Aus dem
Institut für Physiologie
der Medizinischen Fakultät Charité – Universitätsmedizin Berlin

Dissertation

# Chronic Kidney Disease Induces Systemic Microvascular Functional Impairment

zur Erlangung des akademischen Grades eines
Doctor medicinae (Dr. med.)

vorgelegt der Medizinischen Fakultät Charité – Universitätsmedizin Berlin

von

Dr. rer. nat. Johannes Maurer

aus Neckarsulm

Datum der Promotion: 1. März 2019

Für meine Mutter, die mich immer unterstützt hat.

# Foreword

Parts of this work have already been published in:

Prommer, H.U.*, Maurer J.*, von Websky K., Freise C., Sommer K., Nasser H., Samapati R., Reglin B., Guimarães P., Pries A. R. and Querfeld U. 2018. Chronic kidney disease induces a systemic microangiopathy, tissue hypoxia and dysfunctional angiogenesis. Sci Rep. 8(1):5317.

* equal contribution first authorship

Particularly, figure 4 A, figures 12 – 14, figure 16, figure 20, figure 23, figure 26, figure 29, figure 33, figure 36, figure 39, and figure 42 of this work or details thereof, have been released in the above publication.

Table 2 and figure 15 A, B have been included in the Supplementary Data of the above publication.

# Table of Contents

# List of Figures and Tables

## Summary

Chronic kidney disease in young patients is associated with a high mortality rate due to cardiac events, which is in stark contrast to age-matched healthy controls. The mechanisms leading to terminal heart failure in chronic kidney disease are, however, still poorly understood.

Two mouse models of experimental uremia mimicking chronic kidney disease were employed. The data acquired were used for extensive correlation analyses, using serum urea levels and microvessel density in cremaster muscle (derived from identical animals in a related study) as reference parameters.

Functional parameters were measured *in vivo* in the cremaster muscle as a model skeletal muscle by intravital microscopy techniques. The arterial-venous oxygen saturation difference in uremic animals was found to be significantly diminished in a dose-dependent manner. Similarly, in uremic animals, a reduced capability to adjust vessel tone was detected. Despite elevated IL-6 serum levels, no reduction in leukocyte rolling velocity was shown, which is in line with previous results showing an impaired neutrophil recruitment.

*Post mortem* analyses of microvessel density in myocardium showed a significant correlation with microvascular rarefaction in skeletal muscle detected *in vivo,* implying that uremia has a systemic impact. Aortic cross sections of uremic mice, however, showed normal morphology and no differences to controls, suggesting that microvascular rarefaction precedes macrovascular pathology.

These results indicated chronic hypoxic conditions in the respective tissues. Therefore, the expression of genes involved in vessel growth, integrity, and remodeling was determined in cardiac muscle. While VEGF-A, Ang-1, and MMP-2 remained unaffected by uremia, HIF 1$\alpha$, VEGFR-2, Tie-1, Tie-2, Ang-2, and MMP-9 displayed significant downregulation. Thus, VEGF and Ang/Tie-2 signaling was disrupted in uremia, while HIF 1$\alpha$ levels were depleted, suggesting a dysregulated angiogenic response. In fact, uremia resulted in a reversed relationship of hypoxia and angiogenesis.

This study shows that uremia leads, in a dose-dependent manner, to a profound systemic dysregulation of the sensitive interplay between physiological and cellular factors needed to maintain homeostasis, and this process may already be far advanced before becoming clinically apparent. A regulatory network model of feedback loops is presented which may explain the progression of disease. Upon continuous damage, the regulatory network may decompensate, resulting in a sudden onset of progressively amplifying dysregulatory circles, leading to severe complications which may ultimately result in cardiac death. Therefore, microvascular rarefaction is not only an early systemic

marker of cardiovascular impairment in chronic kidney disease but also a promising target for future therapeutic approaches.

# Zusammenfassung

In der pädiatrischen Nephrologie sind chronische Niereninsuffizienz und terminales Nierenversagen mit einer sehr hohen Mortalität verbunden. Auffallend dabei ist, dass jungen Patienten im Gegensatz zu gleichaltrigen gesunden Kontrollgruppen insbesondere an kardialen Ereignissen versterben. Der Pathomechanismus, der bei chronischer Niereninsuffizienz vor allem zum Herztod führt, ist dabei noch wenig verstanden.

In dieser Arbeit wurden zwei Urämie-Mausmodelle zur chronischen Niereninsuffizienz für funktionelle Studien eingesetzt. Mit den gewonnenen Daten wurden umfassende Korrelationsanalysen durchgeführt, wobei Serumharnstoffwerte als Indikator für den Schweregrad der Niereninsuffizienz und die Dichte der Mikrovaskulatur des *Musculus cremaster* (als Modell für einen Skelettmuskel) derselben Tiere aus einer parallel durchgeführten Studie als Referenzen genutzt wurden.

Die arterio-venöse Sauerstoffdifferenz war abhängig vom Urämiegrad der Tiere signifikant reduziert. Entsprechend war in urämischen Tieren auch die Fähigkeit zur Regulation des Gefäßtonus beeinträchtigt. Trotz erhöhter IL-6-Werte im Serum wurde keine Verminderung der Geschwindigkeit des Leukozytenrollens festgestellt. Dies entspricht früheren Studien, in denen bereits eine gestörte Rekrutierung von Neutrophilen beobachtet worden war.

*Post mortem*-Analysen der Mikrovaskulaturdichte im Myokard zeigten eine signifikante Korrelation zur Mikrovaskulatur-Rarefizierung im Skelettmuskel *in vivo*, was auf einen systemischen Effekt der Urämie hindeutete. Aortenquerschnitte urämischer Versuchstiere zeigten jedoch eine normale Morphologie ohne Unterschiede zu Kontrolltieren. Dies legte nahe, dass eine Rarefizierung der Mikrovaskulatur der Pathologie großer Gefäße vorausgeht.

Diese Ergebnisse wiesen auf eine chronische Hypoxie in den untersuchten Geweben hin. Daher wurde die Expression von solchen Genen im Herzmuskel untersucht, die Gefäßwachstum, -stabilität und -remodelling steuern. Während VEGF-A, Ang-1 und MMP-2 durch die Urämie unbeeinflusst blieben, waren die Expression von HIF 1α, VEGFR-2, Tie-1, Tie-2, Ang-2 und MMP-9 signifikant vermindert. Die VEGF- und Ang/Tie-2-Signalwege waren also bei Urämie gestört, während gleichzeitig der HIF 1α-Spiegel vermindert war, was eine Dysregulation der Angiogenese nahelegte. Tatsächlich bestand bei Urämie ein reziprokes Verhältnis zwischen Hypoxie und Angiogenese.

Diese *in vivo* Studie ergab Hinweise darauf, dass Urämie abhängig von ihrem Schweregrad zu einer tiefgreifenden systemischen Dysregulation des empfindlichen Zusammenspiels physiologischer und zellulärer Faktoren führt, die zur Aufrechterhaltung einer zellulären Homöostase notwendig sind. Dieser Prozess kann bereits weit fortgeschritten sein, bevor er sich klinisch manifestiert. Der

Krankheitsfortschritt kann durch ein Netzwerkmodell mit einer Vielzahl von Rückkopplungsschleifen erklärt werden. Sobald die Schädigung einen Schwellenwert überschreitet, kann dies zu einer Dekompensation durch sich zunehmend selbstverstärkende Rückkopplungsmechanismen führen, die schließlich in kardiale Komplikationen münden können. Die Rarefizierung der Mikrovaskulatur bei chronischer Niereninsuffizienz ist daher nicht nur ein früher klinischer Marker für drohende kardiale Ereignisse, sondern auch eine vielversprechende Zielstruktur für zukünftige therapeutische Ansätze.

# 1 Introduction

## 1.1 Impaired Renal Function: Major Cause of Premature Death in the Young

### 1.1.1 Chronic Kidney Disease and End Stage Renal Disease

Cardiovascular complications are the leading causes of death in children, adolescents, and adults with chronic kidney disease (CKD). The pathomechanisms leading to cardiovascular disease (CVD) while the primary defect is located in the kidney, however, are not yet fully understood.

Normal kidney function is pivotal to maintain body homeostasis and covers, among others, (1) the elimination of toxic substances from the blood, (2) the regulation of water and electrolyte balance as well as the acid-base equilibrium, (3) blood pressure control, and (4) hormone production. Kidney failure has therefore profound effects on health, quality of life, and life expectancy in particular.

Corresponding to onset and course of the disease, renal failure is classified into acute kidney injury (AKI, ICD-10 code: N17), and chronic kidney disease (CKD, ICD-10 code: N18). According to ICD-10, AKI is characterized by a sudden loss of renal function with a decrease in glomerular filtration rate, oliguria, a rise in serum urea and serum creatinine concentrations. In principle, AKI may be reversible, the overall mortality and the risk of developing CKD, however, remains increased (Coca *et al.*, 2012). In contrast, CKD develops in most cases as a gradual decrease in renal function and progresses to end stage renal disease (ESRD), an irreversible deterioration of renal function. CKD is classified according to the glomerular filtration rate (GFR) into 5 stages of renal impairment (table 1).

**Table 1:** ***Staging of Chronic Kidney Disease*** (adapted from KDIGO 2012 Clinical Practice Guideline for the Evaluation and Management of Chronic Kidney Disease)

| CKD Stage | GFR [mL/min/1.73m$^2$] | Symptoms | Treatment Options | ICD-10 |
|---|---|---|---|---|
| 1 | ≥ 90 | Normal kidney function | Observation, control of blood pressure | N18.1 |
| 2 | 60-89 | Mildly reduced kidney function | Observation, control of blood pressure and risk factors | N18.2 |
| 3 | 30-59 | Moderately reduced kidney function | Observation, control of blood pressure and risk factors | N18.3 |
| 4 | 15-29 | Severely reduced kidney function | Planning for end-stage kidney failure | N18.4 |
| 5 | < 15 | End-stage kidney failure | Dialysis or transplant | N18.5 |

### 1.1.2 Etiology and Epidemiology of End-Stage Renal Disease

Causes for ESRD differ significantly between adults and children. In adults, main risk factors include diabetes mellitus type 2, hypertension, and smoking. Other risk factors are application of contrast dyes for CT or MRI, the use of analgesics, certain antibiotics, prescription laxatives, or alcohol.

In contrast, the leading causes of ESRD in children are congenital anomalies of the kidney and urinary tract (CAKUT, 33.0 %), glomerular disease (24.6 %), and secondary causes of glomerulonephritis (12.9 %) (cited percentages refer to the period from 2009 to 2013; US Renal Data System 2015 Annual Data Report: Atlas of Chronic Kidney Disease and End-Stage Renal Disease in the United States; Saran *et al.*, 2016). In this survey the most common diagnoses associated with ESRD include renal hypoplasia/dysplasia, congenital obstructive uropathies, focal glomerular sclerosis, and systemic lupus erythematosus.

### 1.1.3 Cardiovascular Mortality as a Major Endpoint in Juvenile End-Stage Renal Disease

The dramatic impact of CKD as an independent risk factor for cardiovascular disease is best illustrated by epidemiological studies in young patients. These studies have shown that the cardiovascular mortality in young adults with hemodialysis treatment is highly increased and resembles that of senescent patients (Foley *et al.*, 1998). Subsequent surveys confirmed that cardiovascular mortality is particularly increased in children with ESRD compared to the age-matched general population (Parekh *et al.*, 2002, Oh *et al.*, 2002). While cardiac causes account for only 3 % of all deaths in the general population of children and young adults (1-24 years, Mathews *et al.*, 2011) they rise to approx. 20 % in children and young adults (1-19 years) with a liver transplant and to approx. 30 % in children and young adults (1-19 years) undergoing hemodialysis or peritoneal dialysis. The most common cause of death in these young patients is cardiac arrest, followed by arrhythmia, cardiomyopathy, and cerebrovascular disease (Saran *et al.*, 2016).

While classical risk factors for CKD in adults were considered rare in children and adolescents, a meta-analysis revealed that more than 90 % of pediatric patients treated with hemodialysis had at least one cardiac risk factor, particularly hypertension and increased serum calcium and phosphate levels (Chavers *et al.*, 2011). In addition, uremia-related risk factors such as anemia, volume overload, hyperparathyroidism, disturbance of mineral metabolism, or chronic increase of inflammation parameters may contribute to the increased cardiovascular mortality, although no study has yet linked single risk factors with CVD mortality (Mitsnefes, 2012). However, patients undergoing hemodialysis or peritoneal dialysis are more severely affected by cardiovascular morbidity and mortality than patients undergoing preemptive transplantation, indicating that uremia plays a key role in the development of cardiovascular disease (Foster *et al.*, 2011).

Established surrogate markers for cardiovascular disease which can often be found in children with ESRD upon thorough investigation are left ventricular hypertrophy (Johnstone *et al.*, 1996), increased intima-media thickness (Mitsnefes *et al.*, 2004), increased pulse wave velocity (Covic *et al.*, 2006), and tissue calcifications including coronary vessels (Milliner *et al.*, 1990; Oh *et al.*, 2002). For this reason, the American Heart Association categorized children with ESRD as a group of patients with the highest risk for cardiovascular morbidity in childhood (Kavey *et al.*, 2006). It is worth noting that vascular and tissue calcifications, a hallmark of cardiovascular disease in patients with CKD (Mizobuchi *et al.*, 2009), result from extensive vascular remodeling and indicate that the pathological process leading to cardiovascular mortality is already advanced and may be on its final path. In recent years, there has been increasing evidence that changes in the microvasculature in cardiac muscle (Amann & Ritz, 2000; Edwards-Richards *et al.*, 2014) and in skeletal muscle (Flisinski *et al.*, 2008) precede the known pathological remodeling or deterioration of the macrovasculature, indicating the need for thorough investigation of small vessel pathology in uremia model organisms.

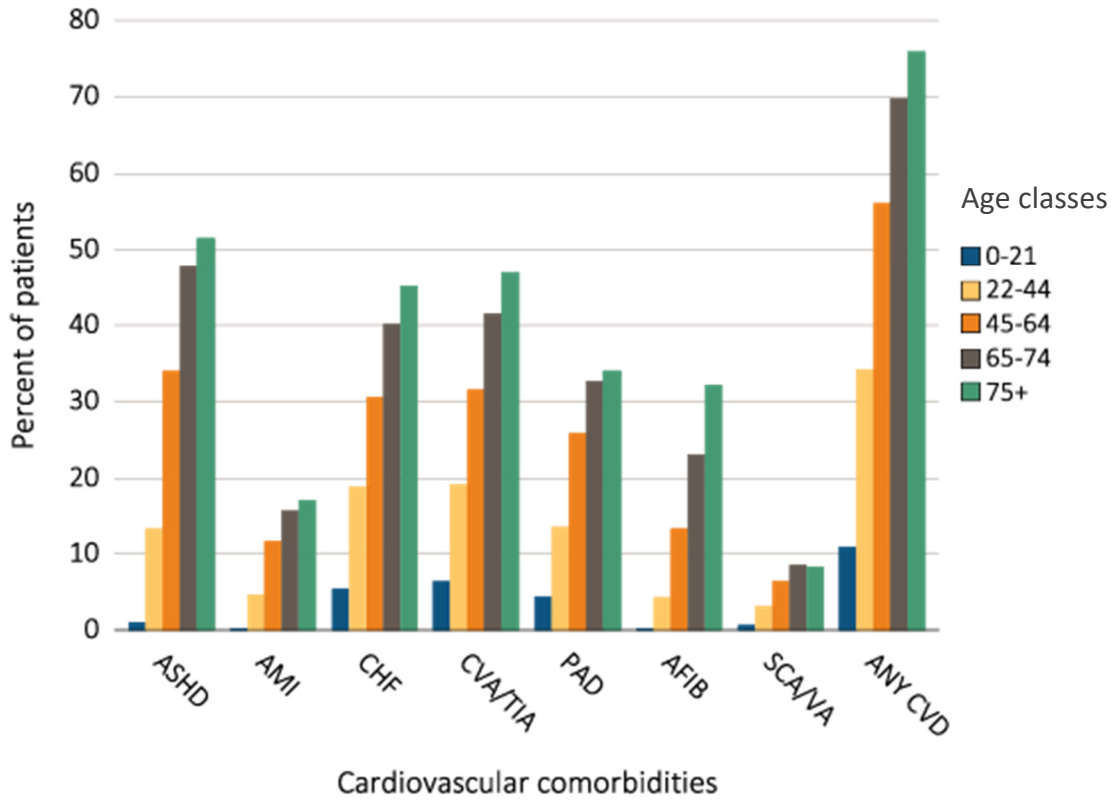


**Figure 1** ***Prevalence of cardiovascular comorbidities in ESRD patients by age classes (2013)***. AFIB: atrial fibrillation; AMI: acute myocardial infarction; ASHD: atherosclerotic heart disease; CHF: congestive heart failure; CVA/TIA: cerebrovascular accident/transient ischemic attack; CVD: cardiovascular disease; PAD: peripheral arterial disease; SCA/VA: sudden cardiac arrest and ventricular arrhythmias (from Saran *et al.*, 2016)

## 1.2 Vessel Development, Maturation, and Maintenance

### 1.2.1 Key Factors Affecting the Vascular Structure

Vascular development, remodeling, and depletion are initiated as microvascular processes. Vasculogenesis (i.e., *de novo* formation of vessels during embryonic development) and angiogenesis (i.e., growth of vessels from existing vasculature) are controlled by a complex system of cytokines and growth factors (Risau, 1997) as well as by hemodynamic factors, such as blood flow (Kochhan *et al.*, 2013), hematocrit (He *et al.*, 2008), vascular tone (Lobov *et al.*, 2011, Chen *et al.*, 2012) and shear stress (Buschmann *et al.*, 2010). Growth factors inducing angiogenesis, such as bFGF, TGF-α, TGF-β, TNF-α, or VEGF, are secreted by endothelial cells and act in an autocrine or paracrine fashion (Folkman, 2006).

The oxygen level in the tissue is measured by the hypoxia-inducible factor (HIF). HIF acts as a heterodimeric transcription factor, binding to specific DNA sequences (hypoxia-responsive elements) and can thus regulate a huge number of effector genes, influencing angiogenesis, erythropoiesis, and energy metabolism (Armulik *et al.*, 2005).

The HIF 1$\alpha$ subunit is constitutively expressed in the tissue; in normoxia, HIF 1$\alpha$ rapidly undergoes prolyl hydroxylation, binds to the von Hippel-Lindau tumor suppressor protein complex, and is degraded in the proteasome. In hypoxia, however, the $\alpha$ subunit escapes prolyl hydroxylation and binds to the stable HIF $\beta$ subunit, forming a functional transcription heterodimer (Kida, 2014). The HIF target gene which plays a key role in vessel development, maturation, and remodeling is the vascular endothelial growth factor (VEGF) (Senger *et al.*, 1983; Ferrara & Henzel, 1989), as it has been shown that hypoxia leads to a profound upregulation of VEGF expression (Shweicki *et al.*, 1992). VEGF plays an important role in both vasculogenesis and angiogenesis. Different VEGF types and splice variants thereof exist, but VEGF-A (hereinafter simply referred to as VEGF) is the most relevant for vessel fate. VEGF initiates the creation of new blood vessels during embryonic development, upon extensive exercise, after injury, or to establish collateral circulation to bypass blocked vessels.

VEGF can bind to two different receptors (VEGFRs): fms-like tyrosine kinase-1 (flt-1), termed VEGFR-1 (de Vries *et al.*, 1992), and kinase insert domain receptor (KDR, in humans) or fetal liver kinase-1 (flk1, in the mouse), termed VEGFR-2 (Terman *et al.*, 1992). VEGFRs are tyrosine kinase receptors which, upon ligand binding, dimerize and become activated through transphosphorylation. It has been shown that most of the complex angiogenic signaling of VEGF (reviewed by Koch & Claesson-Welsh, 2012) is mediated by VEGFR-2. Absolute VEGF concentrations may drive endothelial cell proliferation while varying gradients of VEGF isoforms may trigger endothelial cell migration and differentiation (Carmeliet *et al.*, 2009).

Additional factors, interacting with VEGF signaling, are angiopoietins. Angiopoietins and their receptors form an endothelial-specific signaling system, regulating blood and lymphatic vessel development. Angiopoietin 1 (Ang-1) stabilizes the mature blood vasculature and has a role in the maturation and remodeling of vessels (Eklund & Olsen, 2006), while Angiopoietin 2 (Ang-2) has pro-angiogenic or anti-angiogenic effects, depending on the presence of VEGF (Kim *et al.*, 2000). Ang-1 and Ang-2 both bind to the same receptor, tunica interna endothelial cell kinase (Tie-2) which acts via the anti-apoptotic protein kinase B pathway. The exact mechanism, how the two ligands can transfer different effects via Tie-2 remains controversial. Existing data suggest that Ang-1 and Ang-2 interact, either directly or by competing for Tie-2 binding sites. Therefore, the Ang-1/Ang-2 ratio determines either a pro-angiogenic or anti-angiogenic cellular environment (Maisonpierre *et al.*, 1997). Tie-2 is constitutively expressed in endothelial cells and may thus be required for vessel network integrity (Eklund & Olsen, 2006). Mutations in the Tie-2 gene can lead to vascular anomalies, such as hemangiomas (Wang *et al.*, 2004), while elevated Tie-2 expression in a mouse model may lead to a disease mimicking psoriasis (Voskas *et al.*, 2005). In contrast, Tie-1 is an orphan receptor that does not bind Ang-1 or Ang-2. Tie-1 may play a role in disease as mediator of inflammation. A recent study suggests an interactive model of Tie-1 and Tie-2 function, in which dynamically regulated Tie-1 versus Tie-2 expression determines the net positive or negative effect of Tie-1 on Tie-2 signaling (Savant *et al.*, 2015).

### 1.2.2 Network Formation and Maturation

The mechanisms for the formation, maturation, and maintenance of vessel networks are still poorly understood. Most likely, they follow an overshooting process, where during development an abundance of vasculature is formed that requires subsequent trimming of branches and regression of individual vessels to achieve a customized network, suiting the needs in respective tissues, locations and time (Pries & Secomb, 2014; Korn & Augustin, 2015). This notion is corroborated by the fact that unidirectional tumor growth based on an upregulation of proangiogenic factors (Eggert *et al.*, 2000) results in chaotropic vasculature which is normalized upon anti-angiogenic treatments (Carmeliet & Jain, 2011). Thus, mechanisms of vessel regression or even pruning of larger vessel branches can be considered as part of normal vessel network development, maturation, and adaptation. There is compelling evidence that apoptosis is a major driver for the regression of microvascular networks (Alon *et al.*, 1995). However, other mechanisms that lead to the remodeling or rarefaction of vascular networks exist. Endothelial cells of pruned vessels may also migrate and re-integrate into other segments of a network (Franco *et al.*, 2015) or de-differentiate in a process known as endothelial to mesenchymal transition (Zeisberg *et al.*, 2007).

VEGF acts as an important factor for vessel maintenance, as it is constitutively expressed in adult tissue (Iliescu *et al.*, 2010) while VEGF signaling depletion leads to vessel regression (Meeson *et al.*, 1999). Other pathways involved in keeping the delicate balance between angiogenesis, maintenance and regression may be Ang/Tie-2 signaling, acting through phosphoinositide 3-kinase and protein kinase B which influences apoptosis, as well as Notch, canonical Wnt and non-canonical Wnt signaling (Phng *et al.*, 2009; Korn *et al.*, 2014). Thus, the fate of a network is dependent on the interplay of many factors that may either promote vessel maintenance or regression. VEGF, non-canonical Wnt, and blood flow-induced signaling act as maintenance factors, while Notch and canonical Wnt signaling support vessel regression either by hindering vessel stabilization and proliferation or by promoting vessel constriction and flow stasis, respectively (Korn & Augustin, 2015). The effect of Ang/Tie-2 signaling depends on the prevalence of Ang-1 or Ang-2 (Holash *et al.*, 1999) and, in the latter, on the concentration of VEGF present (Lobov *et al.*, 2002). Loss of microvascular homeostasis may result in chronic tissue hypoxia and eventually in target organ damage (Lockhart *et al.*, 2009).

## 1.3 Target Organ Damage in Chronic Kidney Disease

### 1.3.1 Inflammation and Fibrosis

Persistent inflammation is correlated with cardiovascular mortality rates in ESRD patients (Stenvinkel *et al.*, 2005). In CKD, inflammation is caused, amongst others, by increased oxidative stress resulting from a reduced plasma antioxidant activity (Mimic-Oka *et al.*, 1999) and increased levels of cytokines such as IL-1$\beta$, IL-6, and TNF-$\alpha$. The kidneys are usually involved in the metabolism and removal of modified proteins and protein-associated compounds resulting from oxidative stress. CKD leads to the accumulation of these proteins called advanced glycation end products, AGE (Kaysen *et al.*, 2001). AGE, however, may activate mononuclear cells (i.e. lymphocytes, monocytes, and macrophages) and thus directly spark inflammation. In addition, many other mechanisms contribute to chronic inflammation in CKD (Silverstein, 2009).

Blood leukocytes circulate the vasculature as long as they remain in their quiescent state. Inflammation induces leukocyte capture from the blood flow to the vessel wall. Upon rolling along the vessels' endothelium, leukocytes become activated by endothelial cytokines, gradually slowing them down. Eventually, leukocyte rolling turns into tight adhesion and diapedesis into the adjacent tissue (Sperandio *et al.*, 2006). Adherence of leukocytes to the endothelial surface occurs primarily in postcapillary venules and is facilitated by the lower shear stress present in venules compared to arterioles (Pries & Secomb, 2008). A local vessel dilatation at the region of inflammation may further reduce shear stress (Secomb *et al.*, 2003) and alleviate adherence and subsequent diapedesis.

Permanent inflammation affects functional tissue and triggers regeneration processes leading to fibroblast activation and subsequent fibrosis. In fibrosis, tissue parenchyma is replaced by connective tissue. Fibrosis can be considered as a misguided healing process on the basis of a constant growth stimulus which may impede oxygen diffusion, leading to impairment of organ function, and eventually to organ failure (Mutsaers *et al.*, 2015).

### 1.3.2 Microvascular Rarefaction

Oxygen and nutritional supply of body tissue is achieved via blood flow in vessels and the diffusion of the required substances from the vessels to their target area. Diffusion is effective only over short distances and therefore occurs mainly in the dense microvascular networks pervading tissue and organ parenchyma. To meet the tissue's requirements for both flow and diffusion, a highly organized network structure of the microvasculature is necessary. The microvasculature consists of small resistance arteries, arterioles, capillaries and venules with a diameter below 200 µm which are responsible for 70 % to 90 % of the blood pressure regulation. In this study, microvessels were further differentiated according to their caliber. Measured vessels were classified into the categories of ≤8 µm, >8 to ≤16 µm, >16 to ≤32 µm, >32 to ≤64 µm, >64 to ≤128 µm, and >128 µm, respectively. The low solubility of oxygen and the resulting maximum diffusion distance of 20 to 200 µm make network density the limiting factor for oxygen supply (Pries & Secomb, 2014).

Chronic disease conditions can be detrimental to the microvasculature. There is increasing evidence indicating that microvascular rarefaction in CKD occurs early in the disease process and that these alterations may be subclinical early markers for organ damage (Amann & Ritz, 2000; Edwards-Richards *et al.*, 2014; Burkhardt *et al.*, 2016).

## 1.4 Regulation of Tissue Oxygen Supply

In the microvasculature, effective oxygen exchange is influenced by physical or functional alterations in flow patterns (Pries & Secomb, 2008). The oxygen uptake in tissue is determined by the local vessel density, the blood flow, the hematocrit, and the oxygen saturation of the blood's hemoglobin. Vessel density is a crucial parameter that may change over time but which can be considered stable at a given point in time. Likewise, the hematocrit can vary but can be assumed to be a systemic parameter that is stable and similar in any given part of the body. In contrast, blood flow and oxygen saturation are dynamic functional parameters that can adapt more quickly to changing environmental conditions.

Blood flow through individual arterioles can be regulated locally and is subject to dynamic changes depending on shear stress on the vessel endothelium (Bayliss effect), endocrine factors, or nerval

influences. As described in Poiseuille's law (see below), blood flow is dependent on the fourth power of vessel diameter, rendering this parameter the single most powerful flow regulator.

**Poiseuille's law:** $V = \pi\, p\, r^4 / 8\, \eta\, l$

where

$V$ = *volume flow*
$p$ = *pressure difference between the ends of the vessel*
$r$ = *internal radius of the vessel*
$\eta$ = *blood viscosity*
$l$ = *length of the vessel*

Vessel diameter is controlled by the tone of smooth muscle cells enclosing these vessels. Arterioles have a positive tone of their smooth muscles even in the resting state. Changes in tone are achieved either through the activity of the endothelial cells lining the vessel interior (endothelium-dependent) or the smooth muscle cells surrounding the vessel wall (endothelium-independent).

Oxygen saturation of the blood hemoglobin is a parameter of pulmonary function. The arterio-venous difference in oxygen content ($av\Delta O_2$) of an afferent arteriole and an efferent venule quantifies which oxygen fraction is effectively deposited in a tissue under investigation. A decreased $av\Delta O_2$ may be the result of a decreased microvessel density, a hindered diffusion, or a structural or functional shunt (Pries *et al.*, 2010).

Both vessel tone and $av\Delta O_2$ are subject to multiple nervous, endocrine, cellular, and hemodynamic influences. Hence, for realistic results, they have to be tested *in vivo* rather than in an artificial *in vitro* environment.

## 1.5 Animal Models for the Study of Microvasculature in Uremia

*In vivo* microscopy of the cremaster muscle is an established skeletal muscle model for the study of microvascular networks, as its minor layer thickness renders it translucent and relatively easy to access experimentally. For this investigation, the mouse was the preferred model because the microvasculature is easily accessible for established *in vivo* structural and functional studies. Two established models for the induction of kidney disease were chosen: a remnant kidney model and adenine feeding (Shobeiri *et al.*, 2010). In the remnant kidney model, unilateral nephrectomy and the removal of the poles of the remaining kidney (5/6 nephrectomy, 5/6 NX) reliably produces mild chronic renal disease (Gabizon *et al.*, 1985). In the adenine model, which was first introduced in rats (Yokozawa *et al.*, 1986), adenine is added to the normal diet; intermediate products of the adenine metabolism then precipitate in the kidney tubules, leading to severe CKD. The adenine model is associated with

local and systemic inflammation (Tamura *et al.*, 2009). Both models were used in parallel in this study, to exploit the unique features of each approach, namely differences in the severity of inflammation and uremia, respectively, and to examine whether the effects of uremia were independent of the model.

CKD is characterized by a decreased glomerular filtration rate which can be monitored by increasing blood levels of compounds usually removed from the blood by the healthy kidney. Urea is one of the most abundant substances produced by the liver and is usually disposed of in the kidney via renal urine production. Urea, however, is only one of a plethora of compounds accumulating in the blood of CKD patients, of which many are not yet identified or of which the individual contributions to the accompanying disease process are not clear. The term 'uremia' is therefore used to generally describe symptoms accompanying kidney failure which are thought to be largely due to the accumulation of waste products in the blood such as urea and creatinine (Meyer & Hostetter, 2007). Symptoms of uremia are variable and non-specific and in humans include headache, fatigue, seizures, serositis, nausea, pruritus, peripheral neuropathy, sexual dysfunction, bone disease with fractures, and weight loss. Excessive uremia may lead to encephalopathy, coma, and eventually, death.

No specific values for urea and creatinine demarcate the onset of uremia. In this study, uremia was classified according to blood urea levels as mild, if treated animals developed a urea blood level of up to 250 mg/dL or severe, if blood urea levels exceeded 250 mg/dL).

## 1.6 Aims of this Study

There is convincing evidence that CKD is accompanied physiologically with structural and functional changes in the microvasculature. Clinically, CKD is associated with a highly increased risk of cardiac mortality, which is particularly pronounced in the young, where cardiovascular events are usually rare. It is, however, currently unknown whether the functional changes in the microvasculature precede cardiovascular disease. Moreover, we do not yet know which factors trigger these changes, eventually leading to a pathological dysregulation of tissue homeostasis. Therefore, the goals of this study are the characterization of functional disturbances of the microcirculation in uremic animals as model organisms for CKD:

1. Generate mild to severe uremia in two established animal models of CKD.
2. Characterize *in vivo* the dose-dependent functional impact of uremia on skeletal muscle vasculature.
3. Compare the skeletal muscle vasculature of CKD mice determined *in vivo* with cardiac muscle vasculature of the same animals analyzed *post mortem*.
4. Determine the chronological order of microvascular and macrovascular changes to provide diagnostic indications for an early identification of myocardial changes in CKD.
5. Analyze transcriptional changes in the myocardium of uremic animals as explanatory approach for cardiac microvascular rarefaction in CKD.

# 2 Material and Methods

## 2.1 Laboratory Animals

*In vivo* studies were performed on the microvascular network of the cremaster muscle of BALB/c mice. A total of 39 six-week-old male BALB/c mice with a weight of 17 to 25 g were obtained from Charles River GmbH (Sulzfeld, Germany). The animals were kept in facilities with stable environmental conditions and a twelve-hour artificial light day and night cycle. While all animals underwent intravital microscopy for microvessel density measurement in a separate study (Prommer, 2018), a varying number of animals was employed for further functional analyses. The exact number of animals employed in these individual experiments are given in the respective chapters. All animal experiments were performed in accordance with institutional guidelines for animal care and use and were approved by the Institutional Animal Care and Use Committee and the local State Office of Occupational Health and Technical Safety (Landesamt für Gesundheit und Soziales, Berlin, reference: G 0396/10).

## 2.2 Uremia Induction

Experimental uremia was induced by either adenine feeding or subtotal nephrectomy (5/6 NX) (Prommer *et al.*, 2018). Adenine-induced uremia was deployed as follows: For a period of four weeks, 19 mice received a ROD 18 complete diet for breeding and maintenance of mice (LASvendi, Soest, Germany) including 0.2 % adenine additive (Sigma-Aldrich, St. Louis, USA) *ad libidum*. Eight control mice received ROD 18 diet without additives. Intravital microscopy was performed after four weeks in all animals.

In the 5/6 NX model, uremia was induced via a two-stage surgical procedure in 7 mice. Thirty minutes prior to surgery, animals received preoperative analgesia (metamizol, 200 mg/kg p.o.). Animals were anaesthetized with isoflurane (4 %/L $O_2$ for induction of anesthesia, and 1.5 % to 2.0 %/L $O_2$ for maintenance of anesthesia). The left flank was shaved and disinfected. The skin was cut and the muscles severed. The left kidney was removed completely and the left ureter, renal artery and vein were ligated. The abdominal cavity was closed using absorbable suture material. After a two-week recovery period, the above analgesia, anesthesia procedure, and surgical access was repeated on the right side. The right renal artery and vein were freed and clipped. About 1/3 of the anterior and posterior kidney pole and from the cortex opposite the kidney's hilus were removed with an H-shaped cut, sparing the renal pelvis. The vessel clamps were removed for a few seconds to allow bleeding and subsequent coagulation. After a short period of repeated ischemia, clamps were finally removed. Wound management was conducted as described above.

In 5 sham-operated animals, the same two-stage surgical procedure was applied. The respective kidneys, however, were just exposed and shifted to provide comparable operative stress. Post-surgery, all animals received tramal 10 mg/kg s.c. and subsequently tramal 2.5 mg/100 mL for three days via their drinking water *ad libidum*. After surgery, the animals were kept under standardized housing conditions for a period of 4 months before the start of the intravital microscopy analysis. Body weight was monitored on a daily basis.

## 2.3 Cremaster Preparation

Mice were anesthetized intraperitoneally with urethan i.p. (1,500 mg/kg), and ketamine i.m. (50 mg/kg), placed on a heating mat system equipped with a thermal sensor (Harvard Apparatus, Cambridge, UK) and fixed on a 29 cm x 28 cm acrylic glass stage in dorsal position. During surgery or intravital microscopy, anesthesia was continuously monitored upon pedal withdrawal reflex. Appropriately, ketamine was replenished i.p. (half dose of initial anesthetic). All animals underwent tracheotomy to prevent airway obstruction, catheterization of the right jugular vein for infusion of 0.9 % NaCl to maintain fluid balance as well as catheterization of the left carotid artery for continuous arterial blood pressure and heart rate monitoring. Cremaster preparation followed a modified protocol of Hill *et al.* (1990). The scrotum was cut, the cremaster muscle exposed and fascia and connective tissue were cautiously removed. The cremaster was mounted on the acrylic glass stage to a surface of about 1 $cm^2$ and covered with transparent film (Saran, SC Johnson, Racine, USA) to minimize evaporation. The muscle tissue was regularly moistened using 37°C tempered 0.9 % NaCl solution. After completion of the experiment, pentobarbital i.p. (250 mg/kg) was administered.

## 2.4 Intravital Microscopy

The cremaster muscle's microvasculature was visualized with a modified intravital microscope (Axiotech vario, Carl Zeiss, Jena, Germany) applying a saline immersion objective (20x/NA 0.17) and a 1.6x microscope optical path amplification (Ley *et al.*, 1987). A Xenon AC 100 V lamp equipped with transmitting optical fibers (Leitz, Wetzlar, Germany) was employed as a light source. Light intensity was reduced to prevent tissue damage by employing a green filter (Schott, Mainz, Germany) which also increased contrast between erythrocyte-filled vessels and tissue background. A one-minute sequence of blood stream in the vessels was recorded on videotape using a CCD (charge coupled device) camera system (Kappa Optronics GmbH, Gleichen, Germany) connected to a VHS recorder (DVCAM 64 PDV-64ME, Sony, Japan) and overlaid with a video timer signal (VTG33, FOR-A, Japan). In

this film, vessels, blood streams, and for small vessels, the movement of individual erythrocytes or leukocytes was clearly visualized.

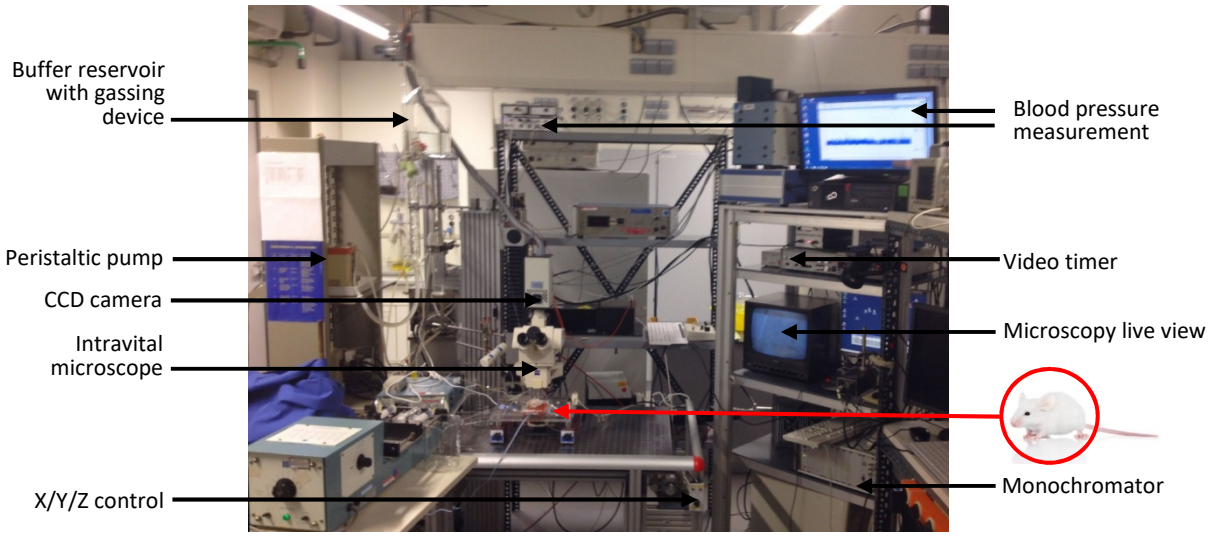


**Figure 2:** ***Experimental setup for intravital microscopy and functional analyses***. Anaesthetized animals with dissected cremaster muscle were placed under the microscope equipped with different light paths for transillumination or reflected light, and an X/Y/Z positioning table for reproducible access of distinct positions within the specimen. The system can be equipped with various cameras, depending on the application. The microscopic visual field can be viewed on a video screen and recorded simultaneously. A peristaltic pump provides an even application of buffer/chemicals to the cremaster muscle. The microperfusion pump used for administration of vasodilatory substances is not visible in this image.

The exact positioning of the fixed cremaster tissue was achieved using a digital X/Y/Z positioning microscopy table (Elesta Elektrotechnik AG, Bad Ragaz, Switzerland). To visualize vessel density in experimental animals, a position adjacent to the first bifurcation of the largest efferent vessels of the cremaster muscle was selected as a starting point for the recordings. An initial visual field of 350 µm x 250 µm muscle tissue area was recorded followed by further visual fields resulting in a 3x3 matrix area (9 visual fields, termed cremaster areas) of approximately 1,050 x 750 µm (neighboring visual fields overlap about 10 %). In total, up to 5 cremaster areas per animal were recorded, corresponding to up to 45 visual fields. Distances between distinct cremaster areas were 1,720 µm horizontally and 2,020 µm vertically.

For analyses of leukocyte rolling velocity, $avΔO_2$, and vascular tone, intravital microscopy was performed using single visual fields. Recordings were subsequently analyzed using an image analysis

software (Vision 3D) allowing for the retracing of vessel distribution, vessel segment lengths, bifurcations, and vessel diameter (Pries, 1988).

## 2.5 Determination of Leukocyte Rolling Velocity

In the video recordings described above, rolling leukocytes could be readily identified in venules without additional staining. The distances covered by individual leukocytes could be measured exactly using the Vision 3D image analysis software (Pries, 1988). The corresponding time was determined and the velocity calculated by metering the overlaid video timer signal. Multiple data points were used to assess the mean leukocyte rolling velocity in the respective animals.

## 2.6 Vascular Oxygen Saturation Imaging Spectroscopy

Oxygen saturation in cremaster muscle microvessels was assessed by using an imaging spectroscopy approach (Styp-Rekowska *et al.*, 2007), taking advantage of changes in the hemoglobin absorption spectrum according to its oxygen saturation (Zijlstra *et al.*, 1983). Feeding arterioles of a tissue area and the draining venules running in parallel were analyzed in an intravital microscopy visual field of 350 µm x 250 µm. The fixed cremaster muscle was transilluminated with a spectrum of 50 consecutive wavelengths, evenly spaced in 2 nm steps from 500 to 598 nm, provided by a monochromator (Polychrome IV LPS150, TILL Photonics, Gräfeling, Germany). Brightness was adjusted using a grey filter (Schott, Mainz, Germany). Each exposure to a certain wavelength was recorded in a distinct image, resulting in a stack of images of the same motif for spectral analysis (monochromator and digital camera are part of an imaging system from TILL Photonics, Gräfeling, Germany). Light intensities were converted into integer data with a resolution of 4095 discrete values by the software of the imaging system (TILL Vision, TILL Photonics, Gräfeling, Germany). For the calculation of oxygen saturation, a dedicated software was used (SOAP - Saturation of Oxygen Analysis Program, Styp-Rekowska *et al.*, 2007). Optical densities for a given wavelength were analyzed for each pixel, subtracting background intensities and calculating the amounts of hemoglobin and oxyhemoglobin after calibration with appropriate reference absorption spectra. The program includes a Fourier algorithm for movement correction, eliminating artifacts due to muscle contraction or breathing. This approach offers simultaneous measurement of the hematocrit levels in individual vessels.

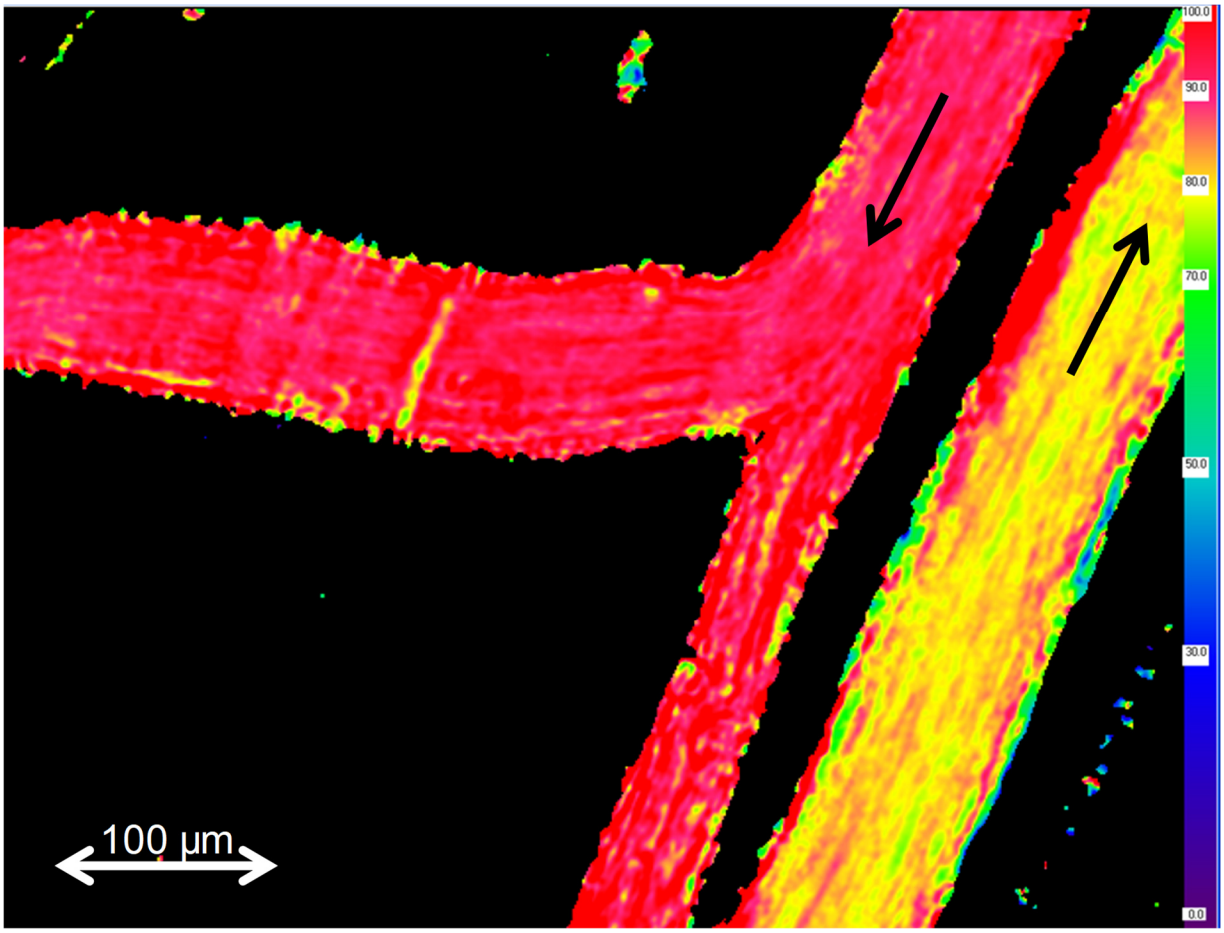


**Figure 3:** ***Spectroscopic avΔO₂ determination***. Sample image from a uremic mouse illustrating the spectroscopic methodology for avΔ$O_2$ determination. An artery with a bifurcation is depicted on the left, the adjacent vein is shown on the right. Flow directions are indicated by black arrows. Scalebar: the double arrow equals 100 µm. Due to a background correction, vessels are clearly singled out from the tissue background. The mean $O_2$ saturation value is 94.6 % for the artery and 81.5 % for the vein. Color coding is given on the right scale bar on a spectrum from deep purple (0 % $O_2$ saturation) to bright red (100 % $O_2$ saturation).

## 2.7 Measurement of Vascular Tone

Arterial vessels display a distinct resting tone, enabling the organism to quickly adjust blood pressure and regional blood supply according to the actual need. To achieve a complete relaxation of the vessels' smooth muscles, a mixture of endothelium-dependent (acetylcholine) and endothelium-independent vasodilatory compounds (adenosine, papaverine, sodium nitroprusside) was applied to the cremaster muscle preparation. This treatment can attain up to 95 % of the maximum vessel dilatation (Klotz *et al.*, 1995). In endothelial cells, acetylcholine triggers a receptor-mediated vasodilatation by inducing the endothelial NO synthetase (eNOS) via muscarinic receptors. The

produced NO diffuses to the smooth muscle cells and leads to vasodilatation. Adenosine, papaverine and sodium nitroprusside act in an endothelium-independent fashion by a direct dilating effect on the smooth muscle cells. Adenosine binds to A2-receptors which belong to the G protein-coupled receptor family. A2 receptor activation leads to an increase of intracellular cAMP levels. Papaverine acts as a PDE inhibitor thus also increasing intracellular cAMP concentrations. Sodium nitroprusside acts as a direct NO donor in smooth muscle cells.

The vascular tone measurement was performed with the intravital microscopy setup as described above, focusing on cremaster arterioles. The buffered superfusion fluid (Duling & Staples, 1976) of 131.9 mM NaCl, 4.7 mM KCl, 2.0 mM $CaCl_2$, 1.2 mM $MgS0_4$, and 18 mM $NaHCO_3$ was preheated to 37°C and aerated with 95 % $N_2$ and 5 % $CO_2$ to maintain a pH of 7.35. The tissue-covering film was removed and the fixed muscle was immediately sprinkled with superfusion fluid for 5 min using a peristaltic pump (Tokyo Rikakikai, Tokyo, Japan) before adding a cocktail of vasodilatory compounds of 0.01 mM acetylcholine (Sigma-Aldrich, St. Louis, USA), 10 mM adenosine (Serva GmbH, Heidelberg, Germany), 0.2 mM papaverine (Sigma-Aldrich, St. Louis, USA), 0.01 mM sodium nitroprusside (Sigma-Aldrich, St. Louis, USA) to the superfusion fluid via a microperfusion pump (Harvard Apparatus Ltd., Edenbridge, UK). Images of the vessels were recorded from identical positions using a digital X/Y/Z positioning microscopy table (Elesta Elektrotechnik AG, Switzerland) before and after administering the vasodilatory cocktail for 5 min.

The Vision 3D image analysis software (Pries, 1988) was used to determine the vessel diameter by dropping a perpendicular line between the limiting vessel walls. Since the inner endothelial layer of the vessels was clearly distinguishable from the vascular lumen in each recording, the vessel diameter could be precisely determined. To calculate the arterial tone, the ratio of the difference between arterial diameter of maximal relaxation $D_{max}$ and arterial diameter at resting state D divided by $D_{max}$ was used according to the following equation (Pries *et al.*, 1995):

$$Tone\ [\%] = \frac{D_{max} - D}{D_{max}} \times 100$$

## 2.8 Blood and Tissue Sample Handling

Following the intravital microscopy analysis, blood samples were drawn for further analyses of serum urea, creatinine, and IL-6 levels. Blood was stored at room temperature for 30 min, centrifuged at 4°C and the supernatant was frozen and stored at -80°C until further use. Urea and creatinine were analysed by 'Labor Berlin' of the Charité Universitätsmedizin Berlin, following standardized protocols.

IL-6 levels were determined using an ELISA test kit with pre-coated plates (BioLegend, Fell, Germany). Moreover, heart, kidneys, aorta, and extensor digitorum longum muscle were harvested. Organs were dissected into 3 portions. One specimen was immediately frozen in liquid nitrogen and stored at -80°C, the remainder was preserved in phosphate-buffered formaldehyde solution 4 % (Roth GmbH, Karlsruhe, Germany) for subsequent paraffin-embedding. Paraffin blocks were sliced in 4 µm or 8 µm layers using a microtome (Leica, Wetzlar, Germany). Hematoxylin-eosin staining with hemalm and eosin (Roth GmbH, Karlsruhe, Germany) and von Kossa staining with sodium thiosulfate (Fluka, Buchs, Switzerland) and silver nitrate (Merck, Darmstadt, Germany) were performed using standard protocols. The intima-media thickness (IMT) of mouse aortas was measured using representative von Kossa-stained paraffin-embedded sections. Using the open source program Image J, the distance from the lumen-intima edge to the media-adventitia edge of the arteries was measured at 12 different spots per section. The average mean of these segments was taken as mean IMT±SD.

## 2.9 Immunohistochemistry

Immunohistochemistry was performed on formalin-fixed tissue sections according to standard methods. Dewaxed and rehydrated tissue sections were incubated in 3 % hydrogen peroxide to block endogenous peroxidases. The heat-induced antigen retrieval was performed in a pressure cooker, using the Dako REAL Target Retrieval Buffer (Dako Cytomation, Glostrup, Denmark). Monoclonal antibodies against Mouse CD31 (1:100) (PECAM-1) (D8V9E) XP Rabbit mAb were purchased from Cell Signaling, Beverly, MA, USA. Bound antibodies were visualized with the Vector NovaRED detection kit (Vector Laboratories, Burlingame, CA, USA). Cell nuclei were counterstained with hematoxylin and eosin and antibody diluents without primary antibodies were used as respective negative controls.

## 2.10 Gene Expression Analysis by qPCR

Gene expression levels in murine heart tissue were determined by quantitative real-time reverse transcription polymerase chain reaction (RT-PCR). Cryo-conserved heart tissues from mice with mild (n = 10) or severe uremia (n = 6) and controls (n = 13, thereof 8 adenine controls and 5 sham-operated controls) were minced in Trizol (Invitrogen, Karlsruhe, Germany) and RNA was isolated according to the manufacturer's protocol, treated with DNase to remove genomic contaminations, and further purified using RNeasy columns (Qiagen, Hilden, Germany). RNA was transcribed into cDNA with the High Capacity RNA to DNA kit (Applied Biosystems, Foster City, CA, USA) and cDNA concentrations were determined by a NanoDrop ND-1000 device (NanoDrop Technologies, Wilmington, NC, USA). Quantitative PCR using SYBR Green Master Mix (Applied Biosystems, Foster City, CA, USA) and

subsequent melting curve analysis was performed using the Mx3000p system (Agilent Technologies, Waldbronn, Germany). Relative RNA amounts were calculated using the 2−ΔΔCt method (Livak & Schmittgen, 2001) and normalized to mean mRNA expressions of the housekeeping genes YWHAZ (tyrosine 3-monooxygenase/tryptophan 5-monooxygenase activation protein, zeta polypeptide) and HPRT1 (hypoxanthine-phophoribosyl transferase). The sequences of the primers (BioTez GmbH, Berlin, Germany) are given in table 2.

**Table 2:** ***Forward and reverse primers used for RT-PCR in the cardiac muscle to determine the quantitative expression of genes involved in angiogenesis***

| Gene | Forward primer | Reverse primer |
|---|---|---|
| HIF 1α | 5'-TCATCAGTTGCCACTTCCCCAC-3' | 5'-CCGTCATCTGTTAGCACCATCAC-3' |
| VEGF | 5'-ACTTGTGTTGGGAGGAGGATGTC-3' | 5'-AATGGGTTTGTCGTGTTTCTGG-3' |
| VEGFR-2 | 5'-TTCCCCCCTGGAAATCCT-3' | 5'-ACAGACCCGGCCAAACAA-3' |
| Ang-1 | 5'-AACCTCACCCTGCAAAGATG-3' | 5'-CACAGATGGCCTTGATGTTG-3' |
| Ang-2 | 5'-CAAGGCACTGAGAGACAC-3' | 5'-TGCGCTTCAGTCTGGTACAC-3' |
| Tie-1 | 5'-GTGCCACCATTTTGACACTG-3' | 5'-CAGGCACAGCAGGTTGTAGA-3' |
| Tie-2 | 5'-GATTTTGGATTGTCCCGAGGTCAAG-3' | 5'-CACCAATATCTGGGCAAATGATGG-3' |
| MMP-2 | 5'-AAAGGACTCGGGTTGTCTGA-3' | 5'-ACTTGGTTCTCCTCCATCCA-3' |
| MMP-9 | 5'-TCCCGAGAGTCCAACTCACT-3' | 5'- CATCTCACCTGGAGGACACA -3' |

## 2.11 Study Organization

Experiments were performed to study either functional alterations of the microvasculature (as documented in this doctoral thesis) or, in a separate study, structural changes of the microvasculature (Prommer, 2018). Structural findings (Prommer, 2018) and functional findings (this study) were derived from identical animals, thus providing a comprehensive, coherent data set. The angioarchitecture of the microvasculature as described by structural measurement during the intravital microscopy experiments of all animals provided the basis for further data analyses and interpretation. The successive functional analyses could often be deduced only from subsets of animals due to a limitation of the overall experimental time, complexity of the respective experimental set-up, possible corruption of subsequent data due to the application of compounds, or stress. Therefore, numbers of animals given in the following chapters represent the quantity of animals successfully investigated in the respective experiments rather than the total number of experimental animals.

## 2.12 Statistical Analysis

Statistical analysis was performed using GraphPad Prism 5.01 (GraphPad, La Jolla, CA, U.S.A.). Numerical values were documented as mean ± standard deviation (SD). Whiskers of boxplot graphs show the standard error of the mean (SEM). The Mann-Whitney test was used to test if two independent samples of observations were drawn from the same distribution, applying a significance threshold of $p < 0.05$. Linear regression of a population was calculated by minimizing the accumulated squares of the residuals (least squares method). The confidence interval represents the range where the true mean exists with a probability > 95 %. The Pearson correlation coefficient r was used as a measure of the linear correlation between two variables. Values between 0.3 and -0.3 were considered nonsense correlations.

# 3 Results

## 3.1 Two Experimental Procedures Generate CKD/Uremia of Different Severity

### 3.1.1 Serum Urea Levels

Both methods employed, adenine feeding and 5/6 NX, led to uremia by destruction of the renal parenchyma. The severity of CKD was assessed by the serum urea level rather than the serum creatinine level, as in mice serum creatinine elevation following renal injury is delayed if compared to serum urea; the increase is less pronounced and is dependent on body mass, which diminishes in the adenine model depending on the adenine concentration of the diet and duration of feeding. (Tamura *et al.*, 2009; Oyama *et al.*, 2010). The level of uremia achieved was variable within respective experimental groups, permitting the investigation of the effect of CKD of different severity on the microcirculation. A four-week 0.2 % adenine diet led to serum urea levels of 39 to 475 mg/dL (median 167 mg/dL). In contrast, 5/6 NX followed by a four-month uremia-inducing period led to serum urea levels of 57 to 249 mg/dL (median 62 mg/dL). For adenine controls and sham-operated mice, the serum urea level was in the range of 21 to 91 mg/dL and 28 to 56 mg/dL, respectively. For stratification, a mildly uremic range (up to 250 mg/dL) and a severely uremic range (250 to 475 mg/dL serum urea) for treated animals was defined. In general, 5/6 NX led to a mild uremia only while adenine feeding on average generated much higher urea levels (7 severe, 12 mild).

### 3.1.2 Serum Creatinine Levels

In the adenine group, control animals (n = 4, as not all of the 8 samples could be successfully analyzed) showed a serum creatinine level of 0.18 ± 0.02 mg/dL, in mildly uremic animals (n = 6) the values were 0.23 ± 0.10 mg/dL (p = 0.25), and in severely uremic animals (n = 7) they were 0.67 ± 0.34 mg/dL (p = 0.033). In the 5/6 NX group, sham-operated animals (n = 5) showed a serum creatinine level of 0.15 ± 0.03 mg/dL and in 5/6 NX mice (n = 7) the values were 0.98 ± 1.08 mg/dL (p = 0.087).

### 3.1.3 Body Weight

Weight loss was observed in adenine-induced uremia. The average animals' body weight at the start of the experiment was 22.6 ± 2.2 g. With adenine feeding, body weight decreased by 2 % ± 9 % for mildly uremic mice and 19 % ± 7 % for severely uremic mice, respectively, whereas controls increased their body weight by 9 % ± 4 %, sham-operated mice by 21 % ± 2 %, and 5/6 NX mice by 14 % ± 11 %. Weight at the time of cremaster surgery was significantly associated with serum urea levels ($r = -0.33$; $p = 0.039$), but not significantly different between uremic groups and their respective controls. The serum urea levels were correlated with relative weight loss in both the adenine-fed mice ($r = -0.72$; $p = 0.0006$) and in the 5/6 NX mice ($r = -0.94$; $p < 0.0001$).

### 3.1.4 Serum Interleukin-6 Levels

Interleukin-6 (IL-6), a marker of inflammation, was significantly elevated in adenine-fed mice with mild uremia (900 pg/mL ± 251 pg/mL; p = 0.032, n = 5) and severe uremia (1199 pg/mL ± 261 pg/mL, p = 0.005, n = 7) compared to controls (516 pg/mL ± 232 pg/mL, n = 5). 5/6 NX mice (n = 7) showed an IL-6 level of 767 pg/mL ± 595 pg/mL compared to sham-operated controls (593 pg/mL ± 662 pg/mL, n = 4). The difference was not significant in the 5/6 NX model (p = 0.79). The levels of IL-6 were significantly correlated with serum urea levels (r = 0.47; p = 0.012, n = 28, figure 4) but not significantly different between groups (p = 0.06). In mice with adenine-induced uremia, but not in 5/6NX animals, IL-6 levels were significantly associated with relative weight change (r = -0.41; p = 0.030).

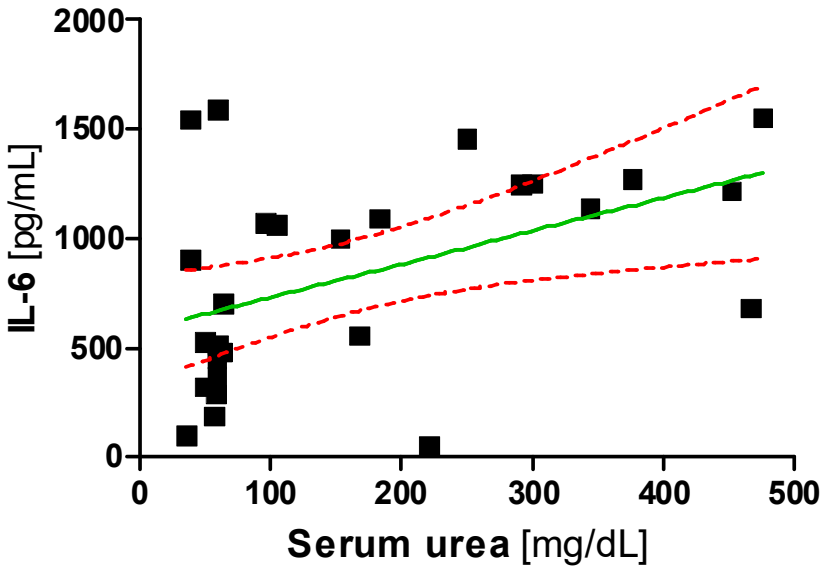


**Figure 4:** ***Correlation of serum IL-6 levels and serum urea levels***. The linear correlation analysis revealed a significant association of IL-6 serum levels to urea serum levels in experimental animals (p = 0.012; r = 0.47, n = 28). The regression line is shown in green, the 95 % confidence intervals are given by the two red dashed curves on either side of the regression line. Each square represents a data pair measured for individual experimental animals.

### 3.1.5 Hematocrit Levels

Hematocrit in arterioles was 0.440 ± 0.043 in controls of the adenine model (n = 8) and 0.355 ± 0.064 in severely uremic animals (n = 7) of the adenine model (p = 0.005). Differences between controls and mildly uremic mice were significant neither in the adenine model (n = 12, p = 0.67) nor in the 5/6 NX (n = 5 for sham-operated animals and n = 7 for 5/6 NX animals) (p = 0.79). Hematocrit levels were negatively associated with serum urea (r = -0.42; p = 0.008), but not significantly different between uremic groups vs. their respective controls.

### 3.1.6 Mean Arterial Blood Pressure

The range of mean arterial blood pressure (MAP) was similar in all groups. Mean MAP was, however, significantly higher in the severely uremic group of the adenine model (79.1 ± 2.7 mmHg, n = 7) compared to their respective controls (73.1 ± 2.8 mmHg, n = 8) (p = 0.0054), but not different between mildly uremic animals of the adenine group (n = 12) and their controls (p = 0.070), and 5/6 NX animals (n = 7) and their sham-operated controls (n = 5) (p = 0.15).

## 3.2 Leukocyte Rolling Velocity in CKD

Leukocyte rolling reflects the direct interaction of leukocytes with the venous endothelial cell layer and is a strong indicator of inflammation. As significantly raised IL-6 levels would suggest systemic inflammation, leukocyte rolling velocity was tested against parameters found to be altered in uremic animals. Leukocyte rolling velocity in the microcirculation depends on the vessel caliber (Prommer, 2018). In order to allow comparability amongst groups, leukocyte rolling velocity was measured only in vessel caliber sizes >64 to ≤128 µm. In no instance, however, could the leukocyte rolling velocity be significantly correlated to any parameter tested. Leukocyte rolling velocity was associated neither with changes in serum urea concentrations (n = 32, p = 0.84, r = -0.038, figure 5), nor with microvascular density in cremaster muscle (n = 32, p = 0.42, r = 0.15, figure 6), nor IL-6 levels (n = 24, p = 0.69, r = 0.087, figure 7).

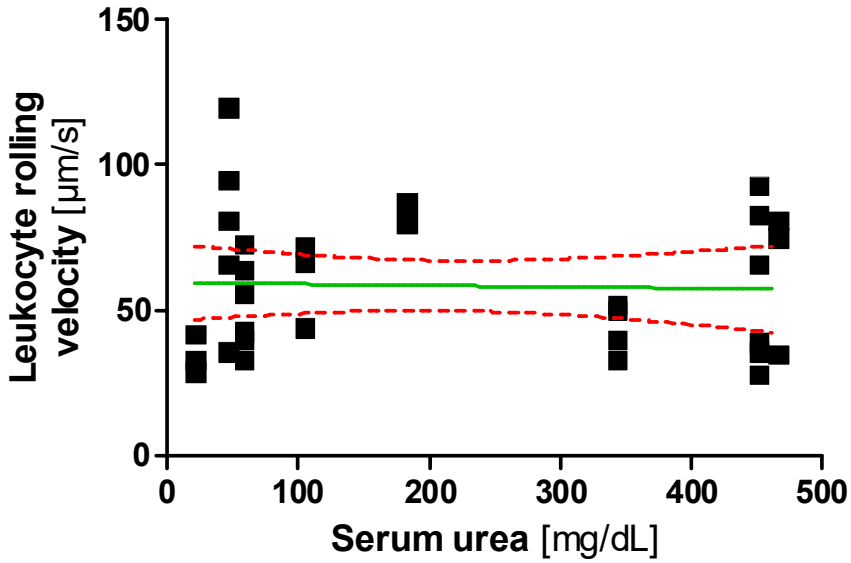


**Figure 5:** ***Linear correlation analysis of leukocyte rolling velocity and serum urea levels.*** No significant correlation between serum urea levels and leukocyte rolling velocity in venules >64 to ≤128 µm was detected (p = 0.84, r = -0.038, n = 32). Designations of the diagram as described in figure 4.

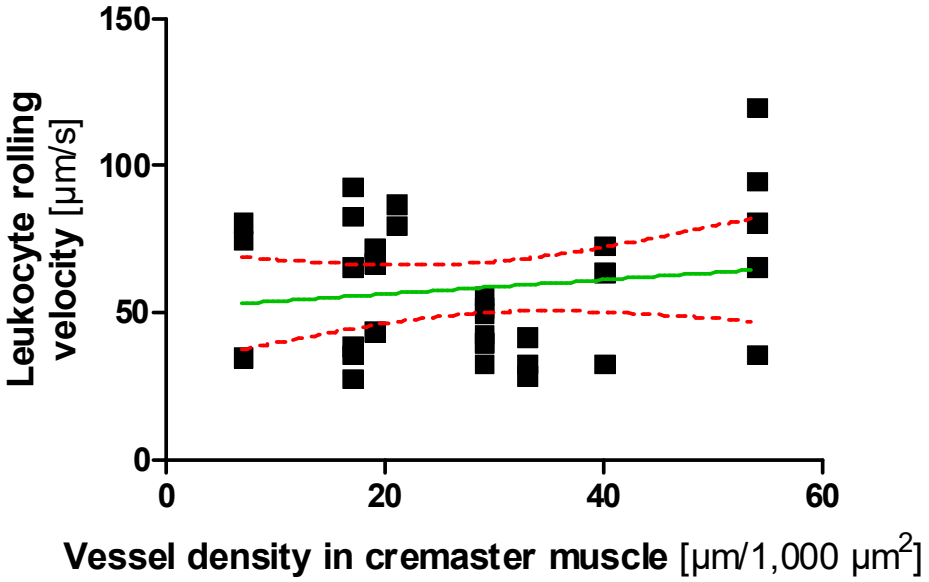


**Figure 6:** ***Linear correlation analysis of leukocyte rolling velocity and microvascular density in the cremaster muscle***. No significant correlation between microvascular density in venules >64 to ≤128 µm and leukocyte rolling velocity was detectable (p = 0.42, r = 0.15, n = 32). Designations of the diagram as described in figure 4.

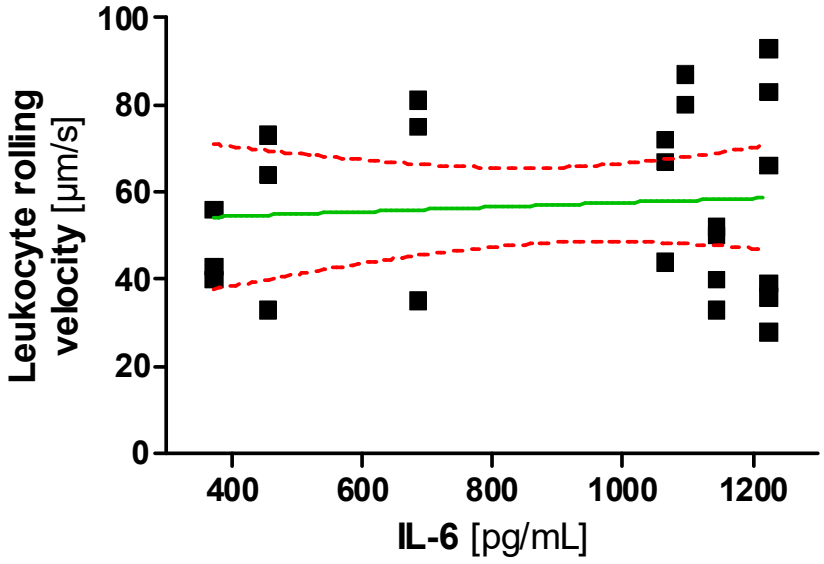


**Figure 7:** ***Linear correlation analysis of leukocyte rolling velocity and serum IL-6 levels***. Although IL6 levels were significantly elevated in severely uremic animals of the adenine model, IL-6 serum levels were not correlated with leukocyte rolling velocity in venules >64 to ≤128 µm (p = 0.69, r = 0.087, n = 24). Designations of the diagram as described in figure 4.

## 3.3 Changes in Arterial-Venous Oxygen Saturation Difference

The av$\Delta O_2$ is one of the drivers for oxygen uptake in skeletal muscle. To determine the effect on peripheral oxygen uptake, the av$\Delta O_2$ in microvessels of caliber >64 to ≤128 µm in 14 mice (8 uremic, 6 controls) was measured. In total, 198 measuring points from 33 vessels were included in the analysis. The av$\Delta O_2$ of control mice (adenine model) was 20.6 % ± 1.5 %, of sham-operated mice 18.1 % ± 2.4 %. 5/6 NX mice had a mean av$\Delta O_2$ of 12.1 ± 2.9 % ($p = 0.0095$ vs. sham), adenine-treated mice with mild uremia 18.0 ± 1.5 % ($p = 0.0635$ vs. controls) and mice with severe uremia 15.6 ± 4.3 ($p = 0.042$ vs. controls). Therefore, the av$\Delta O_2$ was significantly diminished in both models of CKD, ($p < 0.0001$, $r = -0.87$, figure 8).

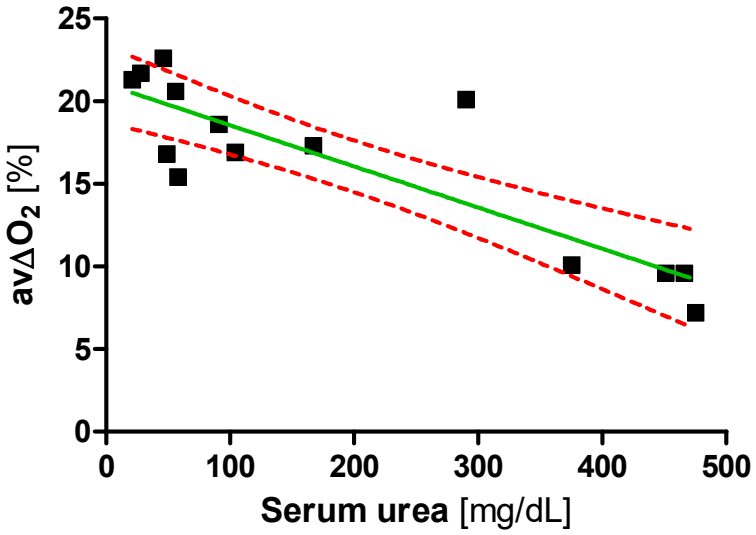


**Figure 8:** ***Linear correlation analysis of arterial-venous difference of oxygen saturation versus serum urea levels.*** Designations of the diagram as described in figure 4. The linear correlation analysis showed an inversely proportional relationship of av$\Delta O_2$ in microvessels of caliber >64 to ≤128 µm and serum urea levels ($p < 0.0001$, $r = -0.87$, $n = 18$), suggesting a decreased tissue oxygen unload in uremia.

## 3.4 Control of Vascular Tone

Change in the efficiency to adjust vascular tone was investigated in arterioles of the adenine model. The relative arterial diameter increase in control mice (n = 4) after administering acetylcholine, adenosine, papaverine, and sodium nitroprusside as previously described (Klotz *et al.*, 1995) was 15.8 ± 1.5 %. Mildly uremic mice (n = 5) showed a relaxation of 13.2 ± 2.5 % ($p = 0.33$ vs. controls), while severely uremic mice (n = 6) showed 8.7 ± 3.6 % relaxation ($p = 0.019$ vs. controls). Diameter change of arterioles was reduced by 17 % in mice with mild uremia and by 45 % in severely uremic animals

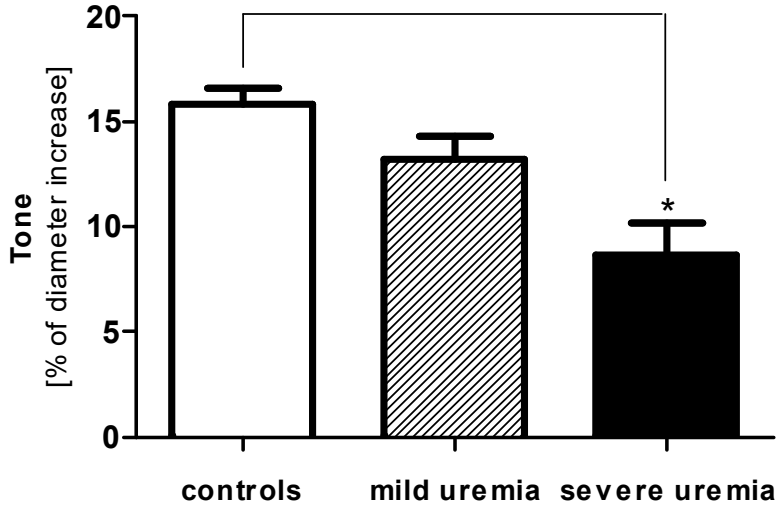


**Figure 9:** ***Vascular tone depending on uremia grade.*** Vascular diameter was measured as difference of vascular diameter before and 5 min after administering vasodilatory substances in controls (n = 4), mildly uremic mice (n = 5), and severely uremic mice (n = 6). Tone was calculated by percentage increase in vessel diameter, as described in the equation given in section 2.7. Severely uremic mice showed a significantly reduced vascular tone (* p = 0.019) when compared to controls.

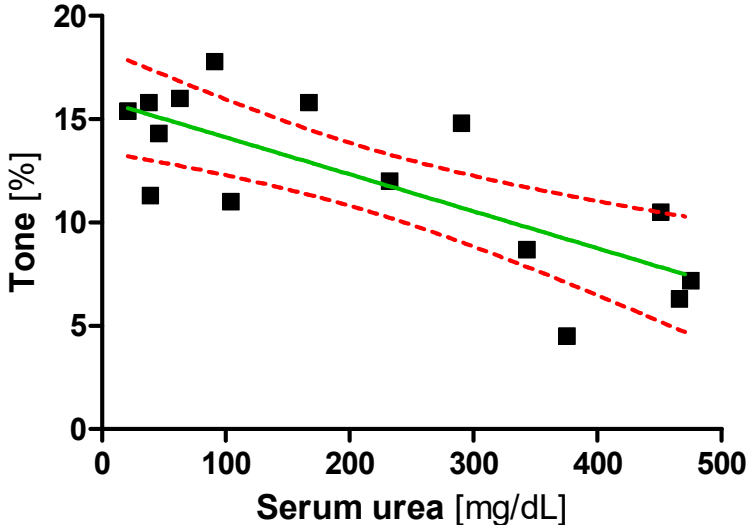


**Figure 10:** ***Linear correlation analysis of vascular tone and serum urea levels.*** Vessel diameter was measured at t = 0 min and t = 5 min after application of endothelium-dependent and endothelium-independent vasodilators. Tone was calculated by percentage increase in vessel diameter, as described in the equation given in section 2.7. The maximum change in vessel diameters upon application of vasodilators correlated inversely with the serum urea levels (p = 0.001, r = -0.76, n = 15). Designations of the diagram as described in figure 4.

if compared to controls (figure 9). The change in vessel diameters correlated inversely with serum urea levels (p = 0.001, r = -0.76, figure 10). Thus, severity of uremia was associated with a diminished vascular tone. The av$\Delta O_2$, quantified in some animals that also underwent measurement of vascular diameter (n = 10), is strongly linked to the change in vascular tone (p = 0.0024, r = 0.84, figure 11).

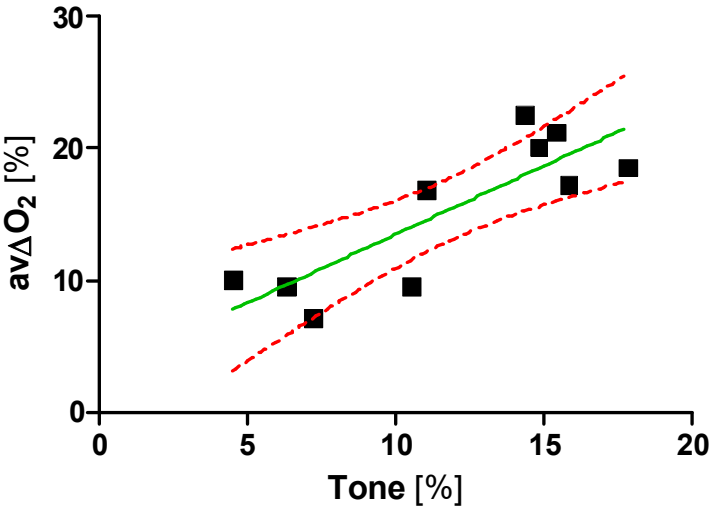


**Figure 11:** ***Linear correlation analysis of arterial-venous difference of oxygen saturation and vessel tone*****.** To determine the vascular tone, vessel diameter was measured in an intravital microscopy setup at t = 0 min and t = 5 min after application of endothelium-dependent and endothelium-independent vasodilators. Tone was calculated by percentage increase in vessel diameter, as described in the equation given in section 2.7. Although this analysis could only be performed for a limited number of animals (n = 10), where av$\Delta O_2$ as well as vascular tone was measured, a strong correlation between the av$\Delta O_2$ and vascular tone was detected (p = 0.0024, r = 0.84). Designations of the diagram as described in figure 4.

## 3.5 Microvascular Rarefaction in Cardiac Muscle Parallels Rarefaction in Skeletal Muscle

In the cremaster muscle, microvessel density (measured as µm/1000µm$^2$) in the intravital microscopy analysis correlated significantly with serum urea levels, independently of the experimental model (Prommer, 2018). Using an immuno-histochemistry approach on the formalin-fixed heart specimen derived from the same animals used for intravital microscopy, a one-to-one verification was achieved. CD31 staining of cardiac muscle revealed a significant decrease in vessel density in uremic mice compared to controls. To diminish bias in the visual analysis of CD31 immuno-histochemical staining, the evaluation of images was performed by a trained third person. Controls (n = 8) were compared to mildly uremic (n = 3, p = 0.012) and severely uremic mice (n = 6, p = 0.0007), thus showing a highly

significant dose-dependent association (figure 12). There was a close correlation of cardiac microvessel density with serum urea levels ($p < 0.0022$, $r = -0.73$, figure 13) and with capillary density in the skeletal cremaster muscle ($p < 0.0001$, $r = 0.90$, figure 14).

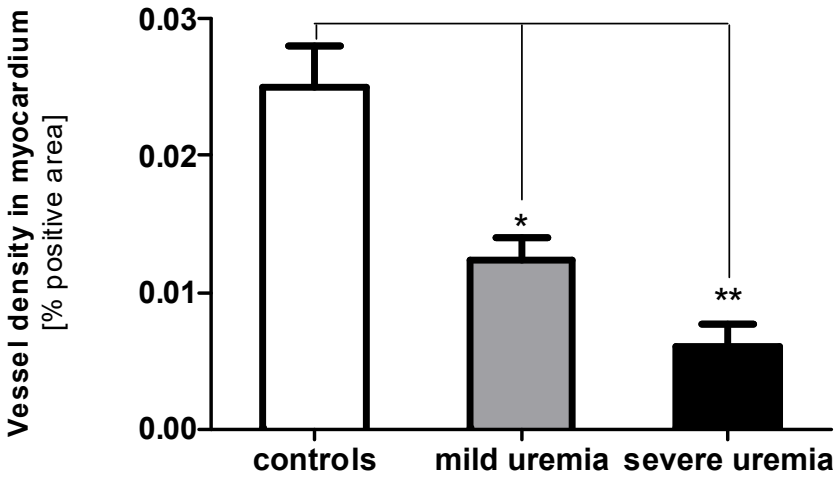


**Figure 12:** ***Microvessel density in myocardium as a function of severity of uremia.*** Microvessel density in the myocardium was measured by CD31 immuno-histochemical staining in controls (n = 8), mildly uremic mice (n = 3) and severely uremic mice (n = 6). Microvascular density was significantly reduced in both mildly (*p = 0.012) and severely uremic animals (**p = 0.0007) if compared to controls.

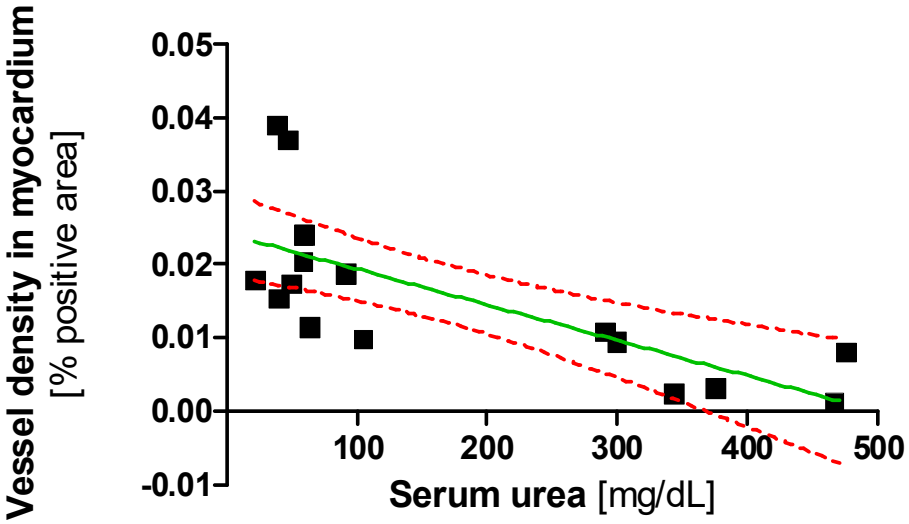


**Figure 13:** ***Linear correlation analysis of microvessel density in the myocardium and serum urea levels.*** The myocardial microvessel density as measured by *post mortem* CD31 immuno-staining in cardiac muscle of experimental mice was inversely correlated to serum urea levels ($p < 0.0022$, $r = -0.73$, $n = 17$). Designations of the diagram as described in figure 4.

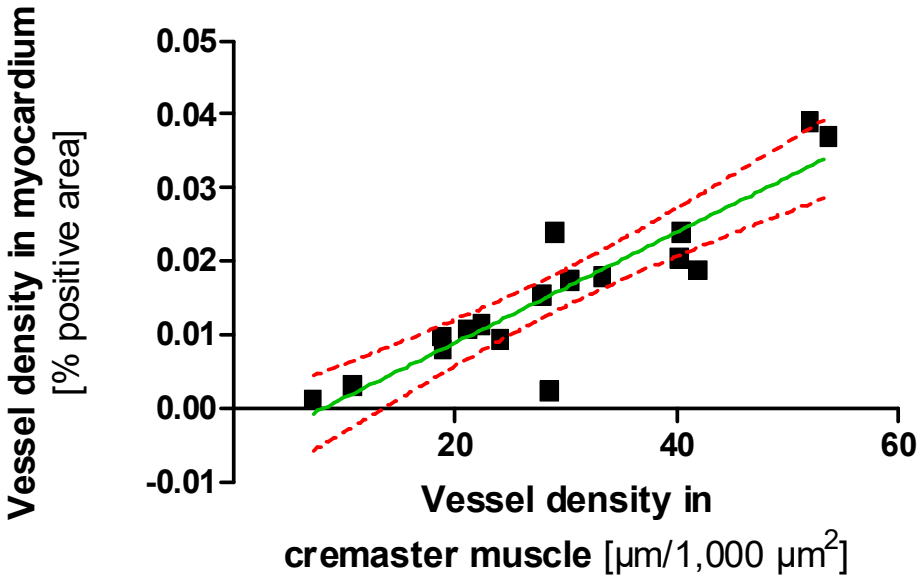


**Figure 14:** ***Linear correlation analysis of microvessel density in the myocardium and microvessel density in the cremaster muscle.*** The myocardial microvessel density was closely correlated to microvessel density in the skeletal cremaster muscle ($p < 0.0001$, $r = 0.90$, $n = 17$). Designations of the diagram as described in figure 4.

## 3.6 Microvascular Rarefaction Precedes Visible Macrovascular Pathology

Capillary density in the cremaster muscle and in the myocardium was significantly reduced in mice with CKD. On cross sections of the aorta (figure 15) of controls and severely uremic mice, the vessel wall layers (endothelium, internal and external elastic membrane, adventitia layer) could be clearly

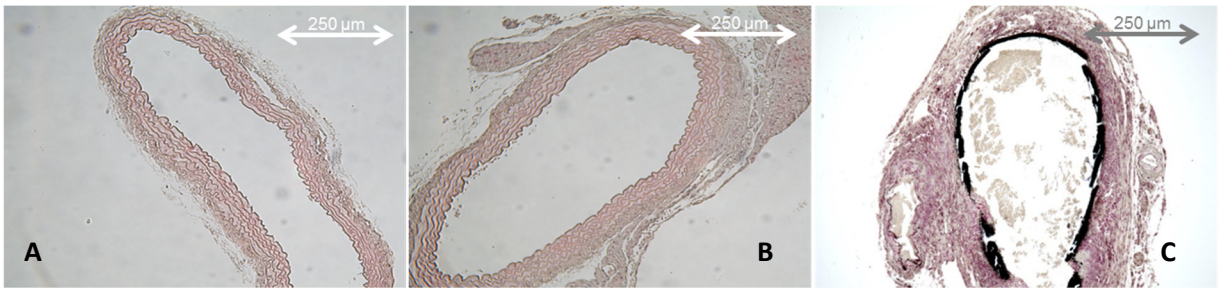


**Figure 15:** ***Arterial cross sections from severely uremic mice and controls do not show any discernible differences.*** Arterial cross sections from uremic animals do not show pathological endothelial alterations. (A) Von Kossa staining of the aorta from a control mouse and (B) a severely uremic mouse to detect aortal calcification. (C) Severely calcified mouse aorta (from a different experiment, photograph courtesy of Veronika Bobb) as a positive control. No significant difference and no signs of arteriosclerotic changes are detectable in the endothelium of severely uremic mice.

distinguished. Two tissue sections were evaluated for each animal (n = 19, 11 uremic, 8 controls). All animals, including severely uremic mice, showed normal morphology by light microscopy and no calcium deposits by von Kossa staining (figure 15 A and B). The intima-media thickness of aortas was not significantly different in uremic mice and controls (48.1 + 7.4 vs. 43.6 + 7.1 µm; p = 0.10).

## 3.7 Dysfunctional Angiogenesis in the Myocardium in Uremic Animals

To elucidate whether renal impairment, measured by elevated blood urea levels, has an effect on the expression of genes in the heart, quantitative RT-PCR on RNA from snap-frozen heart tissue of uremic and control animals (adenine controls and sham) was performed. A focus was set on genes known to be involved in oxygen level measurement, vessel growth and integrity control: HIF 1α, VEGF and its receptor VEGFR-2, Ang-1 and Ang-2 as well as their receptor Tie-2, orphan receptor Tie-1, and finally matrix metalloproteases MMP-2 and MMP-9. For clarity and to facilitate interpretation, the results of the expression analyses are summarized in table 3 at the end of this chapter.

### 3.7.1 HIF 1α Expression in Myocardium is Negatively Correlated to Urea Levels

HIF 1α as a general oxygen sensor of all tissues is of particular interest as it controls the expression of an abundance of effector genes. Therefore, changes in the expression of HIF 1α may trigger expression changes of other genes.

HIF 1α expression levels in the heart were negatively correlated to the urea levels in the blood (figure 16). Controls (n = 13) showed a significantly higher HIF 1α mRNA level than severely uremic mice (n = 6). For severe uremia (blood urea above 250 mg/dL) the average HIF 1α mRNA levels were reduced by about 50 % compared to controls.

The HIF 1α decline (figure 16) appeared particularly in animals with severe uremia and was not significantly different between controls and mildly uremic mice (n = 10, p = 0.73). The difference between controls and severely uremic mice, however, was highly significant (p = 0.008). In addition, the linear regression analysis of the correlation between HIF 1α expression and serum urea levels gave highly significant results (figure 17, p = 0.0021, n = 29, r = -0.55). A similar correlation was detected between HIF 1α expression and the vessel density in the cremaster muscle (figure 18, p = 0.0037, n = 29, r = 0.52), as determined in a related study (Prommer, 2018). HIF 1α mRNA levels were, however, not significantly linked to the $av\Delta O_2$ in the same muscle (figure 19, p = 0.0951, r = 0.53).

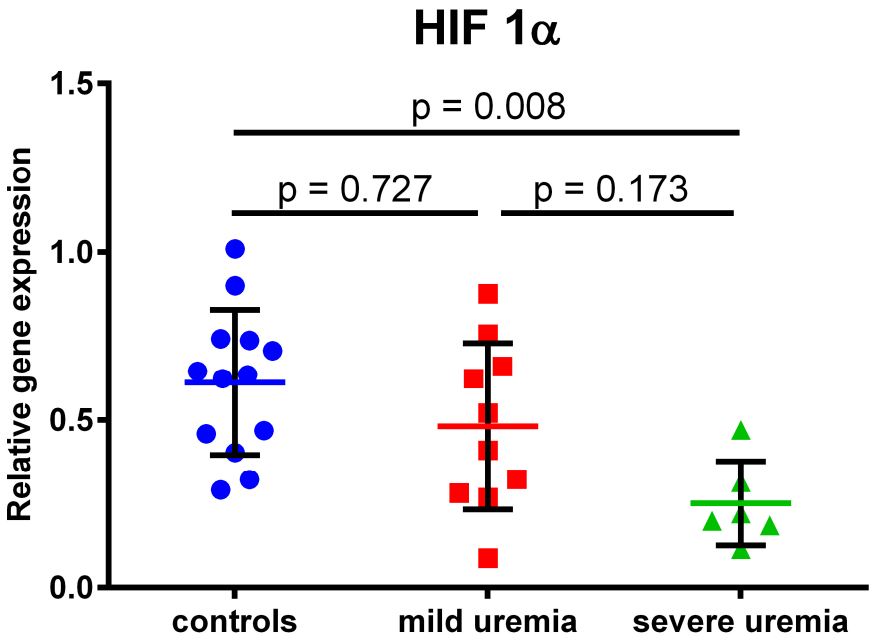


**Figure 16:** ***HIF 1α relative gene expression in the myocardium according to severity of serum uremia.*** HIF 1α gene expression was measured in controls (n = 13), mildly uremic mice (n = 10), and severely uremic mice (n = 6). There is a highly significant decrease of HIF 1α expression in severely uremic animals when compared to controls (p = 0.008).

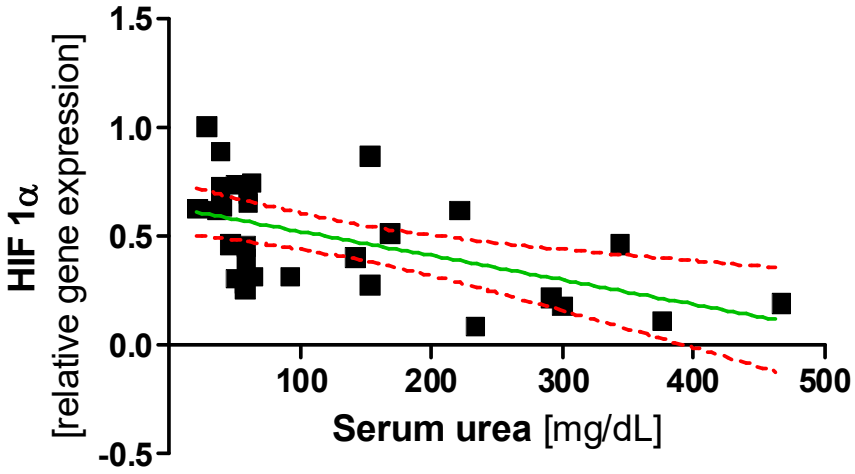


**Figure 17:** ***Linear correlation analysis of HIF 1α gene expression in the myocardium and serum urea levels.*** The decline of HIF 1α expression correlated significantly with increasing serum urea levels (p = 0.0021, n = 29, r = -0.55). Designations of the diagram as described in figure 4.

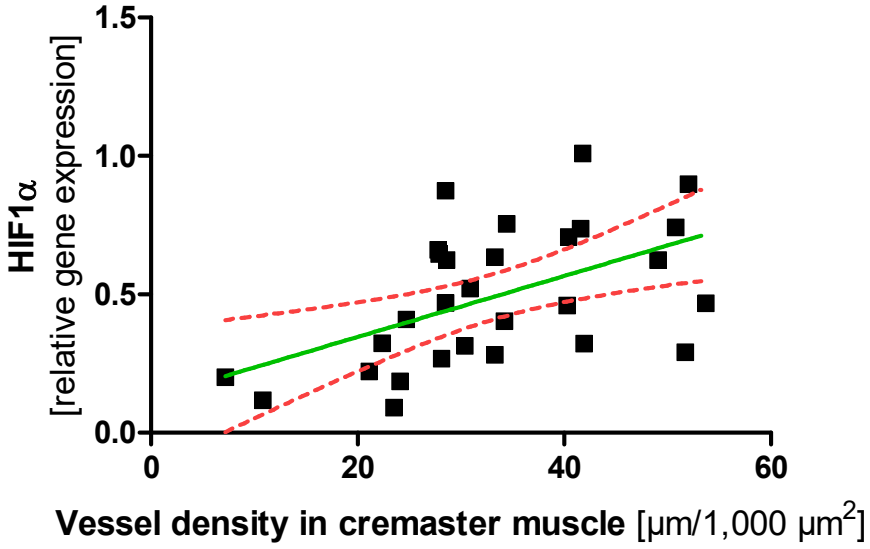


**Figure 18:** ***Linear correlation analysis of HIF 1α gene expression in the myocardium and microvascular density in the cremaster muscle.*** HIF 1α expression also correlated significantly with microvascular density in the cremaster muscle (p = 0.0037, r = 0.52, n = 29). Designations of the diagram as described in figure 4.

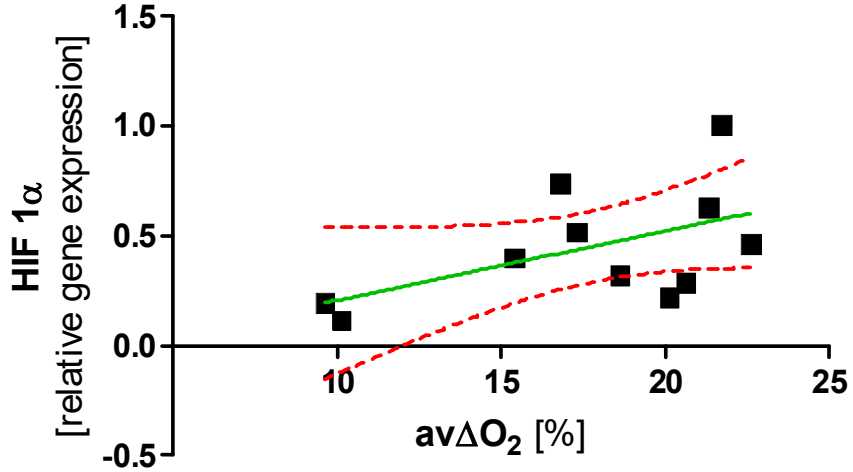


**Figure 19** ***Linear correlation analysis of HIF 1α gene expression in the myocardium and arterial-venous difference in oxygen saturation.*** HIF 1α mRNA expression in the myocardium did not significantly correlate to the av$\Delta O_2$ measured in cremaster muscle tissue (p = 0.0951, n = 11, r = 0.53). Designations of the diagram as described in figure 4.

### 3.7.2 Myocardial VEGF Expression is not Significantly Affected by Uremia

VEGF is thought to be one of the most important regulators of vessel growth and integrity. VEGF is also known as a potential target of HIF gene transcription activation.

Compared to control animals (n = 13), VEGF expression in the heart of mildly uremic animals (n = 10) was not significantly different (figure 20, p = 0.069), and there was no significant difference in expression levels between mildly and severely uremic animals (n = 6, p > 0.999). Also, the comparison of controls (n = 13) with severely uremic animals (n = 6) gave no significant result (p = 0.33). In the linear regression analysis (figure 21), a weak correlation between VEGF expression and serum urea levels was detected which was, however, just under significance level (p = 0.059, r = -0.36, n = 29).

Consistent with this finding, VEGF mRNA expression showed no significant correlation with microvessel density in the cremaster muscle (figure 22, p = 0.052, r = 0.37, n = 29).

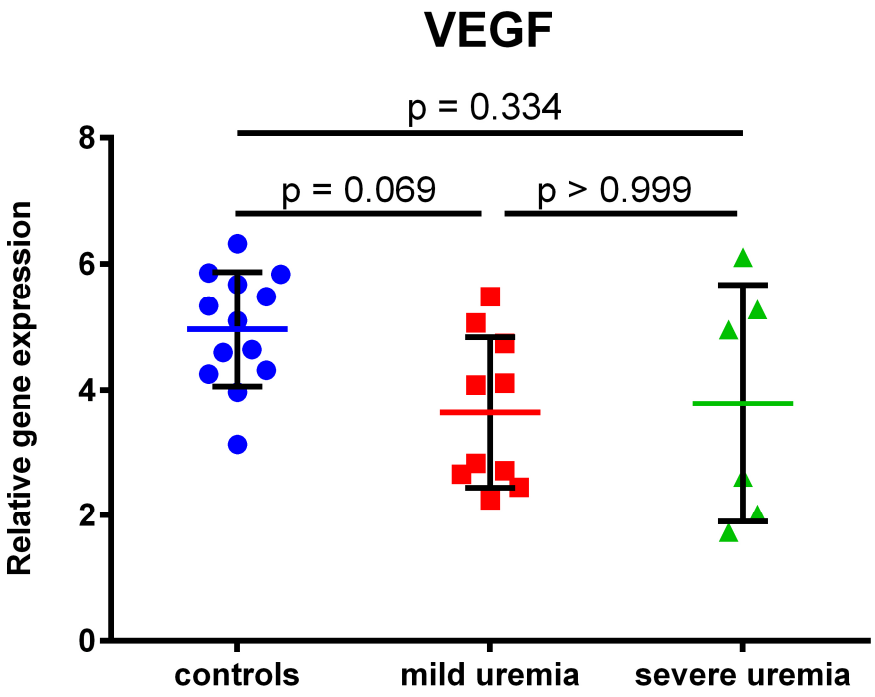


**Figure 20:** ***VEGF relative gene expression in the myocardium as a function of severity of serum uremia.*** VEGF gene expression was measured in controls (n = 13), mildly uremic mice (n = 10), and severely uremic mice (n = 6). No significant correlation of VEGF expression and degree of uremia was detected.

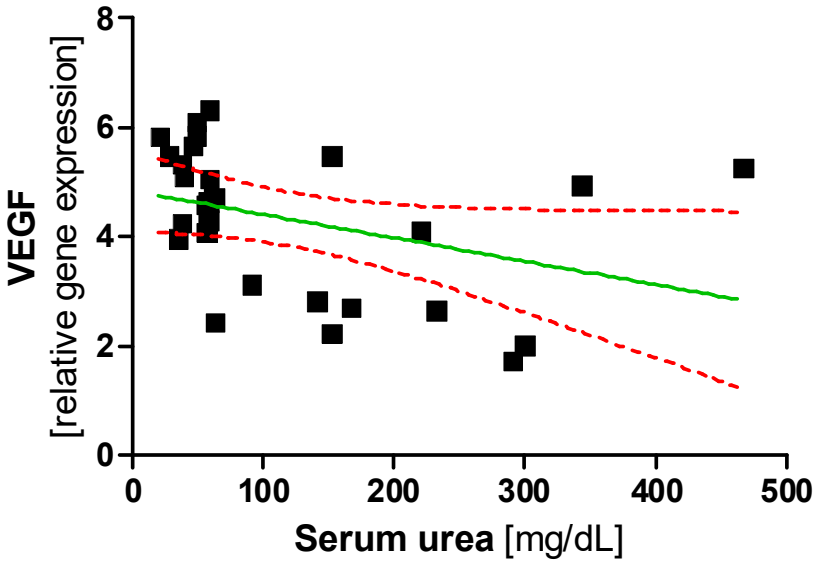


**Figure 21:** ***Linear correlation analysis of VEGF gene expression in the myocardium and serum urea levels.*** Designations of the diagram as described in figure 4. No correlation between VEGF expression and serum urea levels were established (p = 0.059, r = -0.36, n = 29).

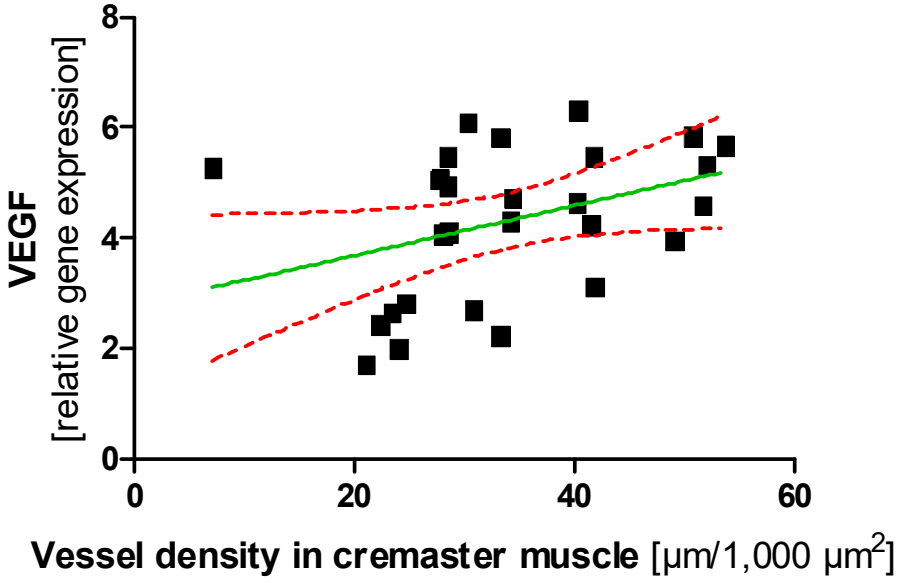


**Figure 22:** ***Linear correlation analysis of VEGF gene expression in the myocardium and microvascular density in the cremaster muscle.*** Likewise, no correlation between VEGF expression in the myocardium and microvascular density in the cremaster muscle was detected (p = 0.052, r = 0.37, n = 29). Designations of the diagram as described in figure 4.

### 3.7.3 VEGFR-2 Shows Decreased Myocardial mRNA Expression in Uremia

VEGFR-2 is the main receptor thought to communicate vascular growth signals transmitted by VEGF. VEGFR-2 mRNA expression gradually deceased as urea levels rose in the respective animals.

Again, the difference in mRNA expression between controls (n = 13) and mildly uremic animals (n = 10) was not significant (figure 23, p = 0.10), neither was the difference between mildly and severely uremic animals (n = 6, p = 0.81). There was, however, a striking difference if severely uremic animals were compared to controls (p = 0.009). Accordingly, linear regression analysis of the association of VEGFR-2 expression with serum urea levels (figure 24) showed a highly significant trend (p = 0.016, r = -0.44, n = 29). Similarly, VEGFR-2 expression declined if cremaster muscle vessels had been rarefacted (figure 25, p = 0.0065, r = 0.49, n = 29).

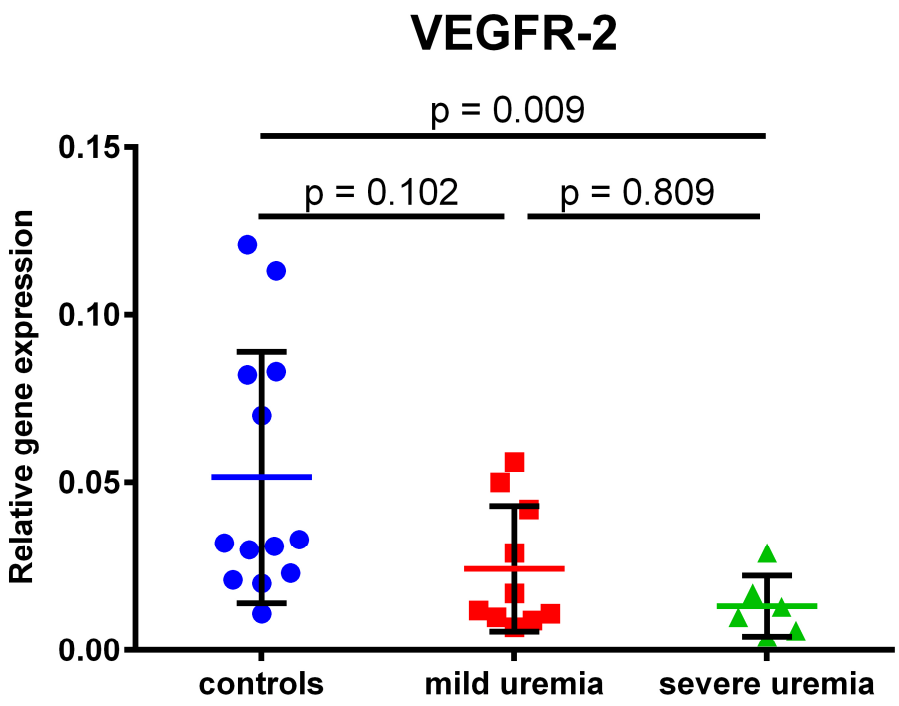


**Figure 23:** ***VEGFR-2 relative gene expression in the myocardium according to severity of serum uremia.*** While there was neither a significant difference of VEGFR-2 expression between mildly uremic mice and controls (p = 0.10) nor between mildly uremic mice and severely uremic mice (p = 0.81), a highly significant difference can be shown between severely uremic animals and controls (p = 0.009).

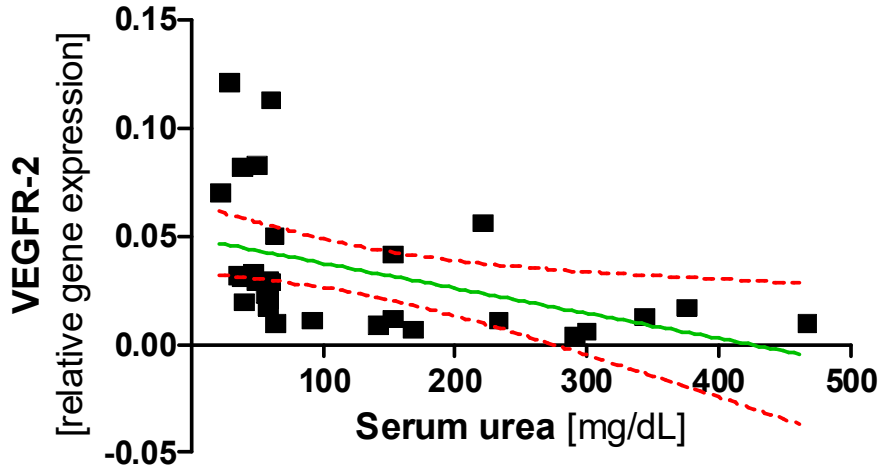


**Figure 24:** ***Linear correlation analysis of VEGFR-2 gene expression in the myocardium and serum urea levels.*** VEGFR-2 gene expression was significantly correlated to serum urea levels (p = 0.016, r = -0.44, n = 29). Designations of the diagram as described in figure 4.

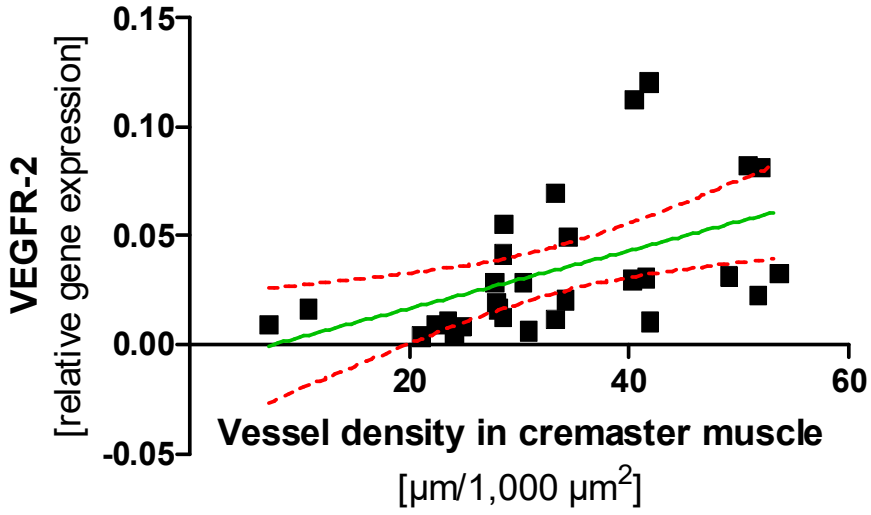


**Figure 25:** ***Linear correlation analysis of VEGFR-2 gene expression in the myocardium and microvascular density in the cremaster muscle.*** Designations of the diagram as described in figure 4. VEGFR-2 expression in the heart correlated significantly with cremaster muscle vessel density (p = 0.0065, r = 0.49, n = 29).

### 3.7.4 Ang-2 but not Ang-1 Transcription is Decreased in the Myocardium of Uremic Mice

The mRNA levels of Ang-1, a main pro-angiogenic compound of the endothelium, were not affected by increasing urea serum levels if mildly uremic animals (n = 10) or severely uremic animals (n = 6)

were compared to controls (n = 13) (figure 26, p = 0.99). The linear regression showed neither a significant correlation between Ang-1 expression and serum urea levels (figure 27, p = 0.51, r = -0.13, n = 29) nor with microvessel rarefaction in the cremaster muscle (figure 28, p = 0.088, n = 29, r = 0.32). In contrast, Ang-2 expression showed a sensitive reaction to increasing urea levels (figure 29). Compared to controls (n = 13), there was already a significant decrease (p = 0.019) in mildly uremic mice (n = 10) and this trend was not further increased in severely uremic animals (n = 6). Linear regression showed a significant correlation between Ang-2 expression decline, serum urea levels (figure 30, p = 0.0094, r = -0.47, n = 29) and microvessel rarefaction in the cremaster muscle (figure 31, p = 0.0075, r = 0.49, n = 29).

This finding showed that with increasing serum urea concentrations, there was a shift in the Ang-1/Ang-2 ratio (figure 32). The Ang-1/Ang-2 ratio, a plain numerical value, rose from approximately 2 in controls to approximately 5 in severely uremic animals. The linear regression analysis showed a highly significant correlation with serum urea levels (p = 0.0064, r = 0.49, n = 29). The same pattern was found, if Ang-1 and Ang-2 were tested against a correlation with microvessel density (data not shown).

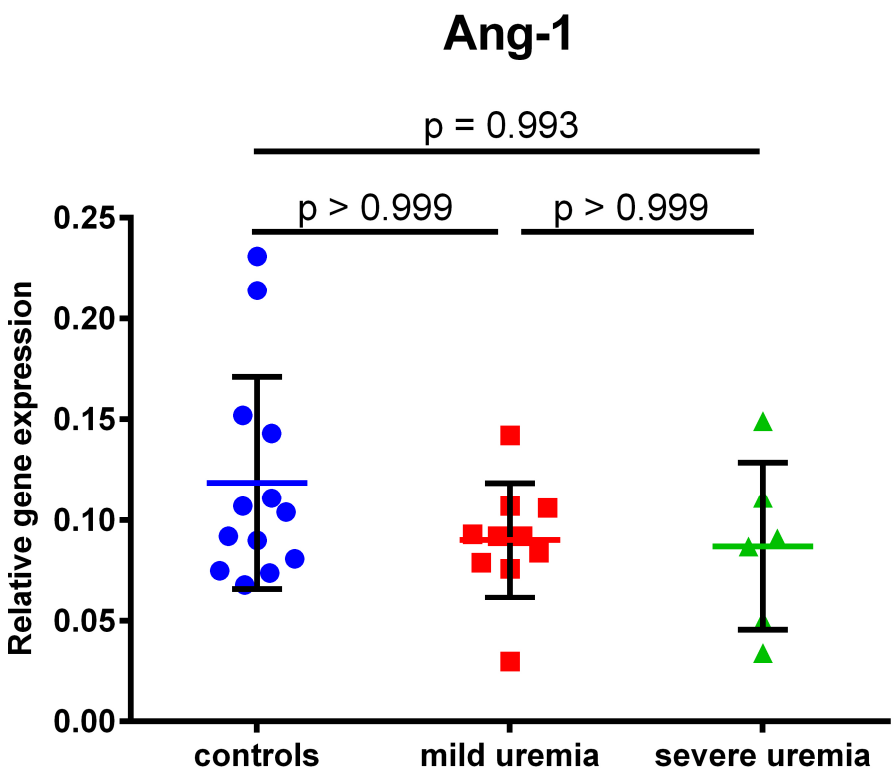


**Figure 26:** ***Ang-1 relative gene expression in the myocardium according to severity of serum uremia.*** Ang-1, a proangiogenic gene regularly expressed in endothelium, showed no significant correlation in myocardial expression levels with the serum urea levels.

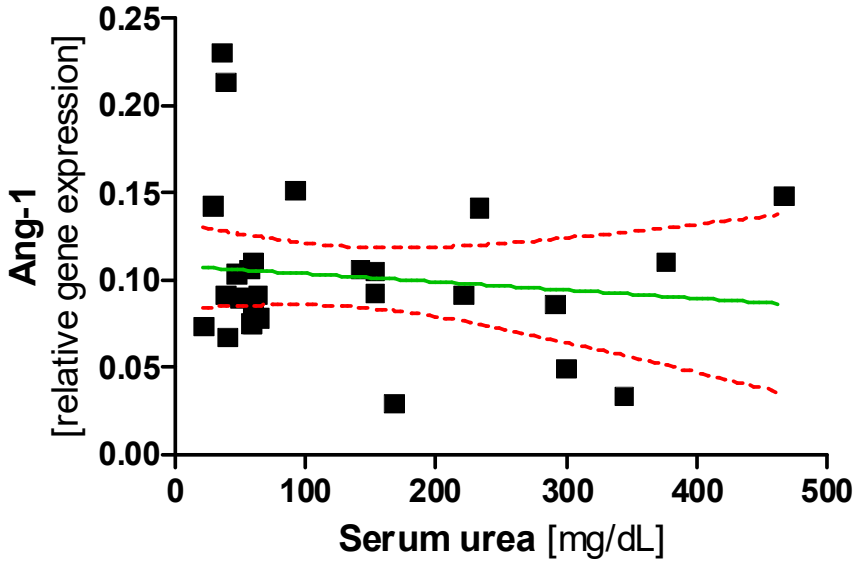


**Figure 27:** ***Linear correlation analysis of Ang-1 gene expression in the myocardium and serum urea levels.*** Ang-1 expression in the myocardium shows a large variation and no significant correlation with serum urea levels (p = 0.51, r = -0.13, n = 29). Designations of the diagram as described in figure 4.

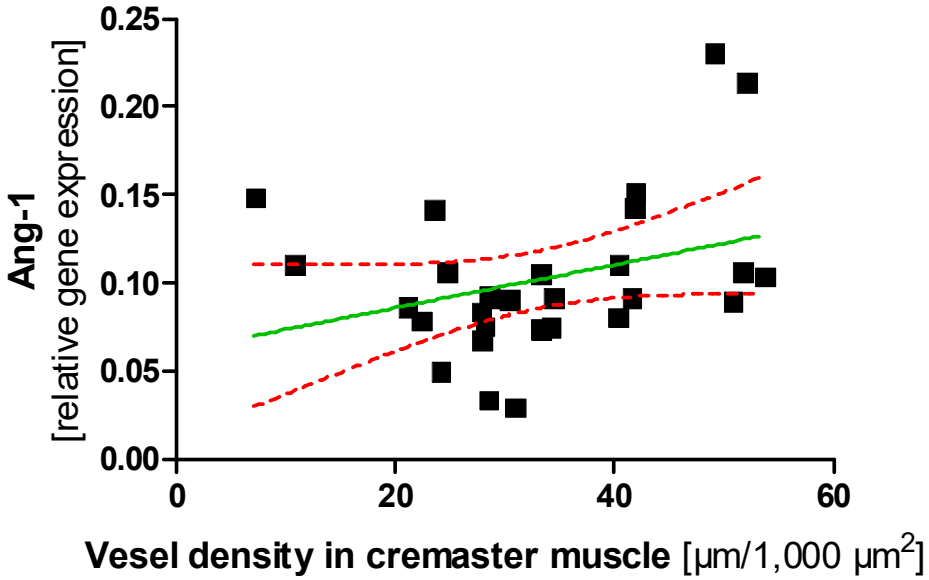


**Figure 28:** ***Linear correlation analysis of Ang-1 gene expression in the myocardium and microvascular density in the cremaster muscle.*** Likewise, no correlation between Ang-1 expression in the myocardium and microvascular density in the cremaster muscle was established (p = 0.088, r = 0.32, n = 29). Designations of the diagram as described in figure 4.

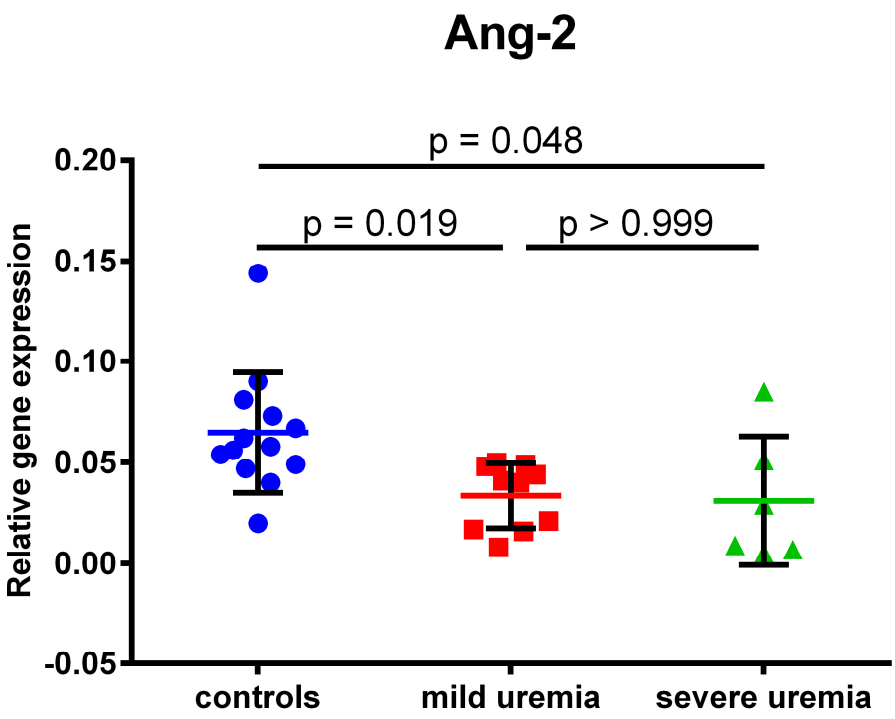


**Figure 29:** ***Ang-2 relative gene expression in the myocardium as a function of severity of serum urea.*** There was a significant difference of Ang-2 expression between mildly uremic mice and controls (p = 0.019), with no further trend between mildly uremic mice and severely uremic mice (p > 0.999). The difference between controls and severely uremic animals was significant at p = 0.048.

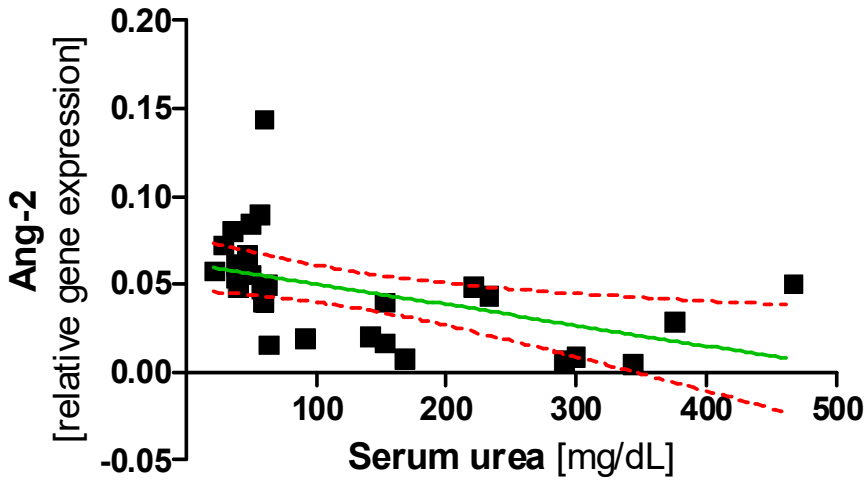


**Figure 30:** ***Linear correlation analysis of Ang-2 gene expression in the myocardium and serum urea levels.*** Designations of the diagram as described in figure 4. Ang-2 gene expression was inversely correlated with serum urea levels (p = 0.0094, r = -0.47, n = 29).

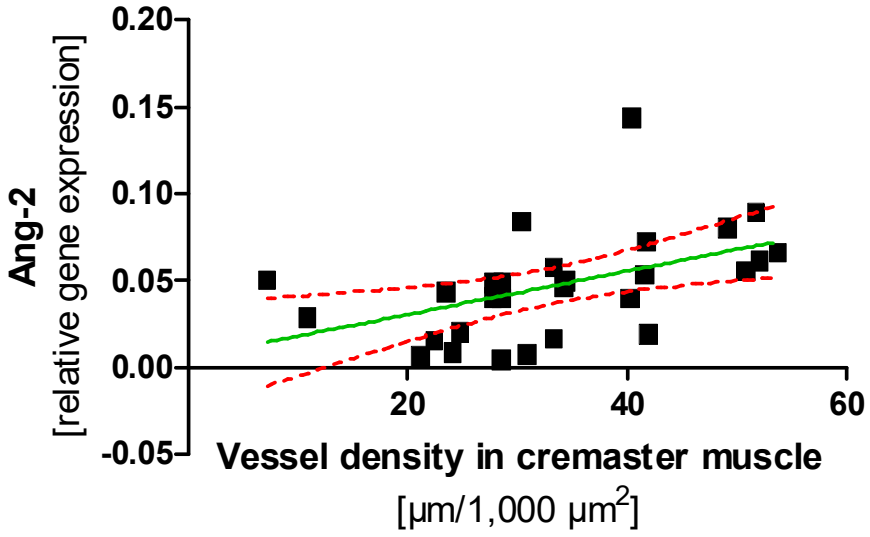


**Figure 31:** ***Linear correlation analysis of Ang-2 gene expression in the myocardium and microvascular density in the cremaster muscle.*** Ang-2 expression in the cardiac muscle is significantly correlated with the cremaster muscle vessel density (p = 0.0075, r = 0.49, n = 29). Designations of the diagram as described in figure 4.

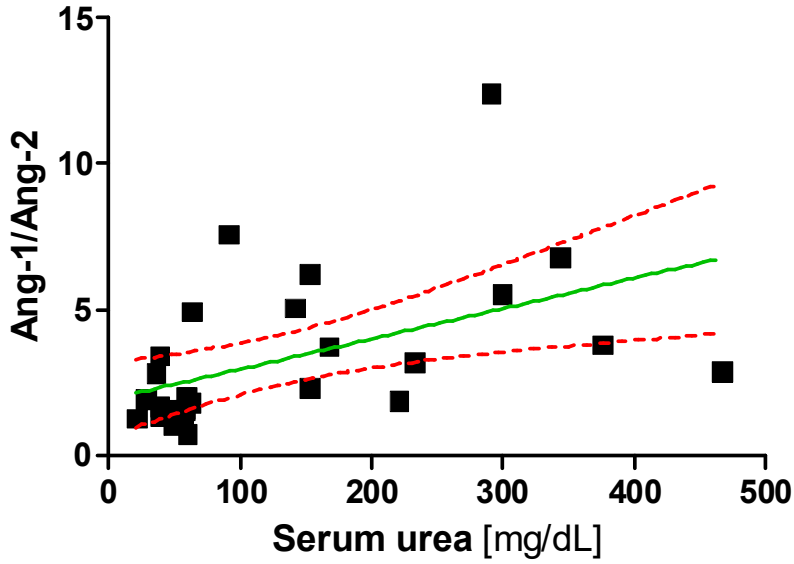


**Figure 32:** ***Linear correlation analysis of Ang-1/Ang-2 gene expression ratio in the myocardium and serum urea levels.*** The ratio of proangiogenic Ang-1 and antiangiogenic Ang-2 gene expression is thought to create a net proangiogenic or antiangiogenic environment, respectively. Therefore, plotting the Ang-1/Ang-2 gene expression ratio against the serum urea levels reveals a highly significant trend towards a proangiogenic environment in the myocardium (p = 0.0064, r = 0.49, n = 29). Designations of the diagram as described in figure 4.

### 3.7.5 Common Ang Receptor Tie-2 Transcription is Downregulated in Severe Uremia

Both Ang-1 and Ang-2 proteins are believed to bind to the Tie-2 receptor. Tie-2 mRNA expression levels in the myocardium showed a significant decrease in severely uremic animals (n = 6) when compared to controls (n = 13) (figure 33, p = 0.024). The differences were not yet significant between controls and mildly uremic mice (n = 10). Consistent with these results, the linear regression analysis (figure 34) showed that Tie-2 expression was negatively correlated with serum urea levels ($p < 0.0001$, $r = -0.68$, $n = 29$) and positively correlated with microvessel density in skeletal muscle (figure 35, $p = 0.0017$, $r = 0.44$, $n = 29$).

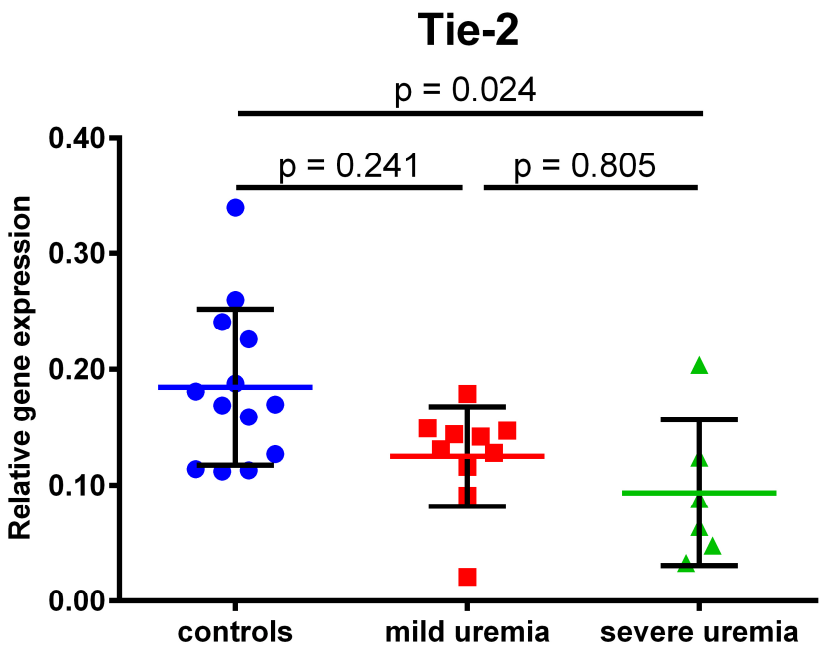


**Figure 33:** ***Tie-2 relative gene expression in the myocardium as a function of severity of serum urea.*** Tie-2 expression was neither significantly different between mildly uremic mice and controls ($p = 0.24$) nor between mildly uremic mice and severely uremic mice ($p = 0.81$). There was, however, a significant difference between severely uremic animals and controls ($p = 0.024$), suggesting that Tie-2 expression in the heart declined particularly at higher serum urea levels.

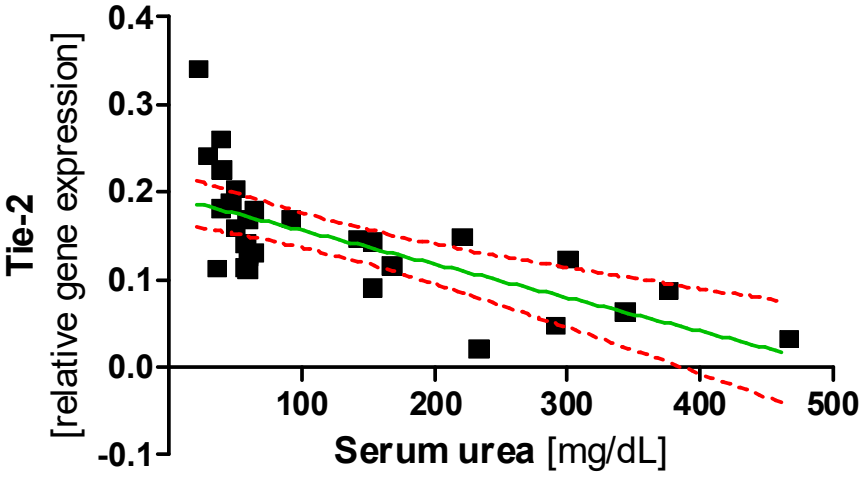


**Figure 34:** ***Linear correlation analysis of Tie-2 gene expression in the myocardium and serum urea levels.*** The myocardial gene expression of Tie-2, which is thought to act as a receptor for Ang-1 as well as for Ang-2, was inversely correlated with serum urea levels ($p < 0.0001$, $r = -0.68$, $n = 29$). Designations of the diagram as described in figure 4

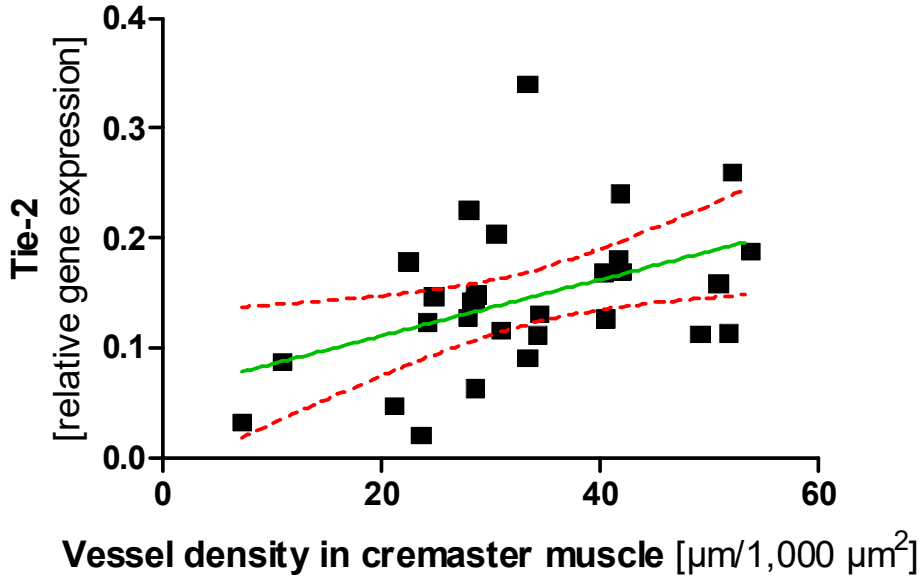


**Figure 35:** ***Linear correlation analysis of Tie-2 gene expression in the myocardium and microvascular density in the cremaster muscle.*** Although cardiac Tie-2 expression showed considerable variation, it was significantly correlated to cremaster muscle vessel density ($p = 0.0017$, $r = 0.44$, $n = 29$). Designations of the diagram as described in figure 4.

### 3.7.6 Orphan Receptor Tie-1 mRNA Levels are Negatively Affected by Uremia

Tie-1 mRNA levels in the heart were significantly lower in severely uremic animals (n = 6) as compared to controls (n = 13) (figure 36, p = 0.036). The drop of gene expression between controls and mildly uremic animals (n = 10) was, however, not significant (p > 0.999), possibly indicating that a stronger metabolic strain is required to produce this effect. Again, there was a consistent negative correlation of Tie-1 mRNA levels and increasing serum urea (figure 37, p = 0.0016, r = -0.56, n = 29) and a positive correlation of Tie-1 mRNA levels and the density of the microvasculature in cremaster muscle (figure 38, p = 0.019, r = 0.43, n = 29).

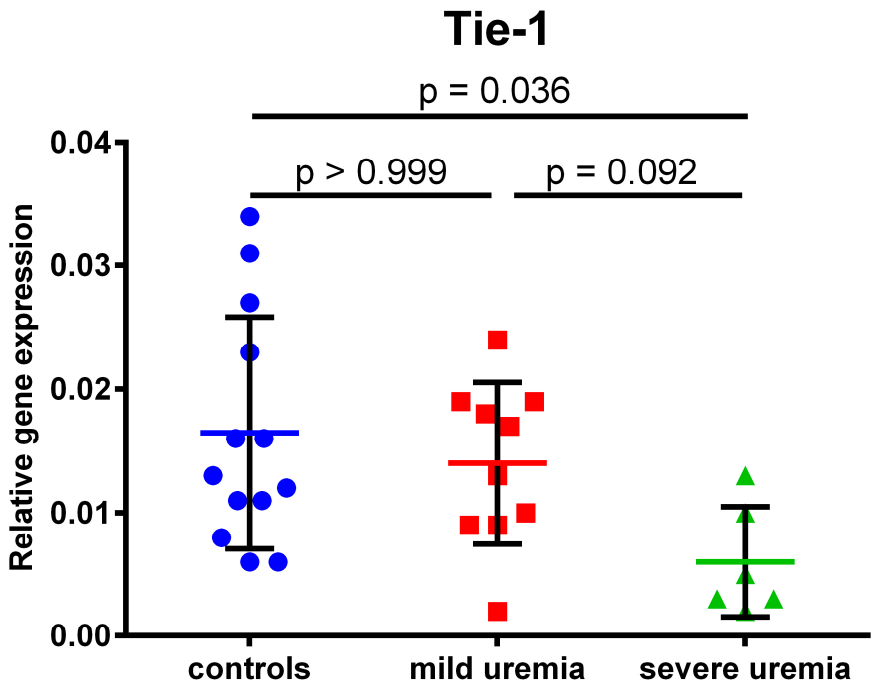


**Figure 36:** ***Tie-1 relative gene expression in the myocardium according to serum urea levels.*** Tie-1 is an orphan receptor that is thought to interact with the Tie-2 receptor. In line with the Tie-2 expression decline in uremic animals, Tie-1 expression is significantly lower in severely uremic animals than in controls (p = 0.036).

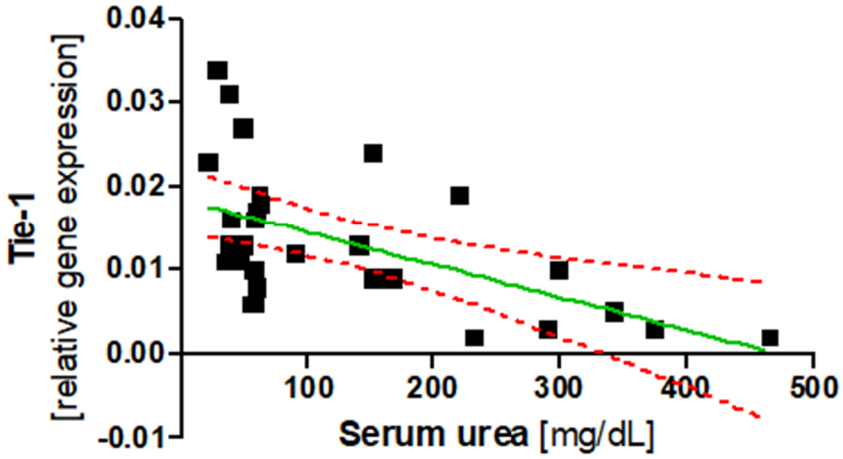


**Figure 37:** ***Linear correlation analysis of Tie-1 gene expression in the myocardium and serum urea levels.*** Expression of orphan receptor Tie-1 in the cardiac muscle was negatively correlated with serum urea levels (p = 0.0016, r = -0.56, n = 29). Designations of the diagram as described in figure 4.

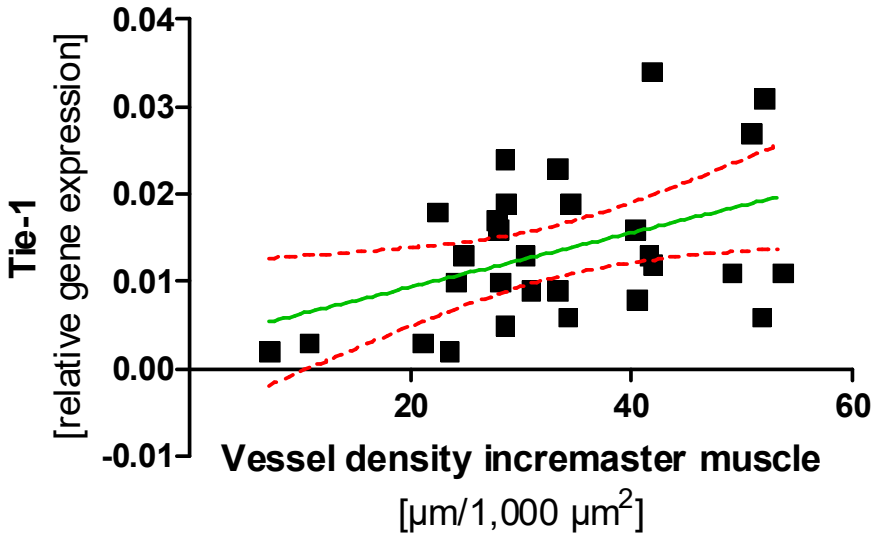


**Figure 38:** ***Linear correlation analysis of Tie-1 gene expression in the myocardium and microvascular density in the cremaster muscle.*** Similar to the Tie-2 receptor which is thought to interact with the Tie-1 receptor, Tie-1 expression was significantly correlated with microvascular density of the cremaster muscle (p = 0.019, r = 0.43, n = 29). Designations of the diagram as described in figure 4.

### 3.7.7 Matrix Metalloprotease MMP-9 but not MMP-2 Transcription is Reduced in Myocardium of Uremic Mice

Vessel regression as well as vessel growth requires the activity of extracellular matrix (ECM) modifying enzymes. There was a significant difference between cardiac MMP-9 expression in controls (n = 13) and severely uremic mice (n = 6, p = 0.024, figure 42). The difference of expression levels was much less pronounced between controls and mildly uremic animals (n = 10) (p = 0.26). Furthermore, the linear regression analysis showed a significant negative correlation of mRNA expression to increasing serum urea levels (figure 43, p = 0.038, r = -0.39, n = 29) and a positive correlation particularly to microvessel density (figure 44, p = 0.0008, r = 0.59, n = 29). In contrast, expression levels of MMP-2 seemed largely unaffected by serum urea levels (figure 39, p > 0.999). Accordingly, linear regression showed no correlation between MMP-2 expression and serum urea (figure 40, p = 0.67, r = 0.08, n = 29) or vessel rarefaction (figure 41, p = 0.77, r = -0.06, n = 29).

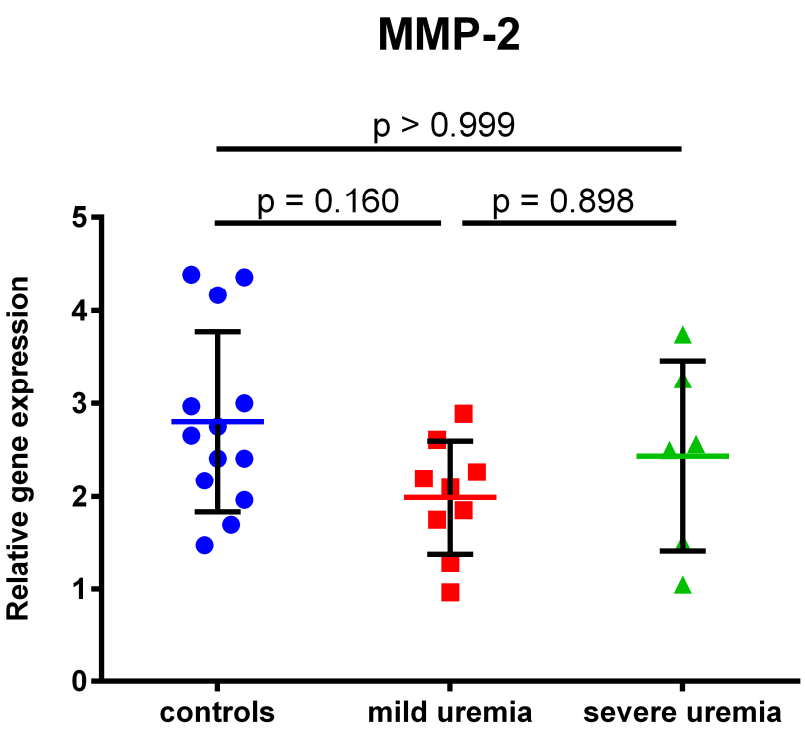


**Figure 39:** ***MMP-2 relative gene expression in the myocardium as a function of levels of serum urea.*** MMP-2, a matrix metalloprotease with an assumed role in vessel remodeling and rarefaction, shows no significant correlation in myocardial expression levels with different classes of serum urea levels (p > 0.999, n = 29).

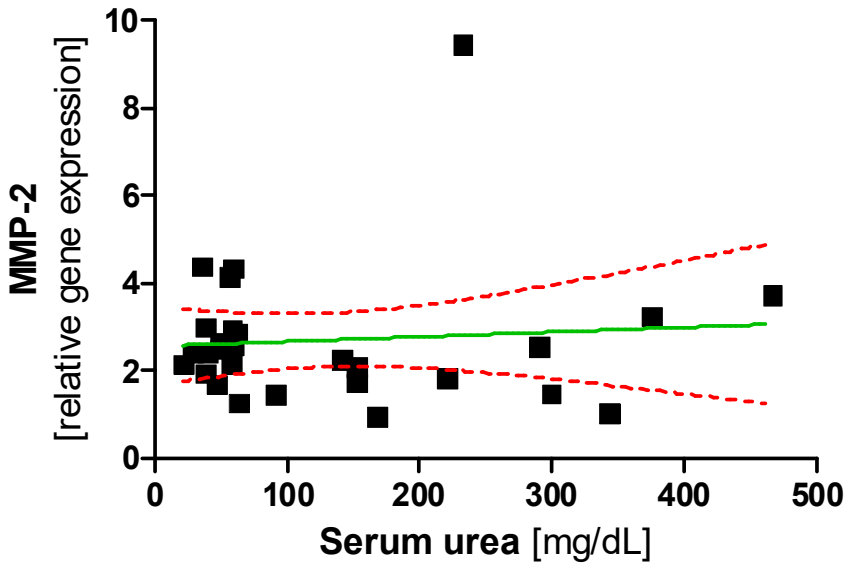


**Figure 40:** ***Linear correlation analysis of MMP-2 gene expression in the myocardium and serum urea levels.*** Although matrix metalloproteases are thought to play a role in vascular remodeling, no correlation of MMP-2 expression in the myocardium and serum urea levels was found (p = 0.67, r = 0.08, n = 29). Designations of the diagram as described in figure 4.

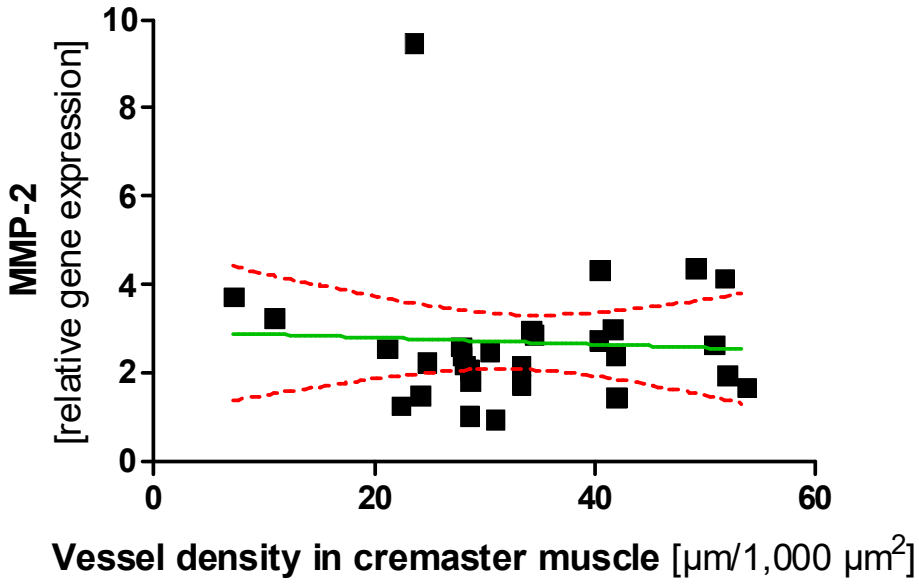


**Figure 41:** ***Linear correlation analysis of MMP-2 gene expression in the myocardium and microvascular density in the cremaster muscle.*** No correlation between MMP-2 expression in the myocardium and microvascular density in the cremaster muscle was detected (p = 0.77, r = -0.06, n = 29). Designations of the diagram as described in figure 4.

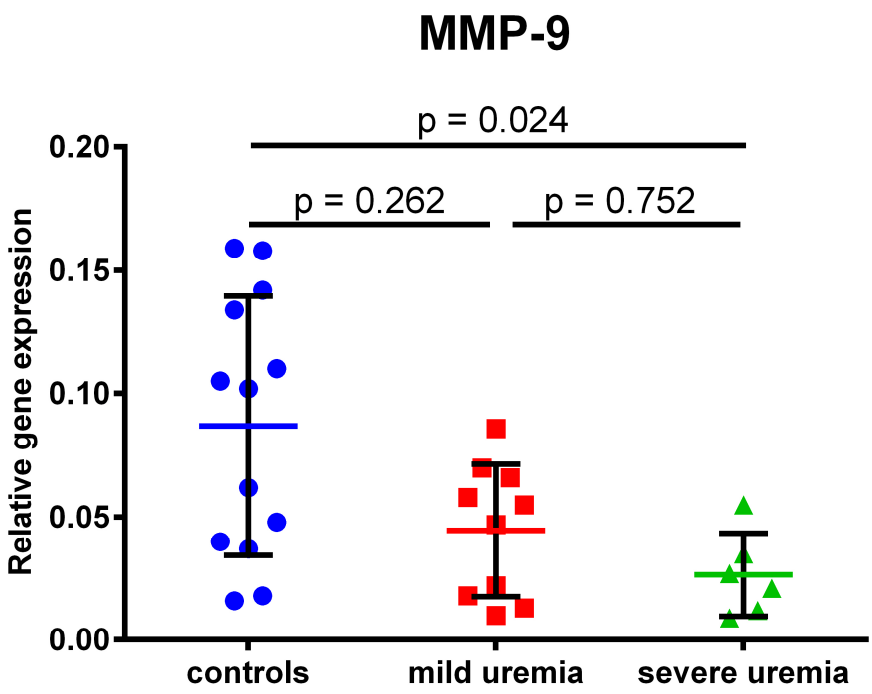


**Figure 42:** ***MMP-9 relative gene expression in the myocardium as a function of severity of serum urea.*** MMP-9, a matrix metalloprotease closely related to but differentially regulated from MMP-2, showed a significant difference in myocardial expression levels (p = 0.024) between severely uremic animals (n = 6) and controls (n = 13).

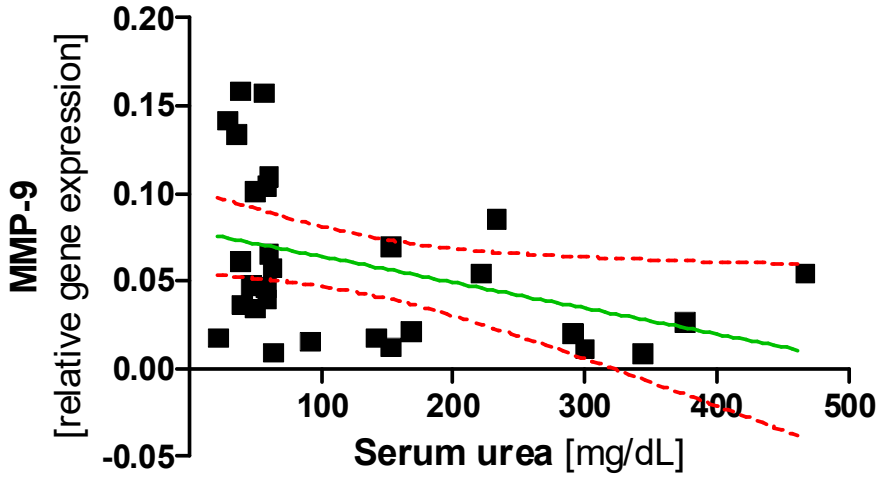


**Figure 43:** ***Linear correlation analysis of MMP-9 gene expression in the myocardium and serum urea levels.*** MMP-9 matrix metalloprotease gene expression was significantly associated with serum urea levels (p = 0.038, r = -0.39, n = 29). Designations of the diagram as described in figure 4.

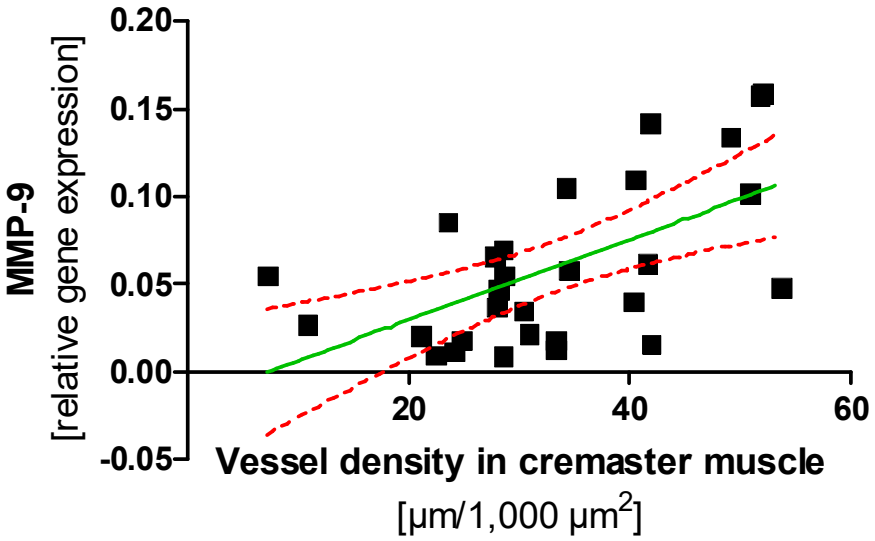


**Figure 44:** ***Linear correlation analysis of MMP-9 gene expression in the myocardium and microvascular density in the cremaster muscle.*** MMP-9 expression was significantly increased with increasing microvascular density of the cremaster muscle ($p = 0.0008$, $r = 0.59$, $n = 29$). Designations of the diagram as described in figure 4.

### 3.7.8 Summary of Myocardial Gene Expression Results in Uremia

In summary, experimental uremia in mice was associated with an expression decline in many of the investigated genes regulating angiogenesis, while others remained not significantly affected. Below (table 3), a comparison of the results provides an overview of the detailed analyses of the previous sections. As certain genes or gene products are linked in signaling pathways or effector cascades, the decline of their expression level may already lead to the disruption of these networks.

**Table 3:** ***Summary of the gene expression levels in cardiac muscle of uremic and control mice.*** Nine genes with a proven involvement in vessel angiogenesis, maintenance and disruption were tested in uremic animals vs. controls. Column 1 gives the gene name. Column 2 shows the significant expression change tendencies which were experimentally observed in uremic animals compared to controls. Column 3 shows an expected tendency in expression change of these genes in a functioning network if hypoxia is assumed (see 1.2.1), while column 4 depicts whether the actual findings are concordant or discordant with these expectations from such a simplistic model. Column 5 shows an assumed correlation of genes or gene products, either as effector genes (green: HIF 1α and its assumed effector genes, Dengler *et al.*, 2014), or as members of the same signaling pathway (taken from the KEGG pathway database, http://www.genome.jp/kegg/pathway.html; yellow: VEGF signaling pathway; pink: Ang/Tie-2 signaling; purple: Tie-2/Tie-1 regulation, Savant *et al.*, 2015; because of their multiple functions, MMPs were not allocated to distinct pathways). Column 6 indicates whether the actual experimentally detected decline in the expression of individual genes is associated with the disruption of an entire signaling pathway or the reduction of the expression of effector genes. N.s.: not significant; ↓ downregulated gene expression, ↑ upregulated gene expression.

| 1 | 2 | | 3 | 4 | 5 | | | | 6 |
|---|---|---|---|---|---|---|---|---|---|
| Gene | Expression Change in Uremia | | Expected Change in Hypoxia | Concordance of Expectation and Observation | Effector Genes or Common Pathway | | | | Probable Disruption of Pathway |
| HIF 1α | ↓ | p=0.008 | ↑ | no | | | | | yes |
| VEGF | n.s. | p=0.334 | ↑ | no | | | | | — |
| VEGFR-2 | ↓ | p=0.009 | ↑ | no | | | | | yes |
| Ang-1 | n.s. | p=0.993 | ↑ | no | | | | | — |
| Ang-2 | ↓ | p=0.048 | ↓ | yes | | | | | — |
| Tie-2 | ↓ | p=0.024 | ↑ | no | | | | | yes |
| Tie-1 | ↓ | p=0.036 | ? | ? | | | | | yes |
| MMP-2 | n.s. | p>0.999 | ? | ? | | | | | — |
| MMP-9 | ↓ | p=0.024 | ? | ? | | | | | — |

# 4 Discussion

## 4.1 Uremia Models

Both methods employed, 5/6 NX and adenine feeding, reliably led to uremia in BALB/c mice. Selection of the appropriate mouse strain is crucial, as not every strain is sensitive to such treatments. It has been reported that C57BL6 mice do not develop CKD upon 5/6 NX (Leelahavanichkul *et al.*, 2010). There was a significant difference in the severity of uremia which was achievable in BALB/c mice with the two methods. While 5/6 NX led to moderate uremia only, adenine feeding partly led to very severe uremic conditions. There was also a striking difference in the pace of uremia development between the two experimental models. 5/6 NX mice developed uremia slowly over a period of 4 months (Fogo, 2003; Ferrari *et al.*, 2014), while adenine-fed mice were severely uremic after a 4 week feeding period. Both approaches showed a considerable heterogeneity within the respective groups in terms of uremia, although the experimental regime was kept uniform during the study period, suggesting that individual differences in the background, behavior or—depending on the methodology—either food intake or surgery, may play a role in uremia development. Particularly in the 5/6 NX microsurgery, subtle differences in the amount and/or region of tissue removal may account for differences in the experimental outcome, as the remaining kidney tissue tends to develop compensatory hypertrophy.

Development of CKD in mice was monitored by determining the serum urea level. The increase in serum creatinine levels, which is regularly used as a marker in CKD patients, is less pronounced in mice and may be delayed, particularly in the adenine model (Tamura *et al.*, 2009; Oyama *et al.*, 2010). Although differences could be detected in creatinine levels between uremic groups and controls, none of these were significant, probably due to the considerable variation in the measured values. Experimental models affect body weight quite differently (Mori-Kawabe *et al.*, 2015); as expected, adenine-fed mice lost considerable amounts of body weight, while 5/6 NX mice in general showed a slight body weight gain over time.

In conclusion, the above data suggest that 5/6 NX is a good model for a slow uremia development, which is seen in many patients who may remain asymptomatic for a long time. In contrast, the adenine model is much more aggressive, as it leads to progressive deterioration of renal function in a short time. There was, however, a strong negative correlation between serum urea levels and microvessel density in the cremaster muscle, irrespective of the uremia-inducing method (Prommer, 2018), suggesting that both experimental approaches resulted in a similar dose-dependent effect on microvessel rarefaction. To rule out the possibility that the observed functional changes were due to emaciation rather than to uremia, a multivariate regression analysis was performed in a related study

(Prommer, 2018), clearly attributing the results of the cohort to the severity of uremia as indicated by serum urea levels.

Inherent to the intravital microscopy technology on cremaster muscle used to study the structural and functional alterations of the microvasculature in uremia is the restriction to male experimental animals. This inevitable preference of one sex may be one limitation of the significance of this study. These basic research findings will have to be tested for their clinical relevance in further gender-balanced studies (Clayton & Collins, 2014). Indeed, there is a slight preponderance of kidney failure as well as in kidney transplant indication in men (Saran *et al.*, 2016). No reports exist up to now, however, which would suggest a significant sex difference in the cardiac morbidity or mortality from CKD in juvenile patients.

## 4.2 Microvascular Rarefaction in Skeletal and Cardiac Muscles

The microvessel density in the skeletal muscle of severely uremic mice was reduced by approximately 50 % (Prommer, 2018). The degree of rarefaction was strongly correlated with serum urea levels. Correspondingly, microvessel density in the cardiac muscle of identical animals was reduced on the same scale, suggesting a systemic effect of uremia (figure 13). In another study, data from *ex vivo* biopsies from the omentum of children with stage 5 CKD showed a reduction of microvessel density from 36 to 51 % (Burkhardt *et al.*, 2016) which is within the same range as the findings of this work. Vascular rarefaction in cardiac muscle was also detected in a *post mortem* study performed on samples from hemodialysis patients (Amann *et al.*, 1998). The fact that microvascular rarefaction is seen in various organs, and even muscle types, suggests that the accumulation of harmful substances in the blood may have a detrimental effect on the entire organism (Vanholder *et al.*, 2008). Systemic microangiopathy, induced by chronic uremia, may occur early in the disease process and could be the sought-after link between CKD and damage to the cardiovascular system (Shroff *et al.*, 2008), crystallizing in the profound increase in cardiac mortality in this patient group.

The molecular mechanisms of microvascular rarefaction remain unclear. Apoptosis is an evident mechanism for the depletion of vessel density. Evidence for apoptosis, however, may be time-dependent and the process may well escape detection if vessels have already vanished at the time of investigation. Pruning of vessel branches may also involve endothelial cells re-assembling into other vessels (Franco *et al.*, 2015) or de-differentiation (Feinberg & Noden, 1991) in an endothelial to mesenchymal transition. This process in turn might contribute to the exacerbation of the existing disease (Zeisberg *et al.*, 2007), as the arising fibroblasts will further constrain the oxygen supply (Charytan *et al.*, 2014). Irrespective of the underlying mechanism, the initial damage to the

microvessels could be the starting point of a downward spiral for the entire organism. The microvasculature is a metabolic tissue in its own right, accumulating to more than 1 kg of human body weight (Clough, 2015). An initial restriction in blood flow could also have a detrimental effect on nutrient and oxygen supply of the vessels itself. This supposed effect would be more pronounced in small vessels because they have an adverse surface to volume ratio. The resulting rarefaction and subsequent oxygen deficiency would first become clinically apparent in the most vulnerable organ systems.

## 4.3 Alterations of Gene Expression in the Myocardium Correlate with Serum Urea Levels and Vessel Density in the Skeletal Muscle

Gene expression in the heart of uremic mice was significantly diminished for several angiogenic factors, while others remained unaffected. Transcription factors, pro- and anti-angiogenic cytokines and their respective receptors, however, make up such a delicate interdependent system that signaling might be impaired even if only individual components of a signaling cascade are downregulated on the mRNA level.

### 4.3.1 Adverse HIF 1α Response

Analysis of microvascular density showed a significant reduction in uremic groups (Prommer, 2018). This vascular rarefaction is associated with a reduced av$\Delta O_2$ and suggests that hypoxia is widespread in tissue with rarefacted microvasculature. Indeed, elevated HIF 1α levels have been reported in kidney tissue of patients with CKD (Nangaku, 2006; Rudnicki *et al.*, 2009). In contrast, in this work a significant decrease of HIF 1α mRNA levels in the myocardium of mice with vascular rarefaction in the cremaster skeletal muscle was shown, suggesting that a systemic effect impairs both cardiac and skeletal muscle. These findings are consistent with a study in rats with advanced renal failure, where reduced HIF 1α levels were detected in response to systemic hypoxia (Flisinski *et al.*, 2012). An activation of HIF 1α—as a fundamental molecular switch to cope with oxygen deficiency—would be expected to protect body tissue from hypoxia and thus from potential loss. There are various possibilities to explain that this is not necessarily the case: (1) The HIF 1α downregulation could be tissue-specific. At rest, the kidney has the highest oxygen consumption proportional to its weight and therefore receives the largest fraction of the cardiac output. Even under physiological conditions, the renal medulla provides a hypoxic environment due to the immense transporter activity and the resulting highly specific vascular formation (Heyman *et al.*, 1997), making HIF 1α upregulation in the kidney likely, while it could be downregulated in other organs. (2) Expression profiling is a snapshot of the current expression level in a certain disease state. The disease could either be not far advanced yet, so HIF 1α is not yet

activated, or could have reached an advanced stage so that the tissue is already exhausted and the general metabolism is impaired (Chade, 2011). (3) Hypoxia is a known stimulus for inflammation (Kong, 2004). Fibroblasts in hypoxia can switch to a fibrogenic phenotype, inducing TIMPs which results in an accumulation of ECM which further hinders blood flow and oxygen diffusion (Fine & Norman, 2008; Haase, 2009). It can be speculated that the depletion of HIF 1$\alpha$ (and possibly some of its target genes) provide a protective mechanism to avoid this vicious circle, even at the cost of hypoxia (Mayer, 2011). Indeed, chronic hypoxia can lead to HIF 1$\alpha$ suppression via several routes (Fu *et al.*, 2016). In this context, it is noteworthy that von Hippel-Lindau knockout mice, which are incapable of degrading HIF 1$\alpha$, show increased interstitial fibrosis (Kimura *et al.*, 2008). Moreover, long-term upregulation of HIF 1$\alpha$ has been associated with the progression of chronic renal injury (Zhu *et al.*, 2011).

In conclusion, in tissue showing severe vessel rarefaction and thus experiencing chronic hypoxia, a strong pro-angiogenic signaling would be expected. Data from this study suggest, however, that in uremic animals, the core response to hypoxia is heavily disturbed on a systemic level. Similar data were derived from a 5/6 NX rat model (Jacobi *et al.*, 2006). Thus, the failure of an adequate pro-angiogenic response to hypoxia may be a critical step towards a downward spiral in chronic kidney disease.

### 4.3.2 Disruption of VEGF Signaling

In this study, VEGF mRNA levels in the myocardium were not significantly affected by uremia/ rarefaction (figure 20). This is contradictory to the finding of some authors (Rudnicki *et al.*, 2009) that VEGF is upregulated in hypoxia. However, VEGF protein was significantly decreased in another study (Iliescu *et al.*, 2010), possibly reflecting post-transcriptional mechanisms or an increased depletion of the protein. It has, however, been shown by others (Kang *et al.*, 2001), that prolonged hypoxia may lead to a drop in VEGF expression. In a rat model of CKD, kidney proximal tubular cells showed an initial increase in VEGF expression followed by a depletion of both, VEGF and VEGFR expression levels with subsequent endothelial cell apoptosis and vessel regression (Ohashi *et al.*, 2002). Interestingly, in the present work, the VEGFR-2 was downregulated in rarefacted heart tissue (figure 23) which is consistent with studies in artery endothelial cell lines (Olszewska-Pazdra *et al.*, 2009). This data corroborates that chronic hypoxia can lead to a downregulation of VEGF signaling although VEGF expression remains stable. It has been shown previously, that VEGF signaling may also be disturbed at the posttranscriptional level in the rarefacted mesentery of hypertensive rats (Tran *et al.*, 2011). A recent study (Shi *et al.*, 2013) found that VEGF signaling may be controlled by a microRNA targeting $\beta$1 integrin which is required for VEGFR-2 phosphorylation (Chen *et al.*, 2010).

### 4.3.3 Disruption of Ang/Tie-2 Signaling

While Ang-1 levels remained insensitive to blood urea levels (figure 27) and microvascular rarefaction (figure 28), Ang-2 levels decreased markably already at mild serum urea levels (figure 29). Ang-1 is usually considered to be pro-angiogenic and Ang-2 is considered to be destabilizing and anti-angiogenic. The Ang-1/Ang-2 ratio is thought to determine a pro-angiogenic or anti-angiogenic environment (Eklund & Olsen, 2006). This study shows that the Ang-1/Ang-2 ratio increased from a numerical value of approximately 2 in controls to approximately 5 in uremic animals, creating a more pro-angiogenic environment (figure 32), suggesting an attempt of the cardiac tissue to counter a possible tissue hypoxia. This finding is consistent with results of a recent study (Burkhardt *et al.*, 2016) which showed in quantitative immuno-histochemical stainings of mesentery biopsies from children suffering from CKD that Ang-1 levels were not significantly altered compared to healthy controls, but Ang-2 levels were significantly decreased, likewise resulting in a profound increase in Ang-1/Ang-2 ratio. The expression of the Tie-2 receptor which binds both angiopoietins, however, decreases with increasing blood urea levels (figure 33). This effect was significant only if severely uremic mice were compared to controls, suggesting that higher urea levels are required to generate this effect. Transferring these findings to CKD patients would imply that Ang/Tie-2 signaling is disturbed only at the advanced disease stage. Therefore, Tie-2 downregulation may lead to an impaired Ang-1 signaling although Ang-1 levels remain relatively stable.

Tie-1, which is thought to be a co-regulator of Tie-2 function (Savant *et al.*, 2015), is also downregulated in rarefacted tissues (figure 38). Although no ligand has been confirmed for the Tie-1 receptor to date, the molecule seems to be involved in the regulation of vessel stability and remodeling. This notion is supported by the fact that Tie-1 mRNA levels in cardiac muscle were significantly lower in severely uremic animals as compared to controls (figure 36).

### 4.3.4 Regulation of Matrix Metalloproteases

Vascular network formation, remodeling, or regression requires alterations in the extracellular matrix (ECM). The ECM is controlled largely by a system of enzymes termed matrix metalloproteases (MMPs) degrading the ECM, and their negative regulators, the tissue inhibitors of matrix metalloproteases (TIMPs). The role of MMPs is ambiguous, as they may play an active role in angiogenesis as well as in vessel regression and can thus have both pro- and anti-angiogenic effects. MMP-2 and its paralog MMP-9 are capable to break down collagen IV of the basal membrane. Despite their similarity, MMP-2 and MMP-9 are thought to be differentially regulated (Galis *et al.*, 2002; Xie *et al.*, 2004), implying distinct biological functions. On the one hand, MMPs can promote angiogenesis by enabling pericytes to detach from vessels, by releasing cell adhesions of endothelial cells, by releasing pro-angiogenic growth factors from the ECM, or by exposing cryptic integrin binding sites in the ECM. On the other

hand, MMPs may also cause angiogenic arrest by producing anti-angiogenic effectors from degraded ECM or by converting plasminogen to angiostatin (Raffetto & Khalil, 2008). In addition, MMPs can modulate cell receptor signaling by cleaving off their ligand-binding domains (Tran *et al.*, 2011).

This work shows that MMP-9 but not MMP-2 decreased in heart tissue of uremic mice. A decrease for both of these enzymes was previously reported in a porcine model of renovascular disease (Chade *et al.*, 2003). In contrast, in spontaneously hypertensive rats with microvascular rarefaction, increased activity of some MMPs, including MMP-9, was found in the mesentery (Tran *et al.*, 2011). In line with data from this study, the authors found no expression change for MMP-2. They showed that along with increased MMP activity, the extracellular domain of the VEGF receptor VEGFR-2 was depleted, possibly indicating that circulating MMPs are responsible for this proteolytic activity. Inhibition of MMPs could also attenuate microvascular rarefaction, suggesting that MMP-mediated decrease of VEGF signaling triggers rarefaction. However, the authors concede, that increased MMP activity was found mainly along venules, while the depletion of the extracellular VEGFR-2 domain was detected along arterioles and capillaries. In addition, the employed MMP inhibitor, doxycycline, is known to have also strong anti-inflammatory effects, even at low doses which do not yet have antibiotic properties (Krakauer & Buckley, 2002). In 2008, this effect even led to the FDA and EMA approval of low dose doxycycline as an anti-inflammatory drug in some chronic inflammatory conditions. It can therefore not be ruled out that the attenuation of rarefaction observed is due to a reduced inflammatory response induced by the MMP inhibitor rather than to the reduced MMP activity itself. It should also be mentioned that MMPs are usually produced as zymogens in a quiescent form which need other MMPs or triggers for activation. Activators of MMPs include reactive oxygen species (ROS) and NO. Therefore, mRNA levels, protein levels, and enzymatic activity of MMPs may diverge considerably and should be analyzed separately in dedicated experimental settings.

### 4.3.5 Myocardial Gene Expression Changes Imply a Systemic Impact of Uremia

Several studies on the skeletal muscle suggest that uremia leads to rarefaction of the microvasculature and subsequent tissue hypoxia in the affected tissues (Flisinski *et al.*, 2014; Prommer, 2018). This study demonstrates that myocardial microvascular changes in uremic animals parallel microvascular rarefaction in the skeletal muscle. Cardiac vessel regression is strongly linked to serum urea levels, implying a systemic impact of uremia on the microvasculature (figure 13). A significant reduction of vessel density is observed already in mildly uremic animals, suggesting that already mild renal impairment may trigger this process.

In healthy tissue, hypoxia induces HIF 1$\alpha$ to produce an extensive cellular response involving many HIF 1$\alpha$ target genes. In chronic uremia, however, this response is reversed. It is not clear, whether the HIF 1$\alpha$ downregulation observed is the cause or the effect of this reversal. Pro-angiogenic signaling is

impaired, because expression of both transferring receptors, VEGFR-2 and Tie2, are decreased. The shift of the Ang-1/Ang-2 ratio towards a more pro-angiogenic environment can be construed as a futile attempt of counterregulation in hypoxic tissue. This regulatory attempt will, however, not be successfully transferred due to a downstream disruption of Tie-2 signaling. In conclusion, these data suggest a systemic effect, leading to an inadequate response to prolonged hypoxia and a profound dysregulation of vessel maintenance which may eventually result in microvascular rarefaction.

## 4.4 Microvascular Rarefaction Precedes Macrovascular Alterations

The data presented above showed a profound structural microvascular depletion in the skeletal (Prommer, 2018) as well as in the cardiac muscle, suggesting that CKD affects the microvasculature on a systemic level. This degradation leads to a functional impairment of the microvasculature, hampering oxygen and nutritional supply to the tissue. Despite these striking effects in the microvasculature, a comparative staining of aortal cross sections did not show any atherosclerotic changes in severely uremic animals (figure 15 A, B). In fact, no difference was detected between aortas from severely uremic animals and those from negative controls. Although it is known that mice hardly develop atherosclerosis, the positive controls, which were nephrectomized and treated with 2 % phosphate and 1 µg/kg calcitriol in a separate experiment, prove that such changes may develop under harsh treatments (figure 15 C). If atherosclerotic changes in the mouse model require very high serum urea and/or phosphate levels to occur, these will be indiscernible in the 5/6 NX model, as it only leads to moderate uremia. In the adenine model, the four-week time period allowed for severe uremia to develop may be too short a time to reveal such macrovascular changes. This result parallels findings in CKD patients. Children with CKD showed a marked microvascular rarefaction in the omentum (Burkhardt *et al.*, 2016). However, signs of atherosclerosis are absent in children with CKD, while elderly CKD patients with accumulated cardiac risk factors generally do show atherosclerosis (Shroff *et al.*, 2008). The presence of early microvascular changes in the myocardium suggests that these may play a crucial role in cardiac events in juvenile CKD patients. Capillary rarefaction in the myocardium will lead to a decreased capillary to myocyte ratio, a so-called capillary to myocyte mismatch (Amann *et al.*, 2000). The resulting deficit in oxygen and nutrient supply could trigger hypoxia and inflammation which ultimately results in fibrotic remodeling of the myocardium. Moreover, cardiac fibrosis may have several secondary deleterious effects such as myocardial stunning, i.e. the transient inability of a myocardial region to contract. Myocardial stunning is shown to be induced by long-term hemodialysis and is associated with increased cardiac mortality in pediatric CKD patients (Hothi *et al.*, 2009). These data suggest that the microangiopathy in CKD patients might be an early sign of an ongoing disease process.

## 4.5 Impairment of Oxygen Delivery in Uremia

### 4.5.1 Oxygen Uptake Impairment

Oxygen diffusion flow in a given environment can be approximated using

| ***Fick's law:*** | $J = -D\,A\,dc/dx$ |
|---|---|

where

*J* = *diffusion flow*
*D* = *diffusion coefficient*
*A* = *diffusion surface*
*dc* = *concentration difference*
*dx* = *diffusion distance.*

A significantly reduced capability of oxygen uptake was shown for both 5/6 NX and adenine uremia models. It may be hypothesized that tissue which is hypoxic due to a rarefacted microvasculature displays a raised concentration difference *dc* compared to normoxic tissue. Oxygen from arterial blood supplying such a hypoxic region would then be extracted more vigorously, contributing to an increased $av\Delta O_2$. The experimental finding in this study, however, was the opposite, as the $av\Delta O_2$ of vessels above 16 µm in rarefacted muscle tissue was significantly diminished compared to controls. There are several explanations for this finding: (1) Rarefaction of capillaries leads to a reduction of diffusion surface *A* and an increase of the diffusion distance *dx* and thus, to a reduced oxygen unload. Moreover, the so-called phase separation effect, leading to an uneven cell and plasma distribution between larger and smaller vessels in their respective branching points, adds to the heterogeneity of rarefacted networks (Pries & Secomb, 2003) and thus to a lower oxygen delivery in microvascular beds. (2) The necessity of blood distribution throughout the tissue requires many junctions between the feeding arteriole and the draining venule, close and remote, resulting in short and long flow pathways (Pries *et al.*, 2010). Wall shear stress is negatively correlated with the length of the respective pathway, i.e. shear stress is higher in short pathways. High shear stress induces vasodilatation, leading to a decreased flow resistance and subsequently to an increased blood flow in the short pathway. Flows in short low resistance pathways bypassing long pathways constitute functional shunts which further raise the diffusion distance *dx* and additionally reduce passage time required for reaching diffusion equilibrium (Pries *et al.*, 2010). (3) To prevent functional shunting, metabolic information from the microvasculature must be transferred to the attached neighboring venules and arterioles. While information transfer in venules can be accomplished with the blood flow, information transfer in arterioles requires an upstream transfer which involves connexins to form gap junctions (Buschmann *et al.*, 2010). A failure of this process could spark functional shunting and thus aggravate hypoxia. It is known that protracted hypoxia can lead to connexin dephosphorylation, resulting in a loss of function (Solan *et al.*, 2007). Also, the restoration of blood flow in damaged microvasculature by angiogenesis

may lead to increased functional shunts (Chade, 2011). It has been shown previously that spontaneously hypertensive rats develop arteriovenous shunts that gradually substitute normal microvascular networks (Murfee & Schmid-Schönbein, 2008). (4) In addition, uremia-associated endothelial damage may lead to leaky microvasculature. Leaking compounds may not only result in the deterioration of surrounding parenchyma but also to a further reduction in transport of nutrients and oxygen to its respective destination area.

### 4.5.2 Uremia Leads to Impaired Regulation of Vascular Tone

Myogenic tone is a property of resistance vessels, small arteries and arterioles that can adapt their caliber depending on neural signals, metabolic signals, or shear stress. Upon experimentally induced complete vessel relaxation, the relative arterial diameter increase in mildly uremic mice was slightly impaired compared to controls while it was very limited in severely uremic mice. According to Hagen-Poiseuille's Law, this deprives the affected tissue of its ability to effectively regulate perfusion, as changes in the vessel radius enter into the formula with their fourth power. Since this effect is much more pronounced in severely uremic animals it can be assumed that circulatory dysregulation is a symptom of an advanced disease process.

At least three different mechanisms may explain the reduced ability to increase vessel diameter: (1) It has been shown previously that in CKD the overall production of NO is reduced (Baylis, 2008). This would render the vessels incapable of fully dilating to their biological limit. A reduction in bioavailability of NO is believed to be a major contributor to altered vasoresponsiveness. The development and progression of vascular disease, including atherosclerosis, coronary heart disease and hypertension have been associated with both a reduced NO production and an increased generation of ROS in conjunction with compromised endogenous antioxidant defenses (Gao *et al.*, 2009). The experimental use of sodium nitroprusside which acts as an NO donor and thus delivers an excess of NO, however, makes this explanation unlikely. (2) Pathological processes in the intima or media of the vessel wall could reduce the vessels' compliance, limiting the maximum achievable vessel diameter. Indeed, it has been shown in CKD patients that calcification of the vessel intima and media leads to increased vessel stiffening and to a reduced compliance. Children with ESRD show an increased arterial stiffness which is comparable to elderly patients (Covic *et al.*, 2006). Acetylcholine and sodium nitroprusside-mediated vasodilatation in adults between 20 and 45 years of age suffering from advanced CKD is decreased and is comparable to both elderly healthy controls and elderly patients suffering from CKD. This suggests a premature aging of the vasculature in CKD patients (Thang *et al.*, 2012). (3) Finally, vessels in rarefacted uremic tissue could already be dilated in order to compensate for an impending hypoxia by increased blood flow so that no further dilation is possible. This adaptive response was already described in acute and chronic hypoxia (Marshall, 2015).

The impaired tone regulation limits the ability of perfusion regulation which ensures the appropriate blood supply of all body regions under physiological conditions. The decrease of vessel tone with increasing rarefaction supports both of the two latter explanations. However, as the goal of this study was to achieve the maximum vasodilatation, the experimental design to determine the vascular tone did not allow for discrimination of endothelium-dependent and endothelium-independent response.

In another study, tension of mouse aortas was studied *post mortem*. First, vessel contraction was induced by phenylephrine. Subsequently, acetylcholine or sodium nitroprusside was added to measure endothelium-dependent or endothelium-independent relaxation, respectively (Mori-Kawabe *et al.*, 2015). The authors found a decreased acetylcholine effect in adenine-fed mice, indicating an endothelial dysfunction, while no difference in endothelium-independent relaxation could be shown. Further experiments have to show which mechanism is the leading cause of the constraint observed.

## 4.6 The Role of Prolonged Inflammation

Both, uremia and hypoxia enhance the expression of a multitude of pro-inflammatory mediators (Fine & Norman, 2008; Rockey *et al.*, 2015). Chronic inflammation may have a deleterious effect on organ function by increased fibrosis, increased generation of ROS, or increased oxygen consumption which further promotes hypoxia. Systemic inflammatory processes have the potential to initiate a vicious circle in which the primary defect further affects the system leading to further deterioration: Renal failure causes retention of toxic compounds in the blood which lead to endothelial damage and continuous systemic inflammation. In addition, inflammation of the cardiac muscle may lead to cardiac failure which in turn causes hypoperfusion and ischemia of the kidneys resulting in a reduced GFR, which is again causative for uremia (Mutsaers *et al.*, 2015).

Therefore, the leukocyte rolling velocity in postcapillary venules was considered a suitable measure to determine the degree of local inflammation in rarefacted tissue. It has been reported previously that the adenine-induced uremia model showed increased signs of inflammation, such as macrophage infiltration or fibrosis (Tamura *et al.*, 2009). This may either reflect a direct effect of the adenine diet or may be a secondary effect of the much higher serum urea levels achieved by this method.

It has been shown that endothelial cells which display an increased expression of ICAM-1 attract leukocytes by binding to leukocyte β2 integrin and thus contribute to a decelerated leukocyte rolling, increased diapedesis and the accumulation of pro-inflammatory cells in uremic tissue (Miyazaki *et al.*, 1997). These results are in contrast to some other authors, who observed diminished activation of β2 integrin and increased leukocyte rolling velocity in mice with CKD ten days after subtotal nephrectomy (Rossaint *et al.* 2016).

In the present study, no correlation was identified between leukocyte rolling velocity and uremia (figure 5), rarefaction (figure 6), or IL-6 levels (figure 7). The significantly elevated IL-6 levels (figure 4), in particular, would have suggested an inflammatory response, measurable in a decreased leukocyte rolling velocity. It can be speculated that in small vessels, the influence of the already lower blood flow velocity and thus the already lower leukocyte rolling velocity, exceeds the effect of cytokine-mediated changes. The effects described by Rossaint *et al.* (2016) could also account for the leukocyte rolling velocity unaffected by inflammatory signals, as found in this study.

Another effect in chronic inflammatory processes is fibrotic remodeling. Adenine-induced CKD leads to a significant increase in pro-inflammatory cytokines such as IL-1β, IL-6 and TNF-α (Santana *et al.*, 2013). A previous study revealed that the most dramatic decrease in VEGF expression in uremic animals could be shown in areas of the most pronounced macrophage infiltration (Kang *et al.*, 2001). The authors showed that pro-inflammatory cytokines (IL-1β, IL-6) reduced VEGF expression in their model. Since VEGF is not only a pro-angiogenic signaling molecule but also a factor determining endothelial cell survival (Gerber *et al.*, 1998), an inflammation-induced drop in VEGF expression could explain the dramatic rarefaction in the microvasculature. The increase observed in IL-6 levels fits well with the concept that cytokines may hamper VEGF expression. While VEGF expression in the heart was not significantly influenced by uremia in this study (figure 20), a disruption of VEGF signaling due to an expression drop of VEGFR-2 (figure 23) could be shown.

In addition, increased TGF-β expression of inflammatory cells stimulates the production of ECM. Elevated TIMP1 levels inhibit MMPs and contribute to a further accumulation of ECM (Mutsaers *et al.*, 2015).

## 4.7 Synopsis: A Hypothetical Model for Exacerbation of Endothelial Dysfunction in CKD

In health, homeostasis of organ function and systemic conditions is usually maintained by a sensitive regulatory network. In recent years, there has been compelling evidence that CKD has a systemic impact on the microvasculature and organ function by interfering with this regulatory network.

Kidney injury leads to the accumulation of detrimental compounds in the blood stream, including but not restricted to urea. The endothelial cell layer is at the forefront of this detrimental influence and it seems likely that endothelial cells and their sensitive signaling pathways to maintain vessel integrity, blood flow, and supply are battered by this condition. This gradual poisoning may lead to vascular

dysregulation and rarefaction, which has its beginning in the microvasculature well before any changes are detectable in larger vessels or end organs.

As shown in this study, uremia leads to systemic microangiopathy which may be the starting point of a deteriorating disease process. Dysregulation and disruption of the terminal vessels may lead to persistent hypoxia which, in turn, may result in a prolonged inflammatory state, inhibiting an adequate response to insufficient oxygen supply on the expression level. This state could be considered a first step of decompensation: once an external confounding factor (as present in CKD, yet similar factors may exist in other conditions such as diabetes mellitus or hypertension) exceeds a certain threshold, this fine balance decompensates and complications of chronic illness may manifest with sudden onset.

In a generic diagram (figure 45) deduced from the current state of understanding (Chade, 2011; Mayer, 2011; Charytan *et al.*, 2014; Korn & Augustin, 2015; Fu *et al.*, 2016) and from results of this study, a number of vicious circles or feedback loops can be identified at first glance which may be established upon an initial endothelial damage. Some are described here in more detail. The rationales of these examples have already been described in the sections above.

(1) Hypoxia–most simply–may lead to vascular rarefaction which in turn can aggravate hypoxia.
(2) Reduced blood flow leads to hypoxia. Chronic hypoxia may lead to a prolonged inflammatory state which can trigger fibrosis. Increased extracellular matrix will hinder diffusion by increasing diffusion distances which in turn will increase hypoxia.
(3) Fibrosis may lead to a reduced vessel compliance and thus, to an impairment of vascular tone regulation. Tone dysregulation may result in decreased blood flow and thus increase hypoxia.
(4) Chronic hypoxia and prolonged inflammation may lead to a failure of HIF 1$\alpha$ transcription induction and thus, to dysregulated angiogenesis and to microvascular rarefaction. The abandoning of terminal vessels will then lead to functional shunting which will eventually further reduce blood flow in the microvasculature, thus increasing hypoxia.

Upon closer analysis, even more complex loops can be identified which an organism—weakened by chronic illness—cannot counterbalance indefinitely. Therefore, once a system is destabilized and has entered into the vicious circles as shown in figure 45, disease condition can build up and progressively amplify: The condition is prone inevitably to worsen over time. Many of these failures may have a direct impact on the cardiovascular system and hence may trigger cardiac events without prior warning signs. These mechanisms may contribute to our understanding why in severe CKD clinically otherwise unobtrusive patients, such as children and adolescents, may suddenly decompensate, and ultimately, die from the condition.

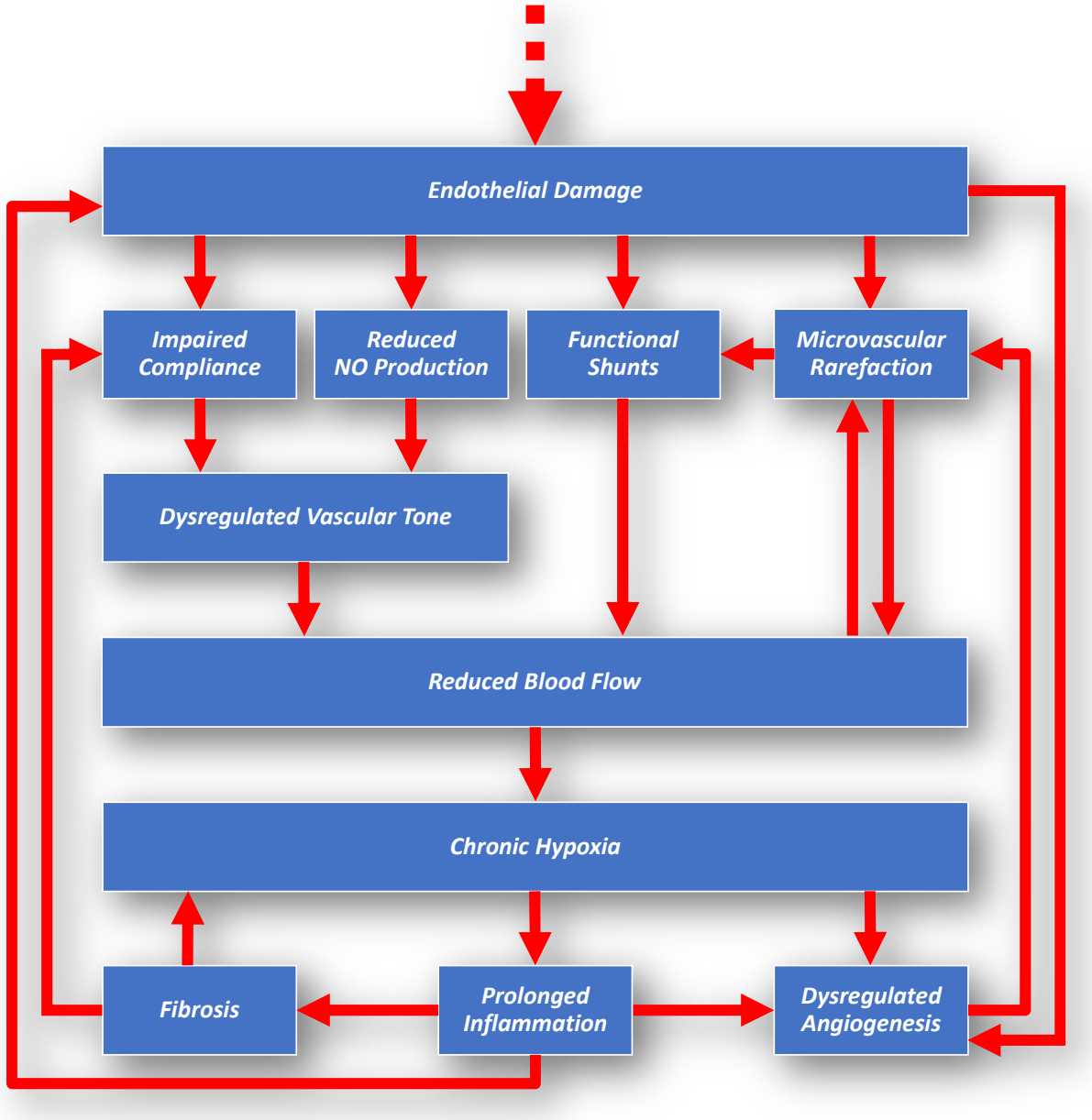


**Figure 45:** ***A vicious circle of exacerbation in CKD.*** Hypothetical model of a dysregulated network in CKD following an initial endothelial damage (top, dashed arrow), e.g. from accumulating uremic toxins. Red arrows symbolize deleterious effects of network components on other elements of the system. The endothelium provides the basis for regulation of vascular tone and delivers essential factors for vessel integrity such as angiopoietins. Disturbance of endothelial function may lead to a reduced blood flow via multiple routes, and thus to tissue hypoxia. Chronic hypoxia triggers inflammatory processes and leads to dysregulated angiogenesis. These effects result in further damage to the endothelium and vessel integrity, respectively, further aggravating the disease process—the start of a vicious circle. Although it is evidently not possible to differentiate clearly between cause and effect in such a complex network, a deeper understanding of this regulatory circuit can provide valuable insight into possible counter-actions to stop or slow down the relentless downward spiral in CKD.

# 5 List of Abbreviations

5/6 NX ..... subtotal nephrectomy removing about 5/6 of renal tissue
AGE ..... advanced glycation end products
AKI ..... acute kidney injury
Ang ..... angiopoietin
$avΔO_2$ ..... arterial-venous difference of oxygen saturation
BALB/c ..... Bagg albino inbred mouse strain c
CAKUT ..... congenital anomalies of the kidney and urinary tract
cAMP ..... 3',5'-cyclic adenosine monophosphate
CCD ..... charge coupled device
CD ..... cluster of differentiation
cDNA ..... copy deoxyribonucleic acid
CKD ..... chronic kidney disease
CVD ..... cardiovascular disease
CT ..... computer tomography
DNA ..... deoxyribonucleic acid
ECM ..... extracellular matrix
EMA ..... European Medicines Agency
eNOS ..... endothelial NO synthetase
ELISA ..... enzyme-linked immunosorbent assay
ESRD ..... end stage renal disease
FDA ..... Food and Drug Administration
FGF ..... fibroblast growth factor
GFR ..... glomerular filtration rate
HIF ..... hypoxia-inducible factor
ICAM ..... intercellular adhesion molecule
ICD ..... International Statistical Classification of Diseases and Related Health Problems
IL ..... interleukin
IMT ..... intima media thickness
i.p. ..... intraperitoneal injection
KDIGO ..... Kidney Disease: Improving Global Outcomes
MAP ..... mean arterial blood pressure
MMP ..... matrix metalloprotease
MRI ..... magnetic resonance imaging
mRNA ..... messenger ribonucleic acid

qPCR ..... quantitative polymerase chain reaction

RNA..... ribonucleic acid

ROS ..... reactive oxygen species

RT-PCR ..... reverse transcription polymerase chain reaction

SD..... standard deviation

SEM..... standard error of the mean

TGF..... transforming growth factor

Tie ..... tunica interna endothelial cell kinase = TEK receptor tyrosine kinase

TIMP .....tissue inhibitor of matrix metalloproteases

TNF.....tumor necrosis factor

VEGF .....vascular endothelial growth factor

VEGFR ..... vascular endothelial growth factor receptor

Wnt..... wingless-related integration site

# 6 References


Alon, T., I. Hemo, A. Itin, J. Pe'er, J. Stone, and E. Keshet. 1995. 'Vascular endothelial growth factor acts as a survival factor for newly formed retinal vessels and has implications for retinopathy of prematurity', *Nat Med*, 1: 1024-8.

Amann, K., M. Breitbach, E. Ritz, and G. Mall. 1998. 'Myocyte/capillary mismatch in the heart of uremic patients', *J Am Soc Nephrol*, 9: 1018-22.

Amann, K., M. Buzello, A. Simonaviciene, G. Miltenberger-Miltenyi, A. Koch, A. Nabokov, M. L. Gross, B. Gless, G. Mall, and E. Ritz. 2000. 'Capillary/myocyte mismatch in the heart in renal failure—a role for erythropoietin?', *Nephrol Dial Transplant*, 15: 964-9.

Amann, K., and E. Ritz. 2000. 'Microvascular disease--the Cinderella of uraemic heart disease', *Nephrol Dial Transplant*, 15: 1493-503.

Armulik, A., A. Abramsson, and C. Betsholtz. 2005. 'Endothelial/pericyte interactions', *Circ Res*, 97: 512-23.

Baylis, C. 2008. 'Nitric oxide deficiency in chronic kidney disease', *Am J Physiol Renal Physiol*, 294: F1-9.

Burkhardt, D., M. Bartosova, B. Schaefer, N. Grabe, B. Lahrmann, H. Nasser, C. Freise, A. Schneider, A. Lingnau, P. Degenhardt, B. Ranchin, P. Sallay, R. Cerkauskiene, M. Malina, G. Ariceta, C. P. Schmitt, and U. Querfeld. 2016. 'Reduced Microvascular Density in Omental Biopsies of Children with Chronic Kidney Disease', *PLoS One*, 11: e0166050.

Buschmann, I., A. Pries, B. Styp-Rekowska, P. Hillmeister, L. Loufrani, D. Henrion, Y. Shi, A. Duelsner, I. Hoefer, N. Gatzke, H. Wang, K. Lehmann, L. Ulm, Z. Ritter, P. Hauff, R. Hlushchuk, V. Djonov, T. van Veen, and F. le Noble. 2010. 'Pulsatile shear and Gja5 modulate arterial identity and remodeling events during flow-driven arteriogenesis', *Development*, 137: 2187-96.

Carmeliet, P., F. De Smet, S. Loges, and M. Mazzone. 2009. 'Branching morphogenesis and antiangiogenesis candidates: tip cells lead the way', *Nat Rev Clin Oncol*, 6: 315-26.

Carmeliet, P., and R. K. Jain. 2011. 'Principles and mechanisms of vessel normalization for cancer and other angiogenic diseases', *Nat Rev Drug Discov*, 10: 417-27.

Chade, A. R. 2011. 'Renovascular disease, microcirculation, and the progression of renal injury: role of angiogenesis', *Am J Physiol Regul Integr Comp Physiol*, 300: R783-90.

Chade, A. R., M. Rodriguez-Porcel, J. P. Grande, X. Zhu, V. Sica, C. Napoli, T. Sawamura, S. C. Textor, A. Lerman, and L. O. Lerman. 2003. 'Mechanisms of renal structural alterations in combined hypercholesterolemia and renal artery stenosis', *Arterioscler Thromb Vasc Biol*, 23: 1295-301.

Charytan, D. M., R. Padera, A. M. Helfand, M. Zeisberg, X. Xu, X. Liu, J. Himmelfarb, A. Cinelli, R. Kalluri, and E. M. Zeisberg. 2014. 'Increased concentration of circulating angiogenesis and nitric oxide inhibitors induces endothelial to mesenchymal transition and myocardial fibrosis in patients with chronic kidney disease', *Int J Cardiol*, 176: 99-109.

Chavers, B. M., C. A. Solid, A. Sinaiko, F. X. Daniels, S. C. Chen, A. J. Collins, D. L. Frankenfield, and C. A. Herzog. 2011. 'Diagnosis of cardiac disease in pediatric end-stage renal disease', *Nephrol Dial Transplant*, 26: 1640-5.

Chen, Q., L. Jiang, C. Li, D. Hu, J. W. Bu, D. Cai, and J. L. Du. 2012. 'Haemodynamics-driven developmental pruning of brain vasculature in zebrafish', *PLoS Biol*, 10: e1001374.

Chen, T. T., A. Luque, S. Lee, S. M. Anderson, T. Segura, and M. L. Iruela-Arispe. 2010. 'Anchorage of VEGF to the extracellular matrix conveys differential signaling responses to endothelial cells', *J Cell Biol*, 188: 595-609.

Clayton, J. A., and F. S. Collins. 2014. 'Policy: NIH to balance sex in cell and animal studies', *Nature*, 509: 282-3.

Clough, G. F. 2015. 'Developmental conditioning of the vasculature', *Compr Physiol*, 5: 397-438.

Coca, S. G., S. Singanamala, and C. R. Parikh. 2012. 'Chronic kidney disease after acute kidney injury: a systematic review and meta-analysis', *Kidney Int*, 81: 442-8.

Covic, A., N. Mardare, P. Gusbeth-Tatomir, O. Brumaru, C. Gavrilovici, M. Munteanu, O. Prisada, and D. J. Goldsmith. 2006. 'Increased arterial stiffness in children on haemodialysis', *Nephrol Dial Transplant*, 21: 729-35.

Dengler, V.L., M. Galbraith, J.M. Espinosa. 2014. 'Transcriptional regulation by hypoxia inducible factors', *Crit Rev Biochem Mol Biol.* 49 (1): 1-15.

de Vries, C., J. A. Escobedo, H. Ueno, K. Houck, N. Ferrara, and L. T. Williams. 1992. 'The fms-like tyrosine kinase, a receptor for vascular endothelial growth factor', *Science*, 255: 989-91.

Duling, B. R., and E. Staples. 1976. 'Microvascular effects of hypertonic solutions in the hamster', *Microvasc Res*, 11: 51-6.

Edwards-Richards, A., M. DeFreitas, C. P. Katsoufis, W. Seeherunvong, N. Sasaki, M. Freundlich, G. Zilleruelo, and C. L. Abitbol. 2014. 'Capillary rarefaction: an early marker of microvascular disease in young hemodialysis patients', *Clin Kidney J*, 7: 569-74.

Eggert, A., N. Ikegaki, J. Kwiatkowski, H. Zhao, G. M. Brodeur, and B. P. Himelstein. 2000. 'High-level expression of angiogenic factors is associated with advanced tumor stage in human neuroblastomas', *Clin Cancer Res*, 6: 1900-8.

Eklund, L., and B. R. Olsen. 2006. 'Tie receptors and their angiopoietin ligands are context-dependent regulators of vascular remodeling', *Exp Cell Res*, 312: 630-41.

Feinberg, R. N., and D. M. Noden. 1991. 'Experimental analysis of blood vessel development in the avian wing bud', *Anat Rec*, 231: 136-44.

Ferrara, N., and W. J. Henzel. 1989. 'Pituitary follicular cells secrete a novel heparin-binding growth factor specific for vascular endothelial cells', *Biochem Biophys Res Commun*, 161: 851-8.

Ferrari, G. O., J. C. Ferreira, R. T. Cavallari, K. R. Neves, L. M. dos Reis, W. V. Dominguez, E. C. Oliveira, F. G. Graciolli, J. Passlick-Deetjen, V. Jorgetti, and R. M. Moyses. 2014. 'Mineral bone disorder in chronic kidney disease: head-to-head comparison of the 5/6 nephrectomy and adenine models', *BMC Nephrol*, 15: 69.

Fine, L. G., and J. T. Norman. 2008. 'Chronic hypoxia as a mechanism of progression of chronic kidney diseases: from hypothesis to novel therapeutics', *Kidney Int*, 74: 867-72.

Flisinski, M., A. Brymora, I. Bartlomiejczyk, E. Wisniewska, R. Golda, A. Stefanska, L. Paczek, and J. Manitius. 2012. 'Decreased hypoxia-inducible factor-1alpha in gastrocnemius muscle in rats with chronic kidney disease', *Kidney Blood Press Res*, 35: 608-18.

Flisinski, M., A. Brymora, G. Elminowska-Wenda, J. Bogucka, K. Walasik, A. Stefanska, P. Strozecki, and J. Manitius. 2014. 'Morphometric analysis of muscle fibre types in rat locomotor and postural skeletal muscles in different stages of chronic kidney disease', *J Physiol Pharmacol*, 65: 567-76.

Flisinski, M., Brymora, A., Elminowska-Wenda, G., Bogucka, J., Walasik, K., Stefańska, A., Odrowaz-Sypniewska, G., and Manitius J. 2008.'Influence of different stages of experimental chronic kidney disease on rats locomotor and postural skeletal muscles microcirculation', *Ren Fail. 30: 443-51.*

Fogo, A. B. 2003. 'Animal models of FSGS: lessons for pathogenesis and treatment', *Semin Nephrol*, 23: 161-71.

Foley, R. N., P. S. Parfrey, and M. J. Sarnak. 1998. 'Clinical epidemiology of cardiovascular disease in chronic renal disease', *Am J Kidney Dis*, 32: S112-9.

Folkman, J. 2006. 'Angiogenesis', *Annu Rev Med*, 57: 1-18.

Foster, B. J., M. Dahhou, X. Zhang, R. W. Platt, and J. A. Hanley. 2011. 'Change in mortality risk over time in young kidney transplant recipients', *Am J Transplant*, 11: 2432-42.

Franco, C. A., M. L. Jones, M. O. Bernabeu, I. Geudens, T. Mathivet, A. Rosa, F. M. Lopes, A. P. Lima, A. Ragab, R. T. Collins, L. K. Phng, P. V. Coveney, and H. Gerhardt. 2015a. 'Correction: dynamic endothelial cell rearrangements drive developmental vessel regression', *PLoS Biol*, 13: e1002163.

Franco, C. A., M. L. Jones, M. O. Bernabeu, I. Geudens, T. Mathivet, A. Rosa, F. M. Lopes, A. P. Lima, A. Ragab, R. T. Collins, L. K. Phng, P. V. Coveney, and H. Gerhardt. 2015b. 'Dynamic endothelial cell rearrangements drive developmental vessel regression', *PLoS Biol*, 13: e1002125.

Fu, Q., S. P. Colgan, and C. S. Shelley. 2016. 'Hypoxia: The Force that Drives Chronic Kidney Disease', *Clin Med Res*, 14: 15-39.

Gabizon, D., E. Goren, U. Shaked, Z. Averbukh, E. Rosenmann, and D. Modai. 1985. 'Induction of chronic renal failure in the mouse: a new model', *Nephron*, 40: 349-52.

Galis, Z. S., C. Johnson, D. Godin, R. Magid, J. M. Shipley, R. M. Senior, and E. Ivan. 2002. 'Targeted disruption of the matrix metalloproteinase-9 gene impairs smooth muscle cell migration and geometrical arterial remodeling', *Circ Res*, 91: 852-9.

Gao, L., and G. E. Mann. 2009. 'Vascular NAD(P)H oxidase activation in diabetes: a double-edged sword in redox signalling', *Cardiovasc Res*, 82: 9-20.

Gerber, H. P., A. McMurtrey, J. Kowalski, M. Yan, B. A. Keyt, V. Dixit, and N. Ferrara. 1998. 'Vascular endothelial growth factor regulates endothelial cell survival through the phosphatidylinositol 3'-kinase/Akt signal transduction pathway. Requirement for Flk-1/KDR activation', *J Biol Chem*, 273: 30336-43.

Haase, V. H. 2009. 'Oxygen regulates epithelial-to-mesenchymal transition: insights into molecular mechanisms and relevance to disease', *Kidney Int*, 76: 492-9.

He, C., H. Hu, R. Braren, S. Y. Fong, A. Trumpp, T. R. Carlson, and R. A. Wang. 2008. 'c-myc in the hematopoietic lineage is crucial for its angiogenic function in the mouse embryo', *Development*, 135: 2467-77.

Heyman, S. N., S. Rosen, and M. Brezis. 1997. 'The renal medulla: life at the edge of anoxia', *Blood Purif*, 15: 232-42.

Hill, M. A., B. E. Simpson, and G. A. Meininger. 1990. 'Altered cremaster muscle hemodynamics due to disruption of the deferential feed vessels', *Microvasc Res*, 39: 349-63.

Holash, J., P. C. Maisonpierre, D. Compton, P. Boland, C. R. Alexander, D. Zagzag, G. D. Yancopoulos, and S. J. Wiegand. 1999. 'Vessel cooption, regression, and growth in tumors mediated by angiopoietins and VEGF', *Science*, 284: 1994-8.

Hothi, D. K., L. Rees, J. Marek, J. Burton, and C. W. McIntyre. 2009. 'Pediatric myocardial stunning underscores the cardiac toxicity of conventional hemodialysis treatments', *Clin J Am Soc Nephrol*, 4: 790-7.

Iliescu, R., S. R. Fernandez, S. Kelsen, C. Maric, and A. R. Chade. 2010. 'Role of renal microcirculation in experimental renovascular disease', *Nephrol Dial Transplant*, 25: 1079-87.

Jacobi, J., M. Porst, N. Cordasic, B. Namer, R. E. Schmieder, K. U. Eckardt, and K. F. Hilgers. 2006. 'Subtotal nephrectomy impairs ischemia-induced angiogenesis and hindlimb re-perfusion in rats', *Kidney Int*, 69: 2013-21.

Johnstone, L. M., C. L. Jones, L. E. Grigg, J. L. Wilkinson, R. G. Walker, and H. R. Powell. 1996. 'Left ventricular abnormalities in children, adolescents and young adults with renal disease', *Kidney Int*, 50: 998-1006.

Kang, D. H., A. H. Joly, S. W. Oh, C. Hugo, D. Kerjaschki, K. L. Gordon, M. Mazzali, J. A. Jefferson, J. Hughes, K. M. Madsen, G. F. Schreiner, and R. J. Johnson. 2001. 'Impaired angiogenesis in the remnant kidney model: I. Potential role of vascular endothelial growth factor and thrombospondin-1', *J Am Soc Nephrol*, 12: 1434-47.

Kavey, R. E., V. Allada, S. R. Daniels, L. L. Hayman, B. W. McCrindle, J. W. Newburger, R. S. Parekh, J. Steinberger, Population American Heart Association Expert Panel on, Science Prevention, Young American Heart Association Council on Cardiovascular Disease in the, Epidemiology American Heart Association Council on, Prevention, Physical Activity American Heart Association Council on Nutrition, Metabolism, Research American Heart Association Council on High Blood Pressure, Nursing American Heart Association Council on Cardiovascular, Disease American Heart Association Council on the Kidney in Heart, Care Interdisciplinary Working Group on Quality of, and Research Outcomes. 2006. 'Cardiovascular risk reduction in high-risk pediatric patients: a scientific statement from the American Heart Association Expert Panel on Population and Prevention Science; the Councils on Cardiovascular Disease in the Young, Epidemiology and Prevention, Nutrition, Physical Activity and Metabolism, High Blood Pressure Research, Cardiovascular Nursing, and the Kidney in Heart Disease; and the Interdisciplinary Working Group on Quality of Care and Outcomes Research: endorsed by the American Academy of Pediatrics', *Circulation*, 114: 2710-38.

Kaysen, G. A. 2001. 'The microinflammatory state in uremia: causes and potential consequences', *J Am Soc Nephrol*, 12: 1549-57.

Kida, Y., B. N. Tchao, and I. Yamaguchi. 2014. 'Peritubular capillary rarefaction: a new therapeutic target in chronic kidney disease', *Pediatr Nephrol*, 29: 333-42.

Kim, I., J. H. Kim, S. O. Moon, H. J. Kwak, N. G. Kim, and G. Y. Koh. 2000. 'Angiopoietin-2 at high concentration can enhance endothelial cell survival through the phosphatidylinositol 3'-kinase/Akt signal transduction pathway', *Oncogene*, 19: 4549-52.

Kimura, K., M. Iwano, D. F. Higgins, Y. Yamaguchi, K. Nakatani, K. Harada, A. Kubo, Y. Akai, E. B. Rankin, E. G. Neilson, V. H. Haase, and Y. Saito. 2008. 'Stable expression of HIF-1alpha in tubular epithelial cells promotes interstitial fibrosis', *Am J Physiol Renal Physiol*, 295: F1023-9.

Klotz, K. F., P. Gaehtgens, and A. R. Pries. 1995. 'Does luminal release of EDRF contribute to downstream microvascular tone?', *Pflugers Arch*, 430: 978-83.

Koch, S., and L. Claesson-Welsh. 2012. 'Signal transduction by vascular endothelial growth factor receptors', *Cold Spring Harb Perspect Med*, 2: a006502.

Kochhan, E., A. Lenard, E. Ellertsdottir, L. Herwig, M. Affolter, H. G. Belting, and A. F. Siekmann. 2013. 'Blood flow changes coincide with cellular rearrangements during blood vessel pruning in zebrafish embryos', *PLoS One*, 8: e75060.

Kong, T., H. K. Eltzschig, J. Karhausen, S. P. Colgan, and C. S. Shelley. 2004. 'Leukocyte adhesion during hypoxia is mediated by HIF-1-dependent induction of beta2 integrin gene expression', *Proc Natl Acad Sci U S A*, 101: 10440-5.

Korn, C., and H. G. Augustin. 2015. 'Mechanisms of Vessel Pruning and Regression', *Dev Cell*, 34: 5-17.

Korn, C., B. Scholz, J. Hu, K. Srivastava, J. Wojtarowicz, T. Arnsperger, R. H. Adams, M. Boutros, H. G. Augustin, and I. Augustin. 2014. 'Endothelial cell-derived non-canonical Wnt ligands control vascular pruning in angiogenesis', *Development*, 141: 1757-66.

Krakauer, T., and M. Buckley. 2003. 'Doxycycline is anti-inflammatory and inhibits staphylococcal exotoxin-induced cytokines and chemokines', *Antimicrob Agents Chemother*, 47: 3630-3.

Leelahavanichkul, A., Q. Yan, X. Hu, C. Eisner, Y. Huang, R. Chen, D. Mizel, H. Zhou, E. C. Wright, J. B. Kopp, J. Schnermann, P. S. Yuen, and R. A. Star. 2010. 'Angiotensin II overcomes strain-dependent resistance of rapid CKD progression in a new remnant kidney mouse model', *Kidney Int*, 78: 1136-53.

Ley, K., A. R. Pries, and P. Gaehtgens. 1987. 'A versatile intravital microscope design', *Int J Microcirc Clin Exp*, 6: 161-7.

Livak, K. J., and T. D. Schmittgen. 2001. 'Analysis of relative gene expression data using real-time quantitative PCR and the 2(-Delta Delta C(T)) Method', *Methods*, 25: 402-8.

Lobov, I. B., P. C. Brooks, and R. A. Lang. 2002. 'Angiopoietin-2 displays VEGF-dependent modulation of capillary structure and endothelial cell survival in vivo', *Proc Natl Acad Sci U S A*, 99: 11205-10.

Lobov, I. B., E. Cheung, R. Wudali, J. Cao, G. Halasz, Y. Wei, A. Economides, H. C. Lin, N. Papadopoulos, G. D. Yancopoulos, and S. J. Wiegand. 2011. 'The Dll4/Notch pathway controls postangiogenic blood vessel remodeling and regression by modulating vasoconstriction and blood flow', *Blood*, 117: 6728-37.

Lockhart, C. J., P. K. Hamilton, C. E. Quinn, and G. E. McVeigh. 2009. 'End-organ dysfunction and cardiovascular outcomes: the role of the microcirculation', *Clin Sci (Lond)*, 116: 175-90.

Maisonpierre, P. C., C. Suri, P. F. Jones, S. Bartunkova, S. J. Wiegand, C. Radziejewski, D. Compton, J. McClain, T. H. Aldrich, N. Papadopoulos, T. J. Daly, S. Davis, T. N. Sato, and G. D. Yancopoulos. 1997. 'Angiopoietin-2, a natural antagonist for Tie2 that disrupts in vivo angiogenesis', *Science*, 277: 55-60.

Marshall, J. M. 2015. 'Interactions between local dilator and sympathetic vasoconstrictor influences in skeletal muscle in acute and chronic hypoxia', *Exp Physiol*, 100: 1400-11.

Mathews, T. J., A. M. Minino, M. J. Osterman, D. M. Strobino, and B. Guyer. 2011. 'Annual summary of vital statistics: 2008', *Pediatrics*, 127: 146-57.

Mayer, G. 2011. 'Capillary rarefaction, hypoxia, VEGF and angiogenesis in chronic renal disease', *Nephrol Dial Transplant*, 26: 1132-7.

Meeson, A. P., M. Argilla, K. Ko, L. Witte, and R. A. Lang. 1999. 'VEGF deprivation-induced apoptosis is a component of programmed capillary regression', *Development*, 126: 1407-15.

Meyer, T. W., and T. H. Hostetter. 2007. 'Uremia', *N Engl J Med*, 357: 1316-25.

Milliner, D. S., A. R. Zinsmeister, E. Lieberman, and B. Landing. 1990. 'Soft tissue calcification in pediatric patients with end-stage renal disease', *Kidney Int*, 38: 931-6.

Mimic-Oka, J., T. Simic, L. Djukanovic, Z. Reljic, and Z. Davicevic. 1999. 'Alteration in plasma antioxidant capacity in various degrees of chronic renal failure', *Clin Nephrol*, 51: 233-41.

Mitsnefes, M. M. 2012. 'Cardiovascular disease in children with chronic kidney disease', *J Am Soc Nephrol*, 23: 578-85.

Mitsnefes, M. M., T. R. Kimball, S. A. Witt, B. J. Glascock, P. R. Khoury, and S. R. Daniels. 2004. 'Abnormal carotid artery structure and function in children and adolescents with successful renal transplantation', *Circulation*, 110: 97-101.

Miyazaki, T., M. Ise, H. Seo, and T. Niwa. 1997. 'Indoxyl sulfate increases the gene expressions of TGF-beta 1, TIMP-1 and pro-alpha 1(I) collagen in uremic rat kidneys', *Kidney Int Suppl*, 62: S15-22.

Mizobuchi, M., D. Towler, and E. Slatopolsky. 2009. 'Vascular calcification: the killer of patients with chronic kidney disease', *J Am Soc Nephrol*, 20: 1453-64.

Mori-Kawabe, M., Y. Yasuda, M. Ito, and S. Matsuo. 2015. 'Reduction of NO-mediated Relaxing Effects in the Thoracic Aorta in an Experimental Chronic Kidney Disease Mouse Model', *J Atheroscler Thromb*, 22: 845-53.

Murfee, W. L., and G. W. Schmid-Schonbein. 2008. 'Chapter 12. Structure of microvascular networks in genetic hypertension', *Methods Enzymol*, 444: 271-84.

Mutsaers, H. A., E. G. Stribos, G. Glorieux, R. Vanholder, and P. Olinga. 2015. 'Chronic Kidney Disease and Fibrosis: The Role of Uremic Retention Solutes', *Front Med (Lausanne)*, 2: 60.

Nangaku, M. 2006. 'Chronic hypoxia and tubulointerstitial injury: a final common pathway to end-stage renal failure', *J Am Soc Nephrol*, 17: 17-25.

Oh, J., R. Wunsch, M. Turzer, M. Bahner, P. Raggi, U. Querfeld, O. Mehls, and F. Schaefer. 2002. 'Advanced coronary and carotid arteriopathy in young adults with childhood-onset chronic renal failure', *Circulation*, 106: 100-5.

Ohashi, R., A. Shimizu, Y. Masuda, H. Kitamura, M. Ishizaki, Y. Sugisaki, and N. Yamanaka. 2002. 'Peritubular capillary regression during the progression of experimental obstructive nephropathy', *J Am Soc Nephrol*, 13: 1795-805.

Olszewska-Pazdrak, B., T. W. Hein, P. Olszewska, and D. H. Carney. 2009. 'Chronic hypoxia attenuates VEGF signaling and angiogenic responses by downregulation of KDR in human endothelial cells', *Am J Physiol Cell Physiol*, 296: C1162-70.

Oyama, Y., T. Hashiguchi, N. Taniguchi, S. Tancharoen, T. Uchimura, K. K. Biswas, K. Kawahara, T. Nitanda, Y. Umekita, M. Lotz, and I. Maruyama. 2010. 'High-mobility group box-1 protein promotes granulomatous nephritis in adenine-induced nephropathy', *Lab Invest*, 90: 853-66.

Parekh, R. S., C. E. Carroll, R. A. Wolfe, and F. K. Port. 2002. 'Cardiovascular mortality in children and young adults with end-stage kidney disease', *J Pediatr*, 141: 191-7.

Phng, L. K., M. Potente, J. D. Leslie, J. Babbage, D. Nyqvist, I. Lobov, J. K. Ondr, S. Rao, R. A. Lang, G. Thurston, and H. Gerhardt. 2009. 'Nrarp coordinates endothelial Notch and Wnt signaling to control vessel density in angiogenesis', *Dev Cell*, 16: 70-82.

Pries, A. R. 1988. 'A versatile video image analysis system for microcirculatory research', *Int J Microcirc Clin Exp*, 7: 327-45.

Pries, A. R., J. Heide, K. Ley, K. F. Klotz, and P. Gaehtgens. 1995. 'Effect of oxygen tension on regulation of arteriolar diameter in skeletal muscle in situ', *Microvasc Res*, 49: 289-99.

Pries, A. R., M. Hopfner, F. le Noble, M. W. Dewhirst, and T. W. Secomb. 2010. 'The shunt problem: control of functional shunting in normal and tumour vasculature', *Nat Rev Cancer*, 10: 587-93.

Pries, A. R., and T. W. Secomb. 2003. 'Rheology of the microcirculation', *Clin Hemorheol Microcirc*, 29: 143-8.

Pries, A.R., and T.W. Secomb. 2008. 'Modeling structural adaptation of microcirculation', *Microcirculation 15: 753-64*

Pries, A. R., and T. W. Secomb. 2014. 'Making microvascular networks work: angiogenesis, remodeling, and pruning', *Physiology (Bethesda)*, 29: 446-55.

Prommer, H.U. 2018. Strukturelle Veränderungen der Mikrozirkulation bei experimenteller Urämie - Quantifizierung, Typisierung, Konsequenzen. Dissertation zur Erlangung des akademischen Grades eines Doctor medicinae (Dr. med.), Charité Universitätsmedizin Berlin

Prommer, H.U., Maurer J., von Websky K., Freise C., Sommer K., Nasser H., Samapati R., Reglin B., Guimarães P., Pries A. R. and Querfeld U. 2018. Chronic kidney disease induces a systemic microangiopathy, tissue hypoxia and dysfunctional angiogenesis. *Sci Rep.* 8(1):5317.

Raffetto, J. D., and R. A. Khalil. 2008. 'Matrix metalloproteinases and their inhibitors in vascular remodeling and vascular disease', *Biochem Pharmacol*, 75: 346-59.

Risau, W. 1997. 'Mechanisms of angiogenesis', *Nature*, 386: 671-4.

Rockey, D. C., P. D. Bell, and J. A. Hill. 2015. 'Fibrosis--a common pathway to organ injury and failure', *N Engl J Med*, 372: 1138-49.

Rossaint, J., J. Oehmichen, H. Van Aken, S. Reuter, H. J. Pavenstadt, M. Meersch, M. Unruh, and A. Zarbock. 2016. 'FGF23 signaling impairs neutrophil recruitment and host defense during CKD', *J Clin Invest*, 126: 962-74.

Rudnicki, M., P. Perco, J. Enrich, S. Eder, D. Heininger, A. Bernthaler, M. Wiesinger, R. Sarkozi, S. J. Noppert, H. Schramek, B. Mayer, R. Oberbauer, and G. Mayer. 2009. 'Hypoxia response and VEGF-A expression in human proximal tubular epithelial cells in stable and progressive renal disease', *Lab Invest*, 89: 337-46.

Santana, A. C., S. Degaspari, S. Catanozi, H. Delle, L. de Sa Lima, C. Silva, P. Blanco, K. Solez, C. Scavone, and I. L. Noronha. 2013. 'Thalidomide suppresses inflammation in adenine-induced CKD with uraemia in mice', *Nephrol Dial Transplant*, 28: 1140-9.

Saran, R., Y. Li, B. Robinson, K. C. Abbott, L. Y. Agodoa, J. Ayanian, J. Bragg-Gresham, R. Balkrishnan, J. L. Chen, E. Cope, P. W. Eggers, D. Gillen, D. Gipson, S. M. Hailpern, Y. N. Hall, K. He, W. Herman, M. Heung, R. A. Hirth, D. Hutton, S. J. Jacobsen, K. Kalantar-Zadeh, C. P. Kovesdy, Y. Lu, M. Z. Molnar, H. Morgenstern, B. Nallamothu, D. V. Nguyen, A. M. O'Hare, B. Plattner, R. Pisoni, F. K. Port, P. Rao, C. M. Rhee, A. Sakhuja, D. E. Schaubel, D. T. Selewski, V. Shahinian, J. J. Sim, P. Song, E. Streja, M. Kurella Tamura, F. Tentori, S. White, K. Woodside, and R. A. Hirth. 2016. 'US Renal Data System 2015 Annual Data Report: Epidemiology of Kidney Disease in the United States', *Am J Kidney Dis*, 67: Svii, S1-305.

Savant, S., S. La Porta, A. Budnik, K. Busch, J. Hu, N. Tisch, C. Korn, A. F. Valls, A. V. Benest, D. Terhardt, X. Qu, R. H. Adams, H. S. Baldwin, C. Ruiz de Almodovar, H. R. Rodewald, and H. G. Augustin. 2015. 'The Orphan Receptor Tie1 Controls Angiogenesis and Vascular Remodeling by Differentially Regulating Tie2 in Tip and Stalk Cells', *Cell Rep*, 12: 1761-73.

Secomb, T. W., M. A. Konerding, C. A. West, M. Su, A. J. Young, and S. J. Mentzer. 2003. 'Microangiectasias: structural regulators of lymphocyte transmigration', *Proc Natl Acad Sci U S A*, 100: 7231-4.

Senger, D. R., S. J. Galli, A. M. Dvorak, C. A. Perruzzi, V. S. Harvey, and H. F. Dvorak. 1983. 'Tumor cells secrete a vascular permeability factor that promotes accumulation of ascites fluid', *Science*, 219: 983-5.

Shi, L., B. Fisslthaler, N. Zippel, T. Fromel, J. Hu, A. Elgheznawy, H. Heide, R. Popp, and I. Fleming. 2013. 'MicroRNA-223 antagonizes angiogenesis by targeting beta1 integrin and preventing growth factor signaling in endothelial cells', *Circ Res*, 113: 1320-30.

Shobeiri, N., M. A. Adams, and R. M. Holden. 2010. 'Vascular calcification in animal models of CKD: A review', *Am J Nephrol*, 31: 471-81.

Shroff, R. C., R. McNair, N. Figg, J. N. Skepper, L. Schurgers, A. Gupta, M. Hiorns, A. E. Donald, J. Deanfield, L. Rees, and C. M. Shanahan. 2008. 'Dialysis accelerates medial vascular calcification in part by triggering smooth muscle cell apoptosis', *Circulation*, 118: 1748-57.

Shweiki, D., A. Itin, D. Soffer, and E. Keshet. 1992. 'Vascular endothelial growth factor induced by hypoxia may mediate hypoxia-initiated angiogenesis', *Nature*, 359: 843-5.

Silverstein, D.M. 2009. 'Inflammation in chronic kidney disease: role in the progression of renal and cardiovascular disease', *Pediatr Nephrol. 24: 1445-52*.

Solan, J. L., L. Marquez-Rosado, P. L. Sorgen, P. J. Thornton, P. R. Gafken, and P. D. Lampe. 2007. 'Phosphorylation at S365 is a gatekeeper event that changes the structure of Cx43 and prevents down-regulation by PKC', *J Cell Biol*, 179: 1301-9.

Sperandio, M., J. Pickard, S. Unnikrishnan, S. T. Acton and K. Ley. 2006. 'Analysis of leukocyte rolling in vivo and in vitro', *Methods Enzymol 416: 346-371.*

Stenvinkel, P., M. Ketteler, R. J. Johnson, B. Lindholm, R. Pecoits-Filho, M. Riella, O. Heimburger, T. Cederholm, and M. Girndt. 2005. 'IL-10, IL-6, and TNF-alpha: central factors in the altered cytokine network of uremia--the good, the bad, and the ugly', *Kidney Int*, 67: 1216-33.

Styp-Rekowska, B., N. M. Disassa, B. Reglin, L. Ulm, H. Kuppe, T. W. Secomb, and A. R. Pries. 2007. 'An imaging spectroscopy approach for measurement of oxygen saturation and hematocrit during intravital microscopy', *Microcirculation*, 14: 207-21.

Tamura, M., R. Aizawa, M. Hori, and H. Ozaki. 2009. 'Progressive renal dysfunction and macrophage infiltration in interstitial fibrosis in an adenine-induced tubulointerstitial nephritis mouse model', *Histochem Cell Biol*, 131: 483-90.

Terman, B. I., M. Dougher-Vermazen, M. E. Carrion, D. Dimitrov, D. C. Armellino, D. Gospodarowicz, and P. Bohlen. 1992. 'Identification of the KDR tyrosine kinase as a receptor for vascular endothelial cell growth factor', *Biochem Biophys Res Commun*, 187: 1579-86.

Thang, O. H., E. H. Serne, M. P. Grooteman, Y. M. Smulders, P. M. Ter Wee, G. J. Tangelder, and M. J. Nube. 2012. 'Premature aging of the microcirculation in patients with advanced chronic kidney disease', *Nephron Extra*, 2: 283-92.

Tran, E. D., M. Yang, A. Chen, F. A. Delano, W. L. Murfee, and G. W. Schmid-Schonbein. 2011. 'Matrix metalloproteinase activity causes VEGFR-2 cleavage and microvascular rarefaction in rat mesentery', *Microcirculation*, 18: 228-37.

Vanholder, R., S. Van Laecke, and G. Glorieux. 2008. 'What is new in uremic toxicity?', *Pediatr Nephrol*, 23: 1211-21.

Voskas, D., N. Jones, P. Van Slyke, C. Sturk, W. Chang, A. Haninec, Y. O. Babichev, J. Tran, Z. Master, S. Chen, N. Ward, M. Cruz, J. Jones, R. S. Kerbel, S. Jothy, L. Dagnino, J. Arbiser, G. Klement, and D. J. Dumont. 2005. 'A cyclosporine-sensitive psoriasis-like disease produced in Tie2 transgenic mice', *Am J Pathol*, 166: 843-55.

Wang, H., Y. Zhang, S. Toratani, and T. Okamoto. 2004. 'Transformation of vascular endothelial cells by a point mutation in the Tie2 gene from human intramuscular haemangioma', *Oncogene*, 23: 8700-4.

Xie, Z., M. Singh, and K. Singh. 2004. 'Differential regulation of matrix metalloproteinase-2 and -9 expression and activity in adult rat cardiac fibroblasts in response to interleukin-1beta', *J Biol Chem*, 279: 39513-9.

Yokozawa, T., P. D. Zheng, H. Oura, and F. Koizumi. 1986. 'Animal model of adenine-induced chronic renal failure in rats', *Nephron*, 44: 230-4.

Zeisberg, E. M., O. Tarnavski, M. Zeisberg, A. L. Dorfman, J. R. McMullen, E. Gustafsson, A. Chandraker, X. Yuan, W. T. Pu, A. B. Roberts, E. G. Neilson, M. H. Sayegh, S. Izumo, and R. Kalluri. 2007. 'Endothelial-to-mesenchymal transition contributes to cardiac fibrosis', *Nat Med*, 13: 952-61.

Zhu, Q., Z. Wang, M. Xia, P. L. Li, B. W. Van Tassell, A. Abbate, R. Dhaduk, and N. Li. 2011. 'Silencing of hypoxia-inducible factor-1alpha gene attenuated angiotensin II-induced renal injury in Sprague-Dawley rats', *Hypertension*, 58: 657-64.

Zijlstra, W. G., A. Buursma, and A. Zwart. 1983. 'Molar absorptivities of human hemoglobin in the visible spectral range', *J Appl Physiol Respir Environ Exerc Physiol*, 54: 1287-91.

# 7 Curriculum Vitae

My curriculum vitae is not shown in the electronic form of my thesis for reasons of data privacy.

Mein Lebenslauf wird aus datenschutzrechtlichen Gründen in der elektronischen Version meiner Arbeit nicht veröffentlicht.

# 8 Publication List

## 8.1 Peer Reviewed Publications

Prommer HU*, **Maurer J***, von Websky K, Freise C, Sommer K, Nasser H, Samapati R, Reglin B, Guimarães P, Pries AR, Querfeld U (**equal contribution authorship*): Chronic kidney disease induces a systemic microangiopathy, tissue hypoxia and dysfunctional angiogenesis. **Scientific Reports 8(1):5317, 2018**

Wiemann S, Pennacchio C,Hu Y, Hunter P, Harbers M, Busse M, Carninci P, Diekhans M, Dunham I, Hao T, Harper W, Hayashizaki Y, Heil O, Hotz-Wagenblatt A, Jang W, Kawai J, Koenig C, Korn B, Lambert C, LeBeau A, Lu S, **Maurer J**, Moore T, Ohara O, Park J, Seiler C, Steel J, Wagner J, Weaver T, Yang S, Vidal M, Gerhard D, LaBaer J, Temple G, Hill D: The ORFeome Collaboration: A community resource for expression of most human protein-coding genes. **Nature Methods 13, 191–192, 2016**

Schofield PN, Bubela T, Weaver T, Portilla L, Brown SD, Hancock JM, Einhorn D, Tocchini-Valentini G, Hrabe de Angelis M, Rosenthal N, Barnes J*, Collis AJ*, Desaintes C*, Dixon JE*, Doyle A*, Eppig J*, Field D*, Grünberger M*, Heim S*, Hicks G*, Hubbard T*, Jennings R*, Kennedy K*, Kennedy G*, Kolar P*, Livingstone A*, Lloyd K*, Masuya H*, Matteoni R*, **Maurer J***, McKenzie A*, McKerlie C*, Moore M*, Muddyman D*, Nguyen T*, Parsons M*, Quackenbush J*, Reuveni E*, Salimova E*, Siegal V*, Skingle M*, Smedley D*, Sugden A*, Wakana S*, Walsh JP* (***extended author list*): Post-publication sharing of data and tools. **Nature 461(7261):171-3, 2009**

Weaver T, **Maurer J**, Hayashizaki Y: Sharing genomes: an integrated approach to funding, managing and distributing genomic clone resources. **Nature Reviews Genetics 5(11):861-6, 2004**

Pusch CM, **Maurer J**, Ramser J, Tomiuk J, Achatz H, Pesch K, Lichtner P, Apfelstedt-Sylla E, Jacobi FK, Berger W, Meindl A, Wissinger B: Complete form of X-linked congenital stationary night blindness (CSNB1): Refined mapping and evidence of genetic homogeneity. **International Journal of Molecular Medicine 7: 155-161, 2001**

Pusch CM, Zeitz C, Brandau O, Pesch K, Achatz H, Feil S, Scharfe C, **Maurer J**, Jacobi FA, Pinckers A, Andreasson S, Hardcastle A,Wissinger B, Berger W, Meindl A: CSNB1, the complete form of CSNB, is caused by mutations in a gene coding for a leucine-rich repeat protein. **Nature Genetics 26: 3, 324 – 327, 2000**

Weiss S, Kremers J, **Maurer J**: Interaction between rod and cone signals in responses of lateral geniculate neurons of dichromatic marmosets (Callithrix jacchus). **Visual Neuroscience 15(5): 931-943, 1998**

## 8.2 Book Chapters

Wirkner U, Maercker C, Selig J, Wagner M, Drzocek H, Kellermann A, Ansorge A, Amarantos I, **Maurer J,** Schwager C, Blake J, Korn B, Wagner W, Ho AD, Abdollahi A, Huber P, Radelof U, Ansorge W: Human Genome Microarray in Biomedical Applications. In: Patrinos G, Ansorge W (Eds.): **Molecular Diagnostics, Elsevier Science, London, 201-210, 2005**

**Maurer J**, Lehrach H: The Human Genome Project – a German perspective. In: Smelser NJ, Baltes PB (Eds.): **International Encyclopedia of Social and Behavioural Sciences, Elsevier Science, Oxford, 6995-6999, 2001**

# 9 Acknowledgements

A big thank you to Prof. Dr. Uwe Querfeld and to Prof. Dr. Axel Radlach Pries for providing this interesting project, for their encouragement to tackle this endeavor, their enthusiasm, and their openness to fruitful discussions at any time.

Special thanks to all at the Charité Institute of Physiology and the Clinic for Pediatric Nephrology / Center for Cardiovascular Research who made this work possible. I like to particularly thank Prof. Dr. Christian Freise for the expression analyses and IMT measurements, Hamoud Nasser for immunohistochemistry, Dr. Karoline von Websky for conducting the subtotal nephrectomy, Dr. Rudi Sampati for valuable assistance in animal preparation, Sylvia Plog for introduction to the surgery technique, and Kerstin Sommer for excellent sample handling and for keeping everything organized.

This work would not have been possible without the close cooperation with Hans-Ulrich Prommer. The two studies refer to each other and extensively cross-fertilized each other. Further thanks to Dr. Bianca Nietzsche, Dr. Bettina Reglin, Björn Hoffmann, Veronika Bobb, Dr. Dorothea Burkhardt, Dr. Claudia Abramjuk and all at the Charité animal facility for continuous help, discussion and support.

Finally, a special thank you to my children for dealing with their bustling dad and to my wife, who went through this with me for the second time.

# Anteilserklärung

Teilumfänge der hier dargelegten Ergebnisse wurden bereits im März 2018 in der folgenden Publikation veröffentlicht:

**Prommer, H.U., Maurer J., von Websky K., Freise C., Sommer K., Nasser H., Samapati R., Reglin B., Guimarães P., Pries A.R. and Querfeld U. 2018. Chronic kidney disease induces a systemic microangiopathy, tissue hypoxia and dysfunctional angiogenesis. Sci Rep. 8(1):5317.**

Hans-Ulrich Prommer und Johannes Maurer sind gleichberechtigte Erstautoren dieser Veröffentlichung.

Johannes Maurer hat an dieser Publikation folgende Anteile:

- Aus seiner Auswertung sind die Grafiken 4 A und B, 5, 6 sowie Teile der Tabelle 1 entstanden.
- Die Kapitel „Abstract“, „Introduction“, „Discussion“, „Methods“ sowie im Kapitel „Results“ der Abschnitt „Two experimental procedures generate CKD/uremia of different severity“ wurden etwa in gleichen Anteilen durch die Erstautoren verfasst – unterstützt durch Prof. Querfeld.
- Im Kapitel „Results“ hat Johannes Maurer maßgeblich folgende Kapitel verfasst:
  - „Blood flow velocity and leucocyte rolling velocity in CKD” (Anteil „Leucocyte Rolling Velocity”)
  - „CKD is associated with diminished vascular tone”
  - „Microvascular rarefaction in the myocardium parallels rarefaction in the cremaster muscle”
  - „CKD induces dysfunctional angiogenesis”
  - „Microvascular rarefaction in mice precedes macrovascular pathology”
- Im „Electronic Supplementary Material“ sind aus seiner Arbeit eingegangen:
  Supplementary Table 3, Daten zu Supplementary Figure 3 B, Supplementary Figure 6

Dr. Johannes Maurer Prof. Dr. Axel Radlach Pries

# Eidesstattliche Versicherung

Ich, Dr. Johannes Maurer, versichere an Eides statt durch meine eigenhändige Unterschrift, dass ich die vorgelegte Dissertation mit dem Thema:

**„Chronic Kidney Disease Induces Systemic Microvascular Functional Impairment“**

selbstständig und ohne nicht offengelegte Hilfe Dritter verfasst und keine anderen als die angegebenen Quellen und Hilfsmittel genutzt habe.

Alle Stellen, die wörtlich oder dem Sinne nach auf Publikationen oder Vorträgen anderer Autoren beruhen, sind als solche in korrekter Zitierung (siehe „Uniform Requirements for Manuscripts (URM)“ des ICMJE -www.icmje.org) kenntlich gemacht. Die Abschnitte zu Methodik (insbesondere praktische Arbeiten, Laborbestimmungen, statistische Aufarbeitung) und Resultaten (insbesondere Abbildungen, Graphiken und Tabellen) entsprechen den URM (s.o.) und werden von mir verantwortet.

Meine Anteile an etwaigen Publikationen zu dieser Dissertation entsprechen denen, die in der obigen gemeinsamen Erklärung mit dem Betreuer angegeben sind. Sämtliche Publikationen, die aus dieser Dissertation hervorgegangen sind und bei denen ich Autor bin, entsprechen den URM (s.o.) und werden von mir verantwortet.

Die Bedeutung dieser eidesstattlichen Versicherung und die strafrechtlichen Folgen einer unwahren eidesstattlichen Versicherung (§§156,161 des Strafgesetzbuches) sind mir bekannt und bewusst.

Berlin, 31.08.2018 Dr. Johannes Maurer